



FEDERAL UNIVERSITY OF CEARÁ – UFC  
TECHNOLOGY CENTER  
ENVIRONMENTAL AND HYDRAULIC ENGINEERING DEPARTMENT – POSDEHA  
CIVIL ENGINEERING POSTGRADUATE PROGRAM  
CONCENTRATION AREA ACADEMIC MASTERS IN GEOTECHNICS

**YURI NUNES SARAIVA**

**ADVANCES IN THE ITERATIVE COUPLING BETWEEN FLOW-  
GEOMECHANICAL SIMULATORS APPLIED TO CASES WITH DIFFERENT  
CONTOUR CONDITIONS**

Fortaleza  
2020



FEDERAL UNIVERSITY OF CEARÁ – UFC  
TECHNOLOGY CENTER  
ENVIRONMENTAL AND HYDRAULIC ENGINEERING DEPARTMENT – POSDEHA  
CIVIL ENGINEERING POSTGRADUATE PROGRAM  
CONCENTRATION AREA ACADEMIC MASTERS IN GEOTECHNICS

**ADVANCES IN THE ITERATIVE COUPLING BETWEEN FLOW-  
GEOMECHANICAL SIMULATORS APPLIED TO CASES WITH DIFFERENT  
CONTOUR CONDITIONS**

A dissertation presented as a partial requirement for obtaining a master's degree by the postgraduate program in Civil Engineering of Environmental and Hydraulic Engineering Department, at the Federal University of Ceará.

Concentration area: Geotechnics.

Research line: Geomechanical behavior analysis.

Advisor: Prof. Francisco Chagas da Silva Filho, PhD.

Co-Advisor: Prof. Luis Glauber Rodrigues, PhD.

Fortaleza  
2020

Dados Internacionais de Catalogação na Publicação

Universidade Federal do Ceará

Biblioteca Universitária

Gerada automaticamente pelo módulo Catalog, mediante os dados fornecidos pelo(a) autor(a)

---

S247a Saraiva, Yuri.

ADVANCES IN THE ITERATIVE COUPLING BETWEEN FLOW-GEOMECHANICAL  
SIMULATORS APPLIED TO CASES WITH DIFFERENT CONTOUR CONDITIONS / Yuri

Saraiva. – 2020.

130 f. : il. color.

Dissertação (mestrado) – Universidade Federal do Ceará, Centro de Tecnologia, Programa de  
PósGraduação em Engenharia Civil: Recursos Hídricos, Fortaleza, 2020.

Orientação: Prof. Dr. Francisco Chagas da Silva Filho.

Coorientação: Prof. Dr. Luis Glauber Rodrigues.

1. Geomechanics. 2. Reservoir Simulation. 3. Coupling. I. Título.

CDD 627

---

**YURI NUNES SARAIVA**

**ADVANCES IN THE ITERATIVE COUPLING BETWEEN FLOW-  
GEOMECHANICAL SIMULATORS APPLIED TO CASES WITH DIFFERENT  
CONTOUR CONDITIONS**

A dissertation presented as a partial requirement for obtaining a master's degree by the postgraduate program in Civil Engineering of Environmental and Hydraulic Engineering Department, at the Federal University of Ceará.

Approver on \_\_\_\_\_

**EXAMINATION COMMISSION**

---

Francisco Chagas da Silva Filho, PhD. – Advisor – President  
Federal University of Ceará

---

Luis Glauber Rodrigues, PhD. – Co-Advisor – Internal Examiner  
Federal University of Ceará

---

Silvrano Adonias Dantas Neto, PhD. – Internal Examiner  
Federal University of Ceará

---

Francisco Pinheiro Lima-Filho, Dsc. – External Examiner  
Federal University of Rio Grande do Norte

## **DEDICATION**

To my Grandfather Mário Sales Nunes (In memoriam) an example of a man who is integrated and a struggler.

To Luana Karine (In memoriam) example of a person who fights for a dream.

## ACKNOWLEDGEMENTS

To God for the gift of life and for being the driving force in the search for knowledge and for overcoming battles.

To my parents, Clésio Jean de Almeida Saraiva and Luci Ane Nunes Saraiva for always supporting my decisions, as well as to my brothers Natália, Mariana, and Jean, who accompany me throughout the journey.

My Girlfriend Natasha Nogueira Prado, who accompanied me through the whole process and constantly supports me.

My advisor Professor Francisco Chagas da Silva Filho, PhD. And my co-advisor Professor Luis Glauber Rodrigues, PhD. For all knowledge and experience shared, as well as for trusting in the dedication and engaged work.

To Professor Silvrano Adonias Dantas Neto, PhD, and Professor Francisco Pinheiro Lima-Filho, Dsc. For accepting the invitation to examine the dissertation and contribute with their vast knowledge and experiences.

To Herberth Arturo Vasques Haro, Dsc. For sharing moments of numerical simulations and search for knowledge, and to Madson Magalhães, Dsc. For sharing knowledge about programming language.

To Petrobras for providing the support, software licenses, computational structure, and laboratory.

To my friends and colleagues Helson, Emanuelle, Tiago, and all the other GSIM lab collaborators for sharing moments of research and knowledge.

This study was financed in part by the Fundação Cearense de Apoio ao Desenvolvimento Científico e Tecnológico – Brasil (FUNCAP).

# ADVANCES IN THE ITERATIVE COUPLING BETWEEN FLOW- GEOMECHANICAL SIMULATORS APPLIED TO CASES WITH DIFFERENT CONTOUR CONDITIONS

## RESUMO

A simulação por análise numérica para cenários de engenharia de reservatórios é necessária devido à importância de se prever e antecipar as consequências e produtos de uma exploração de água ou petróleo, bem como a vasta quantidade de variáveis que estão associadas à engenharia hidráulica, de petróleo e à geomecânica das rochas. Devido a isso, o presente trabalho consiste na apresentação de atividades relativas ao acoplamento de geomecânica e simulação de fluxo baseados no *paper* SPE – 79709 de autoria de Dean *et al.* (2006). Dessa forma, os *softwares* utilizados para o acoplamento foram o simulador IMEX, versão 2019, em acoplamento iterativo explícito, com módulo de fluxo e geomecânica desse simulador e, posteriormente, utilizado o simulador geomecânico FLAC3D 6.0 em conjunto com o módulo de fluxo IMEX e com programação em MATLAB (2018) e FISH, para transferência de dados entre simuladores. Ademais, os resultados demonstram a obtenção de convergência satisfatória dos problemas propostos por Dean *et al.*, no simulador IMEX com geomecânica. Para o acoplamento iterativo entre FLAC3D e IMEX, obteve-se boa convergência de comportamento para o problema 1. Ao final das simulações, é elaborado um modelo de reservatório baseado nesse problema com inclusão de uma fratura horizontal próxima a região do poço produtor. Esse tipo de acoplamento permite um estudo apurado com maior nível de complexidade e inclusão de variáveis ao comportamento do reservatório, como a inclusão de fraturas e modelos constitutivos. Portanto, ao utilizar o melhor de cada simulador, busca-se uma forma de acoplamento que aproxime a realidade e mitigue as incertezas associadas à simuladores de engenharia de reservatórios, e ao realizar o acoplamento iterativo, simplificar métodos numéricos mesmo para cenários elevada complexidade de parâmetros.

**Palavras-chave:** Geomecânica, Simulação de reservatórios, Acoplamento.

## ABSTRACT

Numerical analysis for reservoir engineering scenarios is necessary due to the importance of predict the consequences and products of water or oil exploitation, as well as the vast quantity of variables that are associated with hydraulic engineering, oil, and rock geomechanics. Due to this, the present work consists to show the relative activities for geomechanical coupling and flux simulation based on paper SPE – 79709 of Dean *et al.* (2006). This way, the used software for coupling was IMEX (2019), in the explicit iterative coupling, with geomechanics and flux model of the same simulator and, posteriorly, was used the geomechanics simulator FLAC3D 6.0 associated with the flux model of IMEX and programming with MATLAB and FISH to transfer the data between simulators. In addition, the results demonstrate the satisfactory obtention of convergence of the problems proposed by Dean *et al.* (2006), in IMEX with geomechanics. For iterative coupling between FLAC3D and IMEX was obtained good behavior convergence of problem 1. At the end of the simulations, a reservoir model is elaborated based on this problem with the inclusion of a horizontal fracture near the region of the producing well. This type of coupling allows an accurate study with the highest level of complexity and inclusion of variables to reservoir behavior, as the inclusion of fractures and constitutive models. Therefore, using the best parameters of each simulator is sought as a type of coupling that approximates the reality and mitigates the uncertainties associated with simulators of reservoir engineering, and when performing iterative coupling, simplify numerical methods even for highly complex parameter scenarios.

**Keywords:** Geomechanics, Reservoir simulation, Coupling.



## FIGURES LIST

Figure 1 - Three-dimensional stress state.....	19
Figure 2 - Three-dimensional block stresses.....	19
Figure 3 – Stress state components of a block.....	20
Figure 4 – Typical black oil phase diagram.....	22
Figure 5 – Typical p-T diagram of a multi-component system.....	24
Figure 6 – Wettability illustration.....	24
Figure 7 – Contact angles examples.....	25
Figure 8 – Scale effect on rock masses.....	27
Figure 9 – Reservoir scale system.....	27
Figure 10 – Effective rock compressibility vs. porosity.....	31
Figure 11 – Rupture curve.....	34
Figure 12 – Failure envelope.....	35
Figure 13 – Mohr's circle.....	35
Figure 14 - Hoek-Brown rupture.....	36
Figure 15 - Hoek-Brown criteria.....	37
Figure 16 – Subsidence as a function of standardized distance.....	37
Figure 17 – Well coupling.....	40
Figure 18 – Reservoir with gas solution drive.....	41
Figure 19 – Reservoir changes during depletion.....	42
Figure 20 - In situ stress around a well borehole.....	43
Figure 21 – Oil reservoir subjected to water inflow.....	44
Figure 22 – Flow model mesh.....	45
Figure 23 – Reservoir perspective of problem 1.....	49
Figure 24 – 3D display of problem 1 and initial vertical total stress.....	49
Figure 25 – Reservoir perspective of problem 2.....	50
Figure 26 - 3D display of problem 2 and initial horizontal total stress.....	50
Figure 27 – Reservoir perspective of problem 3.....	51
Figure 28 – 3D problem 3 display and vertical total stress.....	52
Figure 29 – Reservoir pressure.....	53
Figure 30 – 3D problem 4 representation and water saturation.....	55
Figure 31 – Problem 4 3D view and water saturation.....	55

Figure 32 – Geomechanical coupling factor 1 and boundary conditions.....	57
Figure 33 - Geomechanical coupling factor 0 and boundary conditions.....	59
Figure 34 – Process flow between software. ....	63
Figure 35 - FLAC3D flow chart.....	63
Figure 36 – Zone block vertices configuration.....	64
Figure 37 - Fractured reservoir.....	67
Figure 38 – Average reservoir pressure (problem 1).....	68
Figure 39 - Subsidence (problem 1). ....	69
Figure 40 – Average reservoir pressure (problem 2).....	70
Figure 41 - Subsidence (problem 2). ....	70
Figure 42 – Average reservoir pressure (problem 3).....	71
Figure 43 - Subsidence (problem 3). ....	72
Figure 44 – Border pressure (problem 3). ....	72
Figure 45 – Average reservoir pressure (problem 4).....	73
Figure 46 - Subsidence (problem 4). ....	73
Figure 47 – Well’s pressure (problem 4).....	74
Figure 48 – Gas/Oil ratio (problem 4). ....	74
Figure 49 – Water/Oil ratio (problem 4). ....	75
Figure 50 – Average reservoir pressure (problem 1, IMEX). ....	76
Figure 51 – Subsidence (problem 1, IMEX). ....	76
Figure 52 – Average reservoir pressure (problem 2, IMEX). ....	77
Figure 53 - Subsidence (problem 2, IMEX). ....	78
Figure 54 – Average reservoir pressure (problem 3, IMEX). ....	79
Figure 55 – Subsidence (problem 3, IMEX). ....	80
Figure 56 – Subsidence at the top of the reservoir (problem 3, IMEX).....	80
Figure 57 – border pressure (problem 3, IMEX).....	81
Figure 58 – Average reservoir pressure (problem 4, IMEX). ....	82
Figure 59 - Subsidence (problem 4, IMEX). ....	82
Figure 60 – Well’s pressure (problem 4, IMEX).....	83
Figure 61 – Gas/Oil ratio (problem 4, IMEX).....	84
Figure 62 – Water/Oil ratio (problem 4, IMEX). ....	84
Figure 63 - Models without geomechanics.....	86
Figura 64 - Models with geomechanics.....	87
Figure 65 – Volumetric strain.....	88

Figure 66 – Subsidence. ....	89
Figure 67 – Subsidence profile in FLAC3D.....	89
Figure 68 – Comparison of subsidence with the methodologies.....	90
Figure 69 – Mechanical ratio-average limit. ....	91
Figura 70 - Fractured reservoir subsidence .....	91
Figura 71 - Fractured reservoir volumetric strain 3D view .....	92

## TABLES LIST

Table 1 – Rock types and porosity. ....	30
Table 2 – Reasons for simulation. ....	45
Table 3 – Exported file. ....	66
Table 4 - FLAC3D - IMEX models.....	86

## SYMBOLS

$\sigma_h$  – Horizontal stress;

$\sigma_v$  – Vertical stress;

$\tau_{i,j}$  – Shear stress at respective coordinates;

$\sigma_{i,i}$  – Normal stress at respective coordinates;

$\sigma_{os}$  – Interfacial energy between oil and solid;

$\sigma_{ws}$  – Interfacial energy between water and solid;

$\sigma_{ow}$  – Interfacial energy between oil and water;

$\theta_c$  – Angle of contact between oil-water-solid measured through the water phase;

$P$  – Pressure;

$R$  – Universal gas constant;

$T$  – Temperature;

$V$  – Gas volume in ft<sup>3</sup> per one gas mole;

$V_B$  – Bulk volume;

$V_p$  – Pore volume;

$V_G$  – Grain volume;

$\emptyset$  – Porosity;

$\emptyset_i$  – Initial porosity;

$\epsilon_v$  – Volumetric strain;

$\alpha_t$  – Coefficient for incompressible solids equals 1;

$(T - T_i)$ : Temperature variation;

$V_f$  – Final volume;

$V_i$  – Initial volume;

$C_f$  – Rock compressibility;

$K_r$  – Relative permeability;

$K$  – Absolute permeability;

$K_{o,g,w}$  – Effective permeability to the fluid at a given fluid saturation;

$\tau$  – Shear stress;

$\tau_0$  – Cohesive resistance;

$\theta$  – Friction angle;

$\sigma$  – Effective normal stress;

$s_0$  – Final shear stress;  
 $\mu$  – Internal friction coefficient;  
 $\sigma_1$  – Higher main stress;  
 $\sigma_3$  – Lower main stress;  
 $I_f$  – Friction index;  
 $\sigma_c$  – Confinement stress;  
 $I_i$  – Index for intact rock;  
 $m$  e  $s$  – Specific constants for or type of rock;  
 $C_B$  – Bulk compressibility;  
 $C_f$  – Formation compressibility;  
 $h$  – Reservoir net thickness;  
 $\Delta P$  – Pressure depletion;  
 $c_b$  – Porous rock compressibility;  
 $E$  – *Young* modulus;  
 $\alpha$  – *Biot* coefficient;  
 $\nu$  – *Poisson* coefficient;  
 $\sigma_m$  – Mean total stress.

## SUMMARY

<b>1. INTRODUCTION</b> .....	16
1.2. Topic and justification .....	16
1.3. General and specific purpose .....	17
<b>2. THEORETICAL BACKGROUND</b> .....	18
2.1. Stress .....	18
2.2. Effects of fluids on pores .....	20
2.3. Basic phase behavior .....	22
2.4. Wettability .....	24
2.5. State equations .....	26
2.6. Scale effect.....	27
2.7. Porosity .....	28
2.8. Compressibility .....	30
2.9. Permeability .....	32
2.10. Constitutive models of failure criteria.....	33
2.11. Subsidence.....	37
2.12. Reservoir classification .....	38
2.13. Reservoir wells.....	39
2.14. Reservoir behavior .....	43
2.15. Reservoir simulation model .....	44
2.16. New porosity and permeability calculation through iterative coupling .....	46
<b>3. METHODOLOGY</b> .....	48
3.1. Problems description.....	48
3.1.1. Problem 1.....	48
3.1.2. Problem 2.....	50
3.1.3. Problem 3.....	51
3.1.4. Problem 4.....	53
3.2. IMEX 2019 explicit iterative coupling .....	55
3.2.1. Problem 1.....	55
3.2.2. Problem 2.....	58
3.2.3. Problem 3.....	59
3.2.4. Problem 4.....	61
3.3. External explicit iterative coupling with FLAC3D 6.0, IMEX e MATLAB.....	62
3.3.1. Mesh design.....	63
3.3.2. Initial conditions .....	64
3.3.3. Master file.....	65

3.3.4.	Initial pore pressure list .....	65
3.3.5.	FISH programming.....	66
3.4	Fractured model .....	67
<b>4.</b>	<b>RESULTS</b> .....	<b>68</b>
4.1.	Description of results of Dean <i>et al.</i> (2006).....	68
4.1.1.	Problem 1.....	68
4.1.2.	Problem 2.....	69
4.1.3.	Problem 3.....	71
4.1.4.	Problem 4.....	73
4.2.	IMEX 2019 results.....	75
4.2.1.	Problem 1.....	75
4.2.2.	Problem 2.....	77
4.2.3.	Problem 3.....	78
4.2.4.	Problem 4.....	81
4.3.	FLAC3D 6.0 results.....	85
4.3.1.	Volumetric strain .....	87
4.3.2.	Subsidence.....	88
4.3.3.	Average mechanical ratio .....	90
4.4.	Fractured reservoir.....	91
<b>5.</b>	<b>REFERENCES</b> .....	<b>94</b>
<b>7.</b>	<b>APPENDICES</b> .....	<b>97</b>



## 1. INTRODUCTION

Based on the need to control the complexities associated with the oil and water reservoir system, from the preliminary reservoir capacity study to the depletion and abandonment of the fluid extraction field, the simulation of oil and water reservoirs is important because it is possible to mitigate and predict future behaviors, as well as to adjust the analysis with the actual depletion and field tests.

The analysis of the geomechanical behavior through simulation guarantees to follow the development of phenomena such as subsidence and development of the stresses associated with the model, with consequent relief of stresses, or increase of stresses, providing the activation of failures, creation of fractures, or also pressure loss with low production and loss of injection material.

The choice of theme is based on the need for careful monitoring of the geomechanical behavior associated with the reservoir, whether it is confined to rock with fractures that influence the depletion or not, or the reservoir confined with compositional fluid or just black oil.

Initially, studies on preliminary knowledge on reservoir engineering were conducted, with learning and use of specific computer simulators for the analysis of oil and water reservoirs, with associated geomechanics module.

Subsequently, the use of another simulator, specifically for geomechanics, and the application of flow simulators in porous media and rock mechanics in iterative coupling to obtain accurate results of geomechanical behavior.

### 1.2. Topic and justification

Studies and analysis of the behavior of oil and water reservoirs are highly developed due to the importance of the energy capacity that, in the case of oil, it provides, either for fuel generation or the generation of oil products.

The environmental impacts that may occur with an imprecise analysis or without using the due importance to preliminary studies, during the execution phase and later phase of abandonment of the exploration field may be irreparable and provide a drastic impact on mankind.

Therefore, preliminary studies and reservoir simulations are important to predict and mitigate future actions, to provide the preparation for future events during exploration, reducing the uncertainties associated with the oil reservoir system.

### 1.3. General and specific purpose

The general objective is to compare the total coupling proposed by Dean *et al.* (2006) with the iterative coupling developed in this work, using the commercial software CMG IMEX 2019, MATLAB, and FLAC3D 6.0, proposing the numerical analysis of oil reservoirs with the well-defined flow and geomechanical properties. This way, simulations are performed with a simplified method, providing a scenario with a higher level of complexity and representativity of results.

The specific objectives are to monitor the development of geomechanical efforts and reservoir behavior when changing the boundary conditions and properties of the fluid under analysis.

## 2. THEORETICAL BACKGROUND

The theoretical background consists of the analysis of issues related to the flow-stress coupling described below, which involves reservoir flow behavior and geomechanics associated with reservoir rock, properties that affect oil recovery, as well as the safety analysis of depletion development.

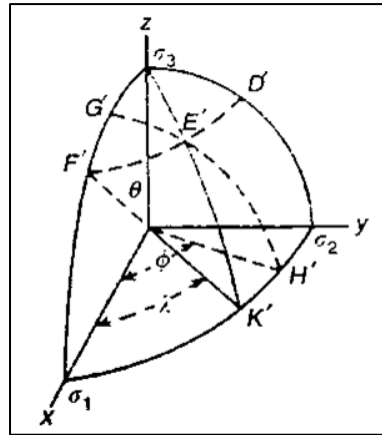
### 2.1. Stress

According to Zoback (2007), depletion can cause changes in the stress state of the reservoir, thus, being beneficial or harmful, to production in different ways. Therefore, knowledge of stresses in depth is fundamentally important to address a wide range of practical problems in geomechanics within oil, gas, geothermal reservoirs, and overlapping formations. Sun *et al.* (2020) state that the numerical uniaxial strain test that represents the reservoir stress path can be used to obtain the changes of porosity and permeability as a function of effective stress.

According to Aadnøy (2014), *in situ* stress data plays a key role at various stages of oil and gas well planning, construction, operation, and production. Knowledge of *in situ* stresses and the mechanical properties of the rock formation is crucial for the assessment of well construction and production, so before performing any rock stress analysis and rupture assessment, it is necessary to have complete knowledge of *in situ* stresses.

Jaeger & Cook (2007) defines the theory of stress in three dimensions as a direct extension of the two-dimensional theory. A generic three-dimensional plane will have a normal unitary vector. Mohr's circular representation of the two-dimensional stress state can be used in three dimensions, as shown in Figure 1.

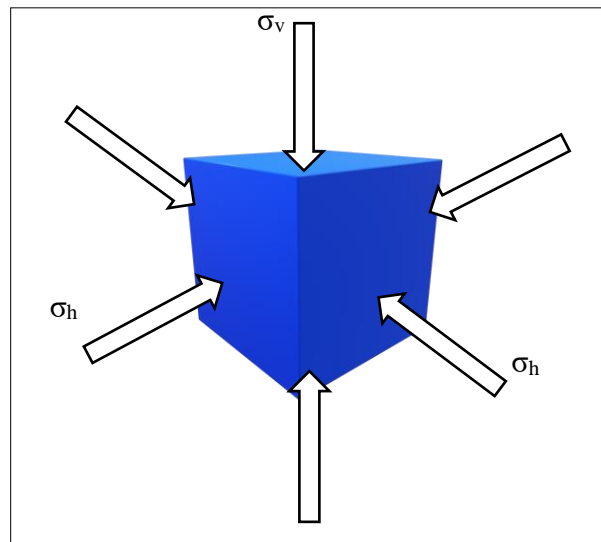
Figure 1 - Three-dimensional stress state.



Source: Jaeger &amp; Cook, 2007.

Three mutually perpendicular stresses exist at each point underground, as shown in Figure 2. Other sources of vertical stress include stresses resulting from geological conditions, such as magma or salt domes penetrating the areas surrounding the rock formation. This overload stress usually tends to propagate and expand the underlying rocks and horizontal lateral directions due to the Poisson effect. This lateral movement is limited by the presence of adjacent materials, which then make the maximum and minimum horizontal stresses form, Aadnøy (2014).

Figure 2 - Three-dimensional block stresses.



Source: Author, 2020.

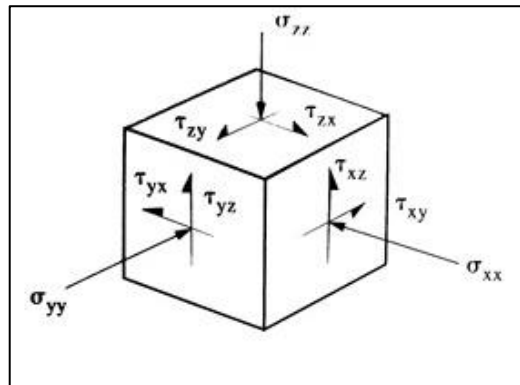
Where:

 $\sigma_h$  – Horizontal stress; $\sigma_v$  – Vertical stress.

Ju *et al.* (2020) defines that stress sensitivity is used to describe petrophysical parameters of oil reservoir rocks that change with the variation in effective stress. Normally, the reservoir rock permeability decreases when the effective stress increases.

According to Hudson and Harrison (1997) it is more convenient to consider normal and shear components concerning a given set of axes, usually a rectangular x, y, z Cartesian system. In this case, the body can be considered sliced into three orientations corresponding to the visible faces of the cube shown in Figure 3.

Figure 3 – Stress state components of a block.



Source: Hudson & Harrison, 1997.

Where:

$\tau_{i,j}$  – Shear stress at respective coordinates;

$\sigma_{i,i}$  – Normal stress at respective coordinates.

For the geomechanics analysis, the stress state is used as a departure point. Usually, it is assumed that  $\sigma_v$  is the principal stress, therefore, the other two lie in the horizontal plane. This assumption should be verified in cases of regional vulcanism, strong structural deformation, high geographical relief, and differential compaction during burial, Dusseault (2011).

## 2.2. Effects of fluids on pores

According to AadnØy (2014), pore pressure is a key factor in production and has a significant effect on well construction and well hole stability. A pore pressure curve is required to select the slurry weights and installation points of the support coatings. Pore pressure derived from profiles and other sources is not accurate, so the pressure curves of the pores have significant uncertainty.

According to Jaeger & Cook (2007), rocks are typically porous to a certain extent, and the pore space of rock will be filled with fluids under pressure. The porous liquid is usually water but can be oil, gas, or molten rock. Porous fluid can affect rock failure in two ways, due

to the purely mechanical effect of pore pressure, or due to chemical interactions between rock and fluid. Concerning the mechanical effect of the pore fluid pressure, this would work as tensile stress. According to Longuemare *et al.* (2002), in conventional formulations of fluid flow, the variation of pore volume only depends on the pore pressure variation through the pore volume compressibility coefficient. In the other hand, Goral *et al.* (2020) observed a minor effect of reservoir confinement in porosity and permeability, related to the morphology of the pore, in the extension of stress and of fluid flow connected paths.

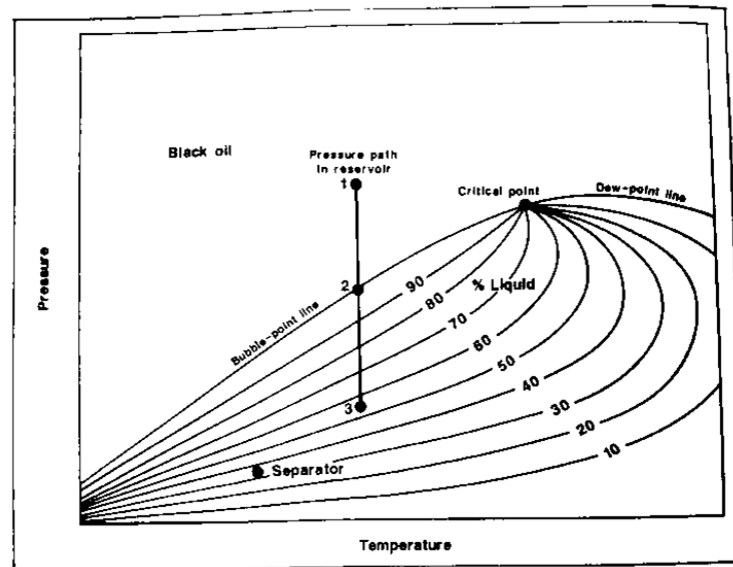
According to Rosa (2002), the properties of the fluids and rocks that make up petroleum reservoirs should preferably be determined experimentally in laboratory analysis. But in some situations, this is not possible due to economic or operational reasons. Therefore, the properties of the fluids and the reservoir rock can be calculated through state equations or estimated using charts, abacuses, or empirical correlations available in the literature. Zhao *et al.* (2020) determine, in the recovery process, the flow of oil, gas, and water by their relative permeability in the reservoir.

Ahmed (2006) defines a porous flow as a complex phenomenon and cannot be described as flows through pipes or conduits. In porous media, flow is different because there are no well-defined flow paths that are used for measurement.

According to McCain (1973), there are five types of reservoir fluids. These are generally named black oil, volatile oil, retrograde gas, wet gas, and dry gas. These five types of reservoir fluids have been defined because each requires different approaches by reservoir engineers and production engineers. The method of fluid sampling, the types and sizes of surface equipment, the calculation procedures for determining oil and gas, the techniques for forecasting oil and gas reserves, the exhaustion plan, and the selection of improved recovery methods are all dependent on the type of reservoir fluid, this reservoir fluid can be confirmed only by observation in the laboratory.

As black oil, which consists of a wide variety of chemical species, including large, heavy, and non-volatile molecules. The phase diagram covers a wide temperature range, and the critical point is well above the slope of the phase envelope. This phase diagram of a typical black oil is shown in Figure 4.

Figure 4 – Typical black oil phase diagram.



Source: McCain, 1973.

According to Ahmed (1946), crude oil covers a wide range of physical properties and chemical components, based essentially on physical properties, gas-oil ratio composition, and pressure-temperature diagram. In general, crude oil is commonly classified by the following types, ordinary black oil, low shrinkage crude oil, high shrinkage (volatile) crude oil, and near-critical crude oil.

According to Segura *et al.* (2016), in fractured environments, fluid flow affects geomechanics in terms of the change in pore pressure that occurs during production or injection, which affects the effective stresses in the distribution in natural fractures, and therefore contributes to their opening or closing.

Ahmed (2006) defines that naturally in oil reservoirs of hydrocarbon systems are found mixtures of organic compounds that exhibit multiphase behavior over a wide range of pressures and temperatures. These hydrocarbon accumulations can occur in the gaseous state, liquid state, solid-state, or various combinations of gas, liquid, and solid. These differences in phase behavior, together with the physical properties of the reservoir rock determine the relative facility with which gas and liquids are transmitted or retained, resulting in various types of hydrocarbon reservoirs with complex behavior.

### 2.3. Basic phase behavior

According to Ahmed (1946), the phase is defined as the homogeneous part of the system and is physically distinct and separated from other parts of the system by defined contours. If a

substance exists in a solid, liquid, or gaseous phase, it is determined by the temperature and pressure acting on the substance. Hydrocarbon systems found in oil reservoirs are known to exhibit multiphase behavior over wide pressure and temperature ranges. The definition of the conditions of these systems is conventionally expressed in different types of diagrams, commonly denominated phase diagrams.

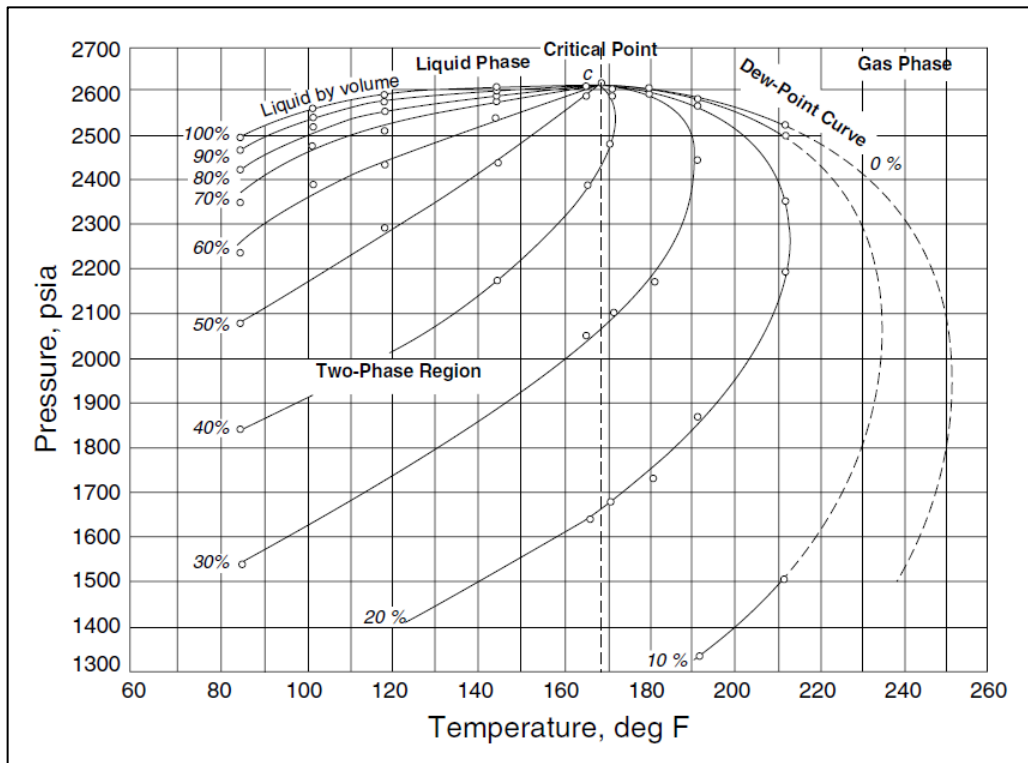
The phase behavior of a multi-component hydrocarbon system in the liquid-vapor region is quite similar to the binary system. However, as the system becomes more complex with the increase in the number of different components, the pressure and temperature ranges in which two phases increase significantly.

Ahmed (2006) describes that oil reservoirs are widely classified as oil or gas. This classification is subdivided depending on the composition of the reservoir hydrocarbon mixture, the initial reservoir pressure and temperature, and the production surface pressure and temperature. These phase behavior conditions are conventionally expressed in different types of diagrams, commonly called phase diagrams. One of these diagrams is named a pressure-temperature (p-T) diagram.

Figure 5 illustrates a typical pressure-temperature diagram of a multi-component system with a specific general composition. For each hydrocarbon system, there is a different phase diagram, but the general configuration is similar. These diagrams are essentially used to classify reservoirs, classify natural hydrocarbon systems, and describe the phase behavior of the reservoir fluid.



Figure 5 – Typical p-T diagram of a multi-component system.

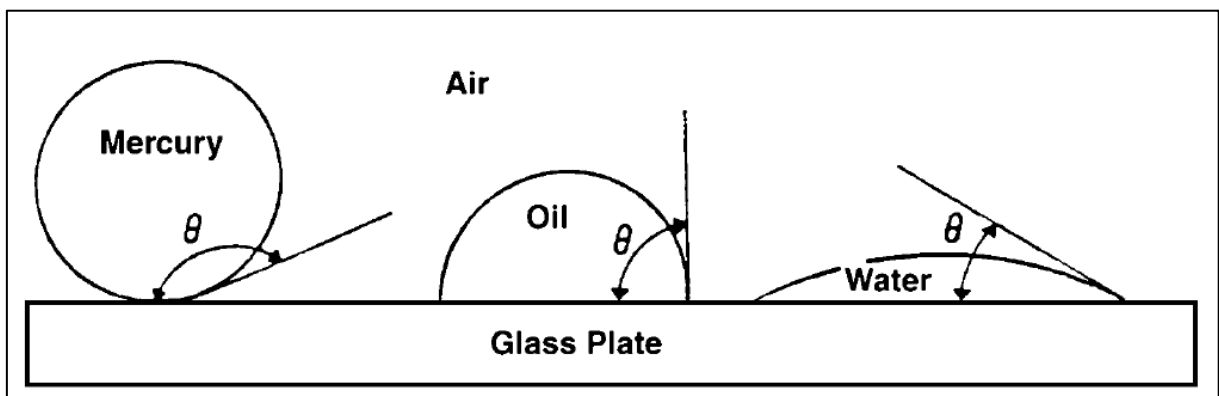


Source: Ahmed, 2006.

#### 2.4. Wettability

Ahmed (2006) defines it as the tendency of a fluid to spread or adhere to a solid surface in the presence of another immiscible fluid. The concept of wettability is illustrated in Figure 6, small drops of three liquids, mercury, oil, and water, are placed on a clean glass plate. It is noted that mercury maintains its spherical shape, oil develops approximately a hemispherical shape, but water tends to spread over the glass surface.

Figure 6 – Wettability illustration.

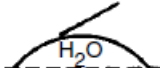
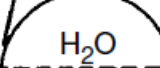
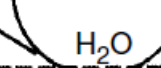
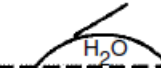
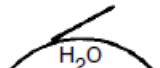
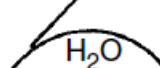
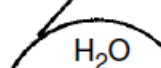
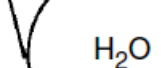


Source: Ahmed, 2006.

This spreading tendency can be conventionally expressed by measuring the angle of contact between the liquid and the solid surface, named contact angle. As the angle decreases, the wettability characteristic of the liquid increases. Complete wettability is evidenced by the zero-contact angle, and complete non-wettability is evidenced by the  $180^\circ$  contact angle. The distribution of fluids in porous media is a function of wettability, due to the forces of attraction, the wettable phase tends to fill small pores of the rock and the non-wettable phase occupies more channels, Ahmed (2006).

Lyons (2010) describes the contact angle ( $\theta_c$ ) existing between two fluids in contact with the solid and measured through the densest phase, is the measure of the relative wettability or the propagation of a fluid on a solid. A zero contact angle indicates complete wettability through the densest phase, and a  $180^\circ$  angle indicates complete wettability through the least dense phase, and a  $90^\circ$  angle means that no fluid is preferentially wettable to the solid, Figure 7 presents examples of various contact angles.

Figure 7 – Contact angles examples.

	$\theta = 30^\circ$	$\theta = 83^\circ$	$\theta = 153^\circ$	$\theta = 35^\circ$
				
SILICA SURFACE				
ORGANIC LIQUID	ISOOCTANE	ISOOCTANE + 5.7% ISOQUINOLINE	ISOQUINOLINE	NAPHTHENIC ACID
	$\theta = 30^\circ$	$\theta = 48^\circ$	$\theta = 54^\circ$	$\theta = 106^\circ$
				
CALCITE SURFACE				

Source: Lyons, 2010.

Oil recovery, as a function of water injection, is higher in water-wet cores than in oil-wet cores, Lyons (2010).

It is important to note that the absolute permeability of the reservoir has no direct influence on the wettability ratio; However, as shown by Craig (1971), the sweeping increases with wettability ratio reduction. With a constant injection rate, only by changing the relative

permeability, it is possible to obtain greater sweeping efficiency for lower relative permeability values of injected fluids, delaying the breakthrough of the injection advance front in production.

But stress changes permeability during production or injection and will influence the relative permeability behavior due to saturation changes. This new relative permeability ratio will influence the wettability ratio, the areal sweep, and the oil recovery factor.

Fanchi (2006) describes that by adding a chemical such as a surfactant, polymer, corrosion inhibitor, or fouling inhibitor, it is possible to alter wettability. Therefore, the contact angle is always measured through the dense phase and related to (2.1) interfacial energy by Equation 2.1:

$$\sigma_{os} - \sigma_{ws} = \sigma_{ow} \cos \theta_c$$

Where:

$\sigma_{os}$  – Interfacial energy between oil and solid;

$\sigma_{ws}$  – Interfacial energy between water and solid;

$\sigma_{ow}$  – Interfacial energy between oil and water;

$\theta_c$  – Angle of contact between oil-water-solid measured through the water phase.

## 2.5. State equations

According to Ahmed (1946), it is an analytical expression that relates pressure to temperature and volume. An appropriate description of this PVT ratio for real hydrocarbon fluids is essential in determining the volumetric and phase behavior of petroleum reservoir fluids by predicting the performance of face separation. The best and simplest example of representation of a state equation is that of an ideal gas, expressed mathematically by Equation 2.2:

$$P = \frac{R T}{V} \quad (2.2)$$

Onde:

$P$  – Pressure;

$R$  – Universal gas constant;

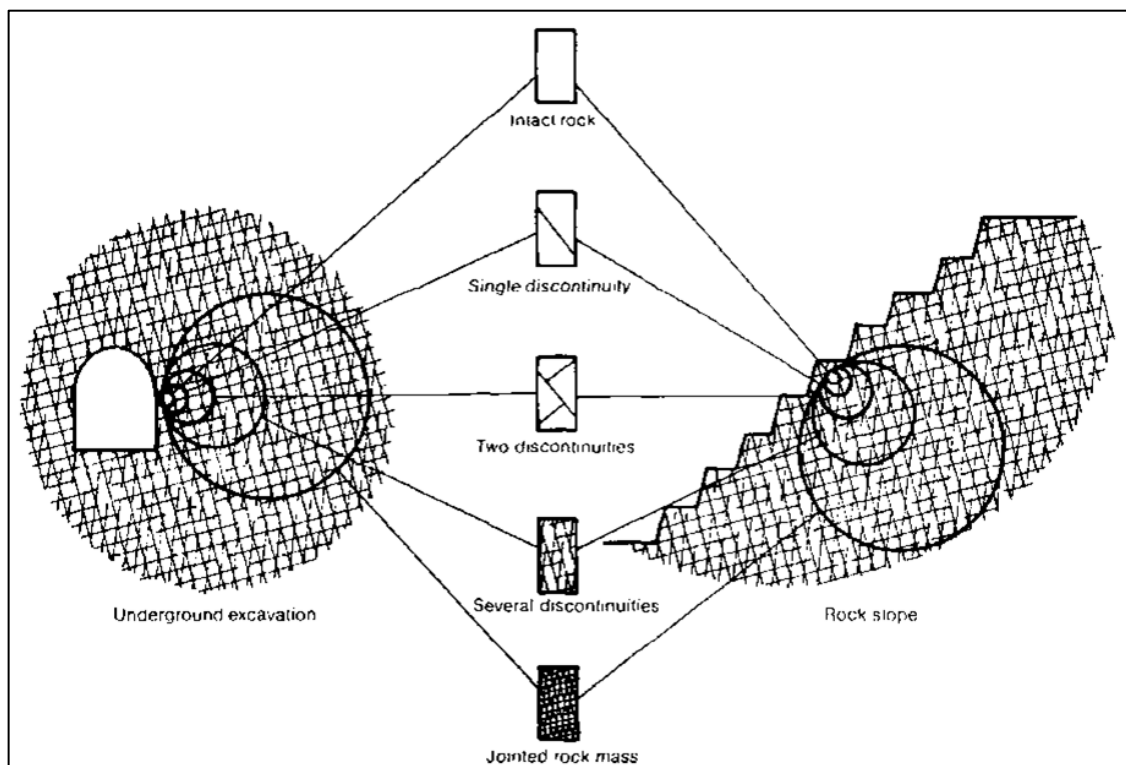
$T$  – Temperature;

$V$  – Gas volume in ft<sup>3</sup> per one mol of gas.

## 2.6. Scale effect

According to Hoek (1983), from a geological description of the rock mass, and a comparison between the size of the structure being projected and the spacing of the discontinuities in the rock mass, as shown in Figure 8, it is decided what type of material and what is the most appropriate behavior for the model, related to the strength of the rock mass. On the relative scale between the sliding surface and the geological structures present in the rock mass, any possible breaking surface passing through a fractured rock mass will be used in the design the shear strength of the rock mass, already on a smaller scale, where only the intact rock remains, the intact rock strength is used in the design.

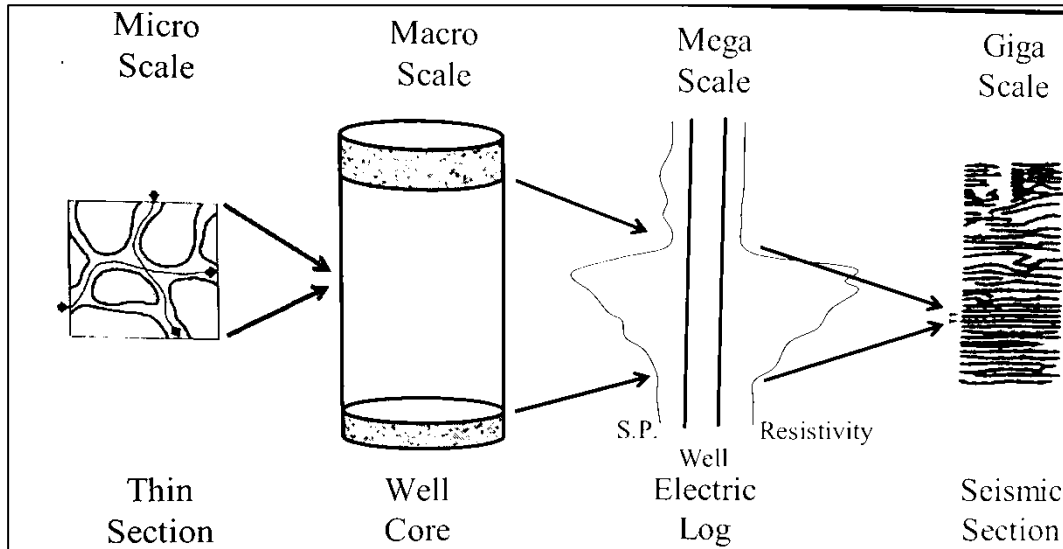
Figure 8 – Scale effect on rock masses.



Source: Hoek, 1983.

According to Fanchi (2006), the size of the scales varies from large to microscopic, variations in the scale of applicability of the data can be distinguished by the definition of conceptual scales. Figure 9 shows the usually adopted reservoir scale system, in the proportion of macro-scale characterizing the level of fracture present in the reservoir rock and that, will influence the flow behavior and permeability of the reservoir.

Figure 9 – Reservoir scale system.



Source: Fanchi, 2006.

## 2.7. Porosity

According to Fanchi (2006), one of the fundamental rock properties that a reservoir flow model should include is porosity, which is the porous medium fraction that is in an empty space. The porous medium bulk volume  $V_B$  is the sum of the pores volume  $V_P$  and the volume of the grains  $V_G$ , as shown in Equation 2.3:

$$V_B = V_P + V_G \quad (2.3)$$

Porosity is the ratio of porous volume to bulk volume, as follows in Equation 2.4:

$$\phi = \frac{V_P}{V_B} \quad (2.4)$$

The porosity calculation, as a volumetric strain function, is elaborated through the following Equation 2.5, defined by Tortike and Farouq Ali (1993), which expresses the porosity as:

$$\phi = \frac{\phi_i + \epsilon\nu - (1 - \phi_i)\alpha t(T - T_i)}{1 + \epsilon\nu} \quad (2.5)$$

Where:

$\phi$  – Porosity;

$\phi_i$  – Initial porosity;

$\epsilon\nu$  – Volumetric strain;

$\alpha t$  – Coefficient for incompressible solids that equals 1;

$(T - T_i)$ : Temperature variation.

The volumetric strain calculation is defined as shown in equation 2.6:

$$\varepsilon_v = \frac{V_f - V_i}{V_i} \quad (2.6)$$

Where:

$V_f$  – Final volume;

$V_i$  – Initial volume.

In an environment where there is no temperature variation, isothermal model, the term  $(T - T_i)$  equals zero. Thus, the following porosity equation becomes as noted in 2.7:

$$\phi = \frac{\phi_i + \varepsilon_v}{1 + \varepsilon_v} \quad (2.7)$$

Ahmed (2006) define rock porosity as a measure of the rock capacity storage, which is capable of retaining fluids. Quantitatively, porosity is the ratio of porous volume to bulk volume. As sediment is deposited and rock is formed during geological times, some voids that are formed become isolated from other voids by excessive cementing. Therefore, many of the voids are interconnected while some porous spaces are isolated. This leads to two distinct types of porosity, the absolute and the effective.

- Absolute porosity: defined by the ratio of total pore space in the rock to bulk volume. A rock can have considerable absolute porosity and still not have fluid conductivity due to lack of interconnected pore;
- Effective porosity: is the percentage of interconnected porous space to bulk volume. It is the used value to represent the interconnected porous space that contains the recoverable hydrocarbon fluids.

The original porosity is that developed by material deposition, while the induced porosity is that developed by some geological process after rock deposition, Ahmed (2006).

Lyons (2010) describes that sandstones with oil have porosity ranging from 15% to 30%, while porosity in limestone and dolomites are typically low. The differentiation between absolute and effective porosity should be performed. Absolute porosity is defined by the ratio of total porous rock volume to rock mass volume while effective porosity is defined by the ratio of interconnected rock porous volume to rock mass volume. Porosity affects factors such as compactness, cementation characteristic and amount, grain shape and amount, and grain size or distribution uniformity.

The porosity values depend on the type of rock, as shown in Table 1. There are two basic techniques for directly measuring porosity, laboratory core analysis, and well logging. Ideally, a correlation can be established between *in situ* measurements, as well as logging and surface measurements, such as core analysis, Fanchi (2006).

Table 1 – Rock types and porosity.

Rock types	Porosity series (%)	Typical porosity (%)
Sandstone	15-35	25
Unconsolidated sandstone	20-35	30
Carbonate		
Intercrystalline limestone	5-20	15
Oolitic limestone	20-35	25
Dolomite	10-25	20

Source: Fanchi, 2006. (Adapted)

In problems involving porosity calculations, it is convenient to remember that porosity of one percent is equivalent to the presence of 77.6 barrels of pore space in a bulk volume of one acre-foot of sand, Lyons (2010).

## 2.8. Compressibility

According to Howard (1953), in an unsaturated reservoir, rock expansion follows the decline in reservoir pressure that such magnitude can materially affect the reservoir performance prediction. The rock compressibility effect will be of greater importance in the oil reserve calculation by pressure decline in unsaturated volumetric reservoirs when the rock limits are unknown or not defined. Compressibility typically decreases with increasing porosity and effective overload pressure, Ahmed (2006).

Lyons (2010) defines isothermal rock compressibility as the change in pore volume to the change in pore pressure, as shown in the following Equation 2.8, where the partial derivative is given at constant temperature:

$$C_f = \frac{1}{V_p} \left( \frac{\partial V_p}{\partial P} \right)_T \quad (2.8)$$

Where:

$C_f$  – Rock compressibility;

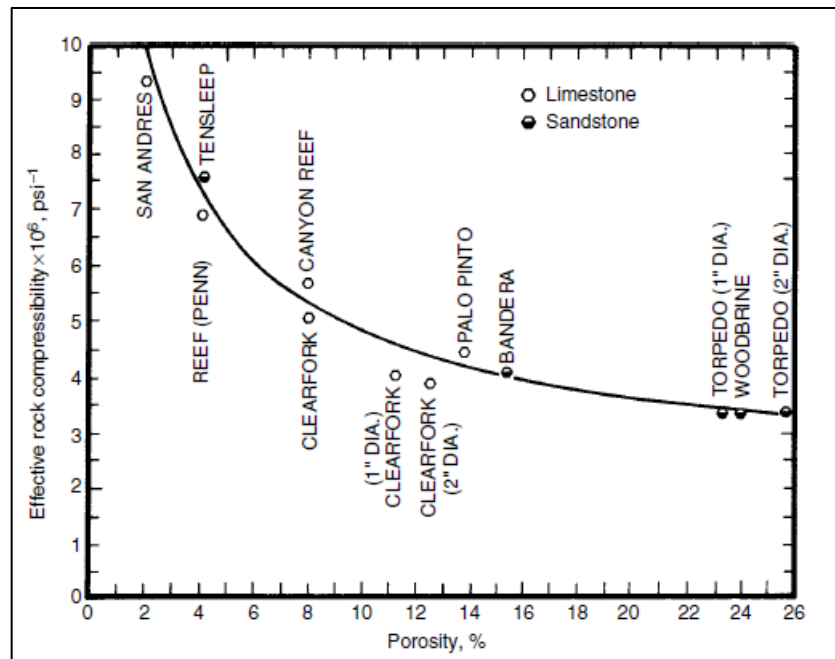
$V_p$  – Porous volume;

$P$  – Pressure;

$T$  – Temperature.

The effective rock compressibility is considered a positive amount that is added to the fluid compressibility; therefore, porous volume decreases with decreasing fluid pressure, a common correlation between rock compressibility and porosity is presented in Figure 10.

Figure 10 – Effective rock compressibility vs. porosity.



Source: Lyons, 2010.

Inoue and Fontoura (2009) defined a coupling between flow and stress problem. The coupling is achieved through an approximation between of the flow equation of the conventional reservoir simulation and the flow equation of the fully coupled scheme. This way, the effect of solids compressibility is removed from the fully coupled scheme and the effect of volumetric strain of the porous medium is added to conventional reservoir simulation. The parameters responsible for the coupling is presented in Equation 2.9:

$$Cr = \frac{\varepsilon v^{n+1} - \varepsilon v^n}{\phi_0(P^{n+1} - P^n)} \quad (2.9)$$

Where:

$Cr$  – Rock compressibility;

$\varepsilon v$  – Volumetric strain;

$\phi_0$  – Initial porosity;

$P$  – Pressure.



## 2.9. Permeability

Ahmed (2006) describes the property of the porous medium that measures the ability and capacity of the formation to transmit fluids. Permeability controls the directional motion and flow rate of reservoir fluids in the formation.

Lyons (2010) define permeability is measured by the ease with which fluids pass through the rock. It is denoted by the symbol  $K$  and commonly expressed in Darcy units, but for convenience, a practical unit for permeability is the miliDarcy (mD) which is worth 0.001 Darcy. If a porous system is completely saturated with a single fluid, permeability is a property of the rock and not a property of the fluid, with exception of low-pressure gases. This 100% saturation permeability of a single fluid is denominated absolute permeability.

Ahmed (2006), indicates that several laboratory studies have concluded that the effective permeability of any reservoir fluid is a function of the saturation of the reservoir fluid and the wetting characteristic of the formation. It is therefore necessary to specify fluid saturation when declaring the effective permeability of any fluid in a given porous medium.

Since  $K$  is universally accepted as a symbol for absolute permeability,  $K_o$ ,  $K_g$ , and  $K_w$  are accepted as symbols for effective permeability of oil, gas, and water, respectively. The saturation  $S_o$ ,  $S_g$ , and  $S_w$  must be specified to completely define the conditions under which effective permeability exists. Therefore, absolute permeability is a property of the porous medium and is a measure of the medium's ability to transmit fluids. When two or more fluids flow at the same time, the relative permeability of each phase at a specific saturation is the ratio of effective phase permeability to absolute permeability, as shown in Equations 2.10, 2.11, and 2.12:

$$K_{ro} = \frac{K_o}{K} \quad (2.10)$$

$$K_{rg} = \frac{K_g}{K} \quad (2.11)$$

$$K_{rw} = \frac{K_w}{K} \quad (2.12)$$

Where:

$K_r$  – Relative permeability;

$K$  – Absolute permeability;

$K_{o,g,w}$  – Effective permeability to the fluid at a given fluid saturation.

Fanchi (2006) defines that changes in wettability conditions can significantly affect relative permeability. Ideally, relative permeability should be measured in the laboratory under the same wettability conditions as in the reservoir. In practice, relative permeability data are obtained using cores restored in the laboratory.

According to Tortike and Farouq Ali (1993), assuming that the solid grains are incompressible, and neglecting the change in surface area of a grain underground thermal expansion area because it is of lesser order than that of the associated volumetric change, the following expression for the permeability is found (2.13):

$$K^{n+1} = K_0 \frac{\left(1 + \frac{\varepsilon v^{n+1}}{\phi_0}\right)^3}{1 + \varepsilon v^{n+1}} \quad (2.13)$$

Where:

$K$  – Permeability;

$K_0$  – Initial permeability;

$\varepsilon v$  – Volumetric strain;

$\phi_0$  – Initial porosity.

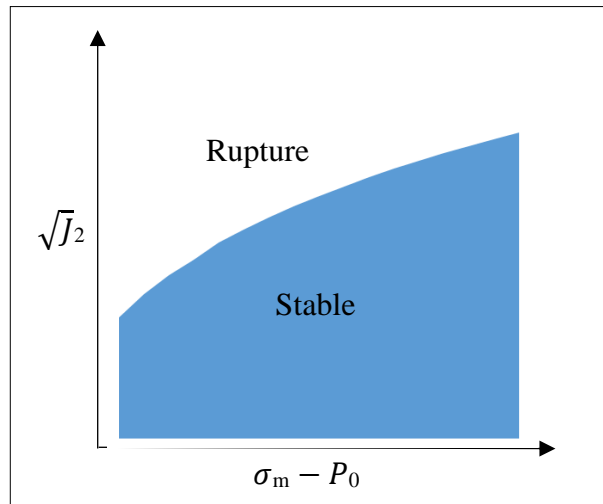
## 2.10. Constitutive models of failure criteria

According to Aadnøy (2014), the failure criteria is based on the ductility or fragility of the material under analysis. Many empirical tests have been developed to predict the rupture of the rocky mass, in general, are used for creating rupture envelopes, separating safe and rupture regions. Therefore, failure rock criteria analysis is presented:

- Von-Mises criteria:

According to Aadnøy (2014), one of the most reliable, it is based on the second invariant deviant and the average effective stress. This second deviating invariant is plotted against the mean effective stress for various axial loads and confinement pressures. The resulting curve, known as the rupture curve, defines two regions, one below the curve, safe and stable, and the other, above the curve, unstable and rupture, as shown in Figure 11.

Figure 11 – Rupture curve.



Source: Author, 2020.

- Mohr-Coulomb criteria:

It relates the shear strength to the contact and friction forces and the physical bonds between the rock grains, Jaeger & Cook (1979). Linear approximation of these criteria is given by equation 2.14:

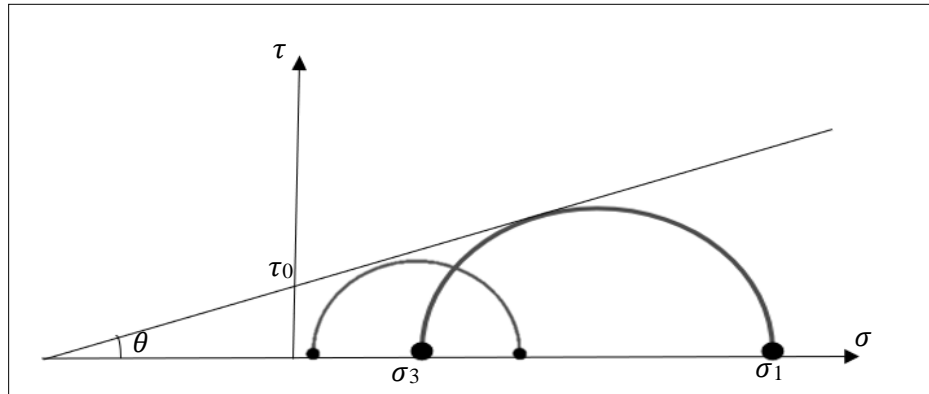
$$\tau = \tau_0 + \sigma tg\theta \quad (2.14)$$

Where:

- $\tau$  – Shear stress;
- $\tau_0$  – Cohesive strength;
- $\theta$  – Friction angle;
- $\sigma$  – Effective normal stress.

The cohesive force is the rock shear strength when no normal stress is applied, in drilling, the internal friction angle is equivalent to the inclination angle of a surface separating a block in two parts, sufficient to produce the displacement of the upper part over the lower, these are linearity coefficients and should be determined experimentally. The failure envelope is determined from several Mohr's circles, as shown in Figure 12, where each circle represents a triaxial test, AadnØy (2014).

Figure 12 – Failure envelope.



Source: Author, 2020.

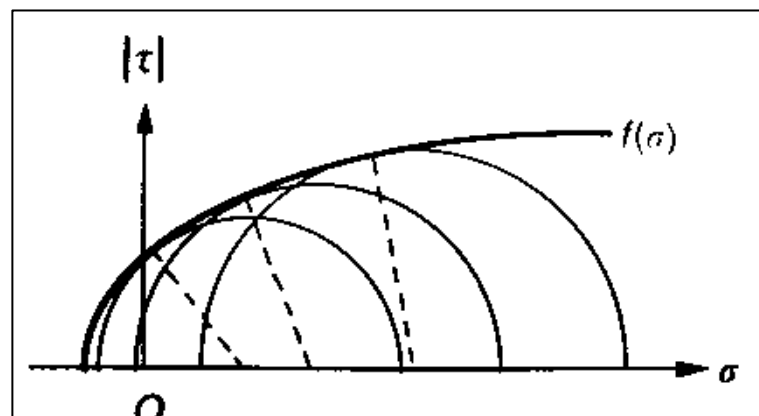
According to Jaeger & Cook (2007), in Coulomb's theory, failure will occur on a plane when normal and shear stresses act on that plane satisfying condition 2.15. And Mohr's circle corresponding to any stress state leading to the failure will be the tangent to that line, as shown in Figure 13.

$$|\tau| = s_0 + \mu\sigma \quad (2.15)$$

Where:

- $\tau$  – Shear stress;
- $s_0$  – Finite shear stress;
- $\mu$  – Internal friction coefficient;
- $\sigma$  – Effective normal stress.

Figure 13 – Mohr's circle.



Source: Jaeger & Cook, 2007.

- Hoek-Brown Criteria:

According to AadnØy (2014), this criterion is purely empirical and generally used in naturally fractured reservoirs, it is based on triaxial test data and it is expressed by the following equation 2.16:

$$\sigma_1 = \sigma_3 + \sqrt{I_f \sigma_c \sigma_3 + I_i \sigma_c^2} \quad (2.16)$$

Where:

$\sigma_1$  – Higher main stress;

$\sigma_3$  – Lower main stress;

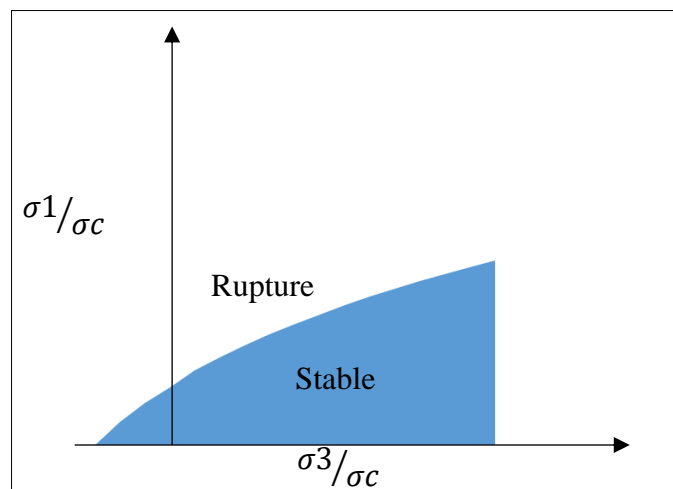
$I_f$  – Friction rate;

$\sigma_c$  – Confinement stress;

$I_i$  – Intact rock rate.

As shown in Figure 14, it provides poor results in ductile rupture, but it is used to predict rupture in naturally fractured formations.

Figure 14 - Hoek-Brown rupture.



Source: Author, 2020.

According to Hudson & Harrison (1997), this empirical criterion is based on a better fit curve for experimental failure data plotted in space  $\sigma_1 - \sigma_3$  as shown in Figure 15. The hoek-brown criteria have been reformulated to consider the experience gained over the 10 years since its development. The criteria are expressed as shown in equation 2.17:

$$\sigma_1 = \sigma_3 + (m\sigma_c\sigma_3 + s\sigma_c^2)^{0,5} \quad (2.17)$$

Where:

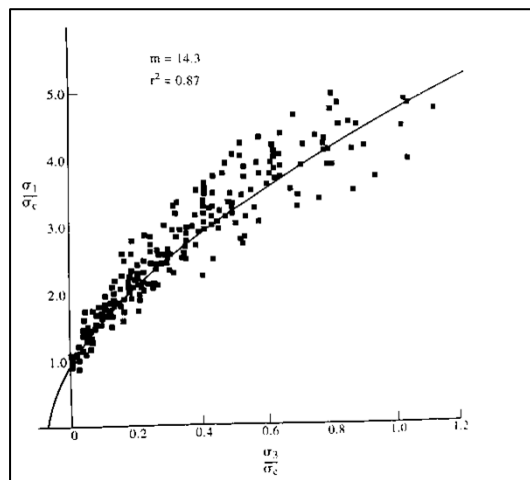
$\sigma_1$  – Higher main stress;

$\sigma_3$  – Lower main stress;

$\sigma_c$  – Confinement stress;

$m$  e  $s$  – Rock type specific constants.

Figure 15 - Hoek-Brown criteria.

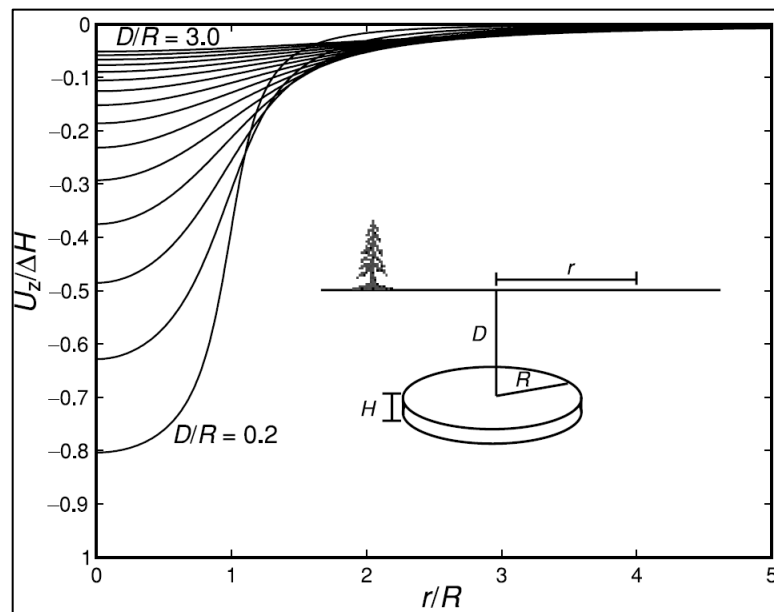


Source: Hudson & Harrison, 1997.

## 2.11. Subsidence

According to Zoback (2007), based on pore elastic theory, subsidence due to a uniform reduction in pore pressure,  $\Delta P_p$ , can be treated as the perpendicular displacement to the free surface as a result of the deformation core to a small but finite volume. Figure 16 illustrates the amount of surface displacement as a function of the normalized distance from the center of the reservoir. It is observed that for very shallow reservoirs ( $D/R \sim 0.2$ ), the amount of subsidence directly above the reservoir is  $\sim 0.8$  of compaction.

Figure 16 – Subsidence as a function of standardized distance.



Source: Zoback, 2007.

According to Fanchi (2006), compaction is a compressibility effect that depends on the geomechanics of the interval produced and its overload. The compaction, or change in thickness  $\Delta h$  of the reservoir can be estimated from the compressibility and pressure depletion of the system using equation 2.18:

$$\Delta h = C_B h \Delta P = \phi C_f h \Delta P \quad (2.18)$$

Where:

$C_B$  – Bulk compressibility;

$C_f$  – Formation compressibility;

$h$  – Reservoir net thickness;

$\phi$  – Porosity;

$\Delta P$  – Pressure depletion.

In many cases, subsidence has little or no adverse environmental effect. In some cases, however, subsidence can be a significant concern.

Chitsazan *et al.* (2020) describe subsidence as the distortion and abrupt sinking of discrete portions of the floor surface. The displacement is essentially downward, and the horizontal deformation tends to have harmful consequences. Soil subsidence is a downward movement of the soil surface caused by changes in stress. This phenomenon can occur naturally or by human activity, causing a natural imbalance, so it is crucial to investigate this phenomenon. The consequences are irreversible, and control is difficult, several factors influence this phenomenon, the most important being the excessive use of alluvial aquifers.

In general, subsidence is defined as the compressibility effect, which depends on the geomechanics between the produced interval and its overburden. In many cases, subsidence has little or no adverse environmental effects; however, in some cases, subsidence can be a significant concern, Fanchi (2006). The terms subsidence and compaction have different concepts. Subsidence is related to a descending movement of the surface, while compaction refers to the top reservoir thickness contraction.

## 2.12. Reservoir classification

According to Ahmed (1946), reservoirs requires knowledge of the thermodynamic behavior of the phases present in the reservoir and the forces responsible for the production mechanism. In general, reservoirs are commonly classified based on the location of the

representative point of the initial pressure of the reservoir and the temperature concerning the p-T diagram of the reservoir fluid. Reservoirs can, therefore, be classified essentially into two types:

- Oil reservoirs: when the reservoir temperature is lower than the critical reservoir fluid temperature;
- Gas reservoirs: when the reservoir temperature is higher than the critical temperature of the hydrocarbon fluid.

Depending on the initial pressure, oil reservoirs may be subclassified in the following categories:

- Unsaturated oil reservoirs: when the initial reservoir pressure is higher than the bubble pressure of the reservoir fluid;
- Oil saturated reservoirs: when the initial reservoir pressure equals the bubble pressure of the reservoir fluid;
- gas cap reservoirs: when the reservoir pressure is below the bubble pressure of the reservoir fluid.

Lyons (2010) defines that oil and gas accumulations occur underground by structural or stratigraphic characteristics. A reservoir is a portion containing oil and/or gas in a hydraulically connected system. Oil and gas can be recovered by fluid expansion, fluid displacement, gravity drainage, or capillary expulsion. As an initial condition, hydrocarbon fluids in reservoirs may exist as single-phase or two phases. The single-phase can be a gas phase or a liquid phase in which all the gas present is dissolved in oil. When there are hydrocarbons vaporized in the gas phase or which are recovered as liquids at the surface, the reservoir is called a condensed gas, and the liquid produced is referred to as condensate or distillate. For two-phase accumulations, the vapor phase is determined from the gas cap and the subsequent liquid phase is called the oil zone. In the case of two phases, hydrocarbon recovery includes gas free from the gas cap, gas involving oil, liquid recovered from the gas cap, and crude oil from the oil zone.

### 2.13. Reservoir wells

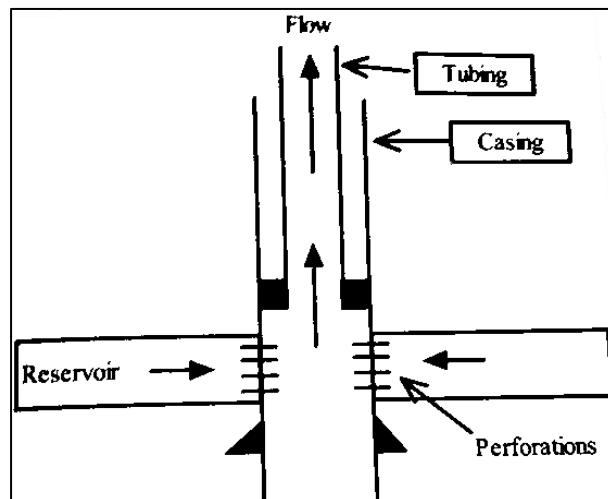
According to Aadnøy (2014), opening a circular hole and applying drilling and completion fluids in a previously stable formation is considered the reason for phenomena that generally result in well hole instability and casing collapse. Therefore, there is a need to develop



mathematical models to simulate the physical problems that result from drilling and production processes. The main causes of instability are high pore pressure in the formation, disturbance induced by drilling of a stable formation, and the possible chemical reactions between the reservoir formation and drilling and fluid completion.

For Fanchi (2006), fluid flow in pipes can vary from laminar to turbulent flow. The fluid does not move transversally in the direction of mass flow in laminar fluid flow. On the other hand, the velocity components of fluid flow fluctuate in all directions concerning the direction of mass flow when the fluid flow is turbulent. In Figure 17, the well coupling system is presented.

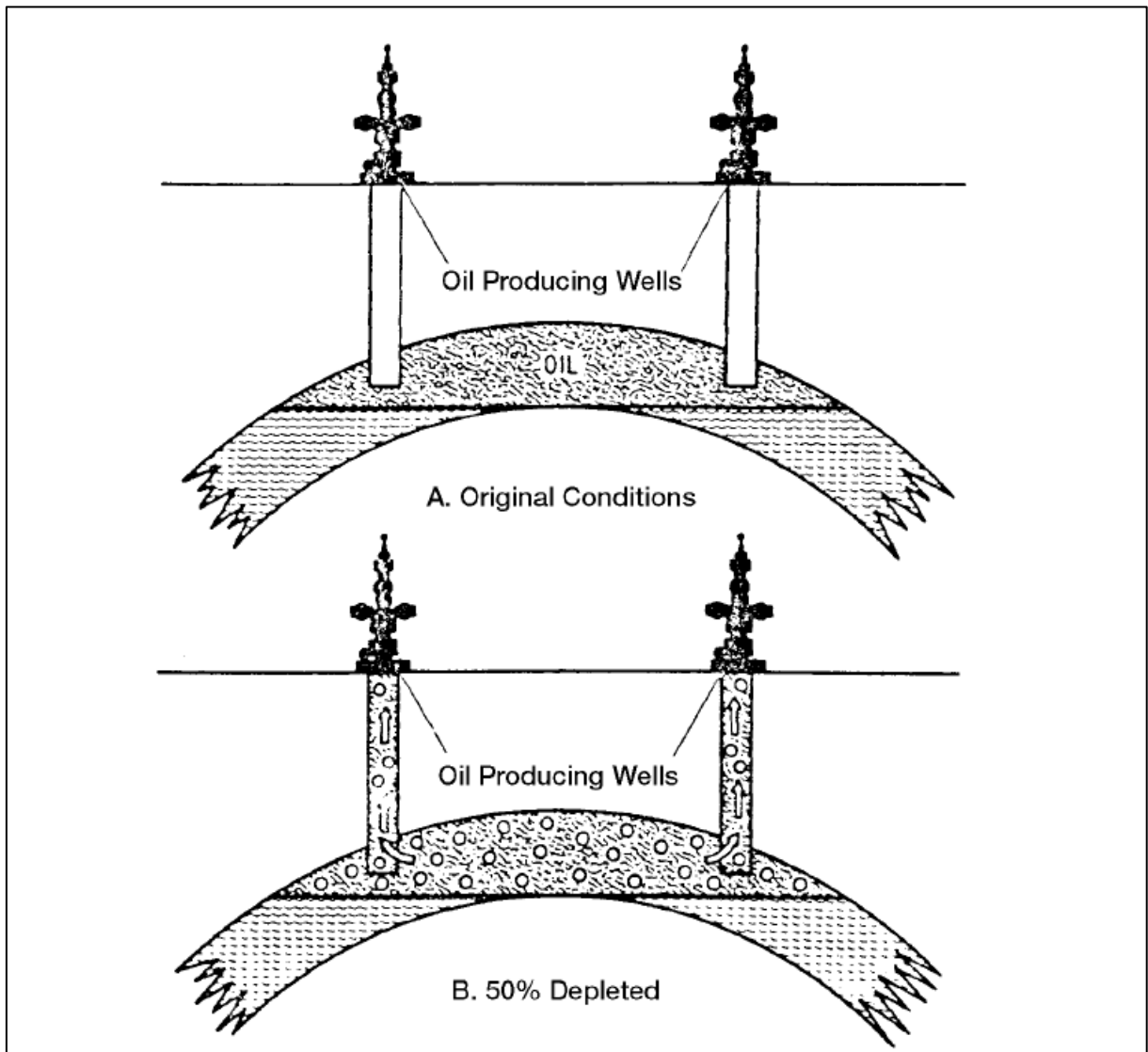
Figure 17 – Well coupling.



Source: Fanchi, 2006.

Ahmed (2006) describes that the oil recovery by any natural mechanism is named primary recovery. The term refers to the production of hydrocarbons from a reservoir without using any process, such as fluid injection, to supplement the reservoir's natural energy. In the depletion mechanism, the main energy source is the result of gas release as reservoir pressure is reduced. As the pressure drops below the bubble point pressure, gas bubbles are released into microscopic porous spaces. These bubbles expand and force crude oil out of the pore space as shown in Figure 18, reservoir pressure declines rapidly and continuously, and depletion is characterized by the rapid increase in the gas-oil ratio of all wells regardless of structural position. After the reservoir pressure has been reduced below the bubble pressure, the gas evolves from the solution throughout the reservoir. When the gas saturation exceeds the critical gas saturation, the free gas begins to flow towards the well hole and the gas-oil ratio increases.

Figure 18 – Reservoir with gas solution drive.



Source: Ahmed, 2006.

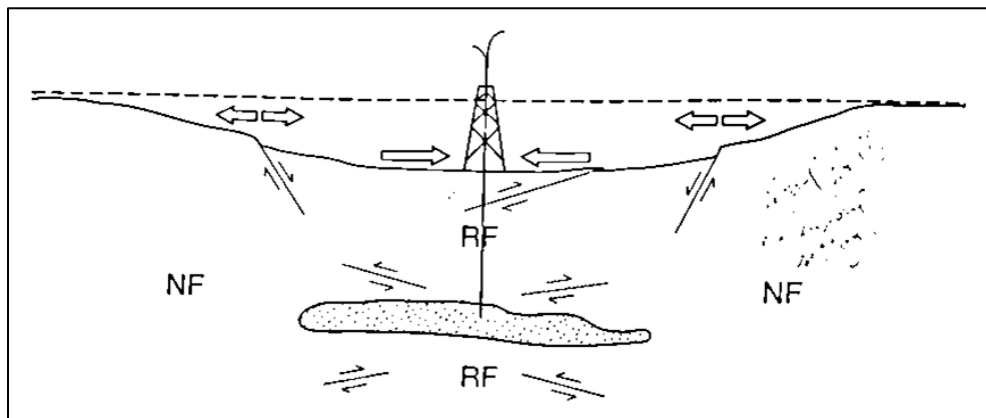
Oil production by the primary method of depletion is usually the least efficient method of recovery. Oil recovery by the primary method of depletion can vary from 5% to 30%. This low recovery of this type of reservoir suggests that large amounts of oil remain in the reservoir and therefore depletion reservoirs are considered the best candidates for secondary recovery application, Ahmed (2006).

Lyons (2010) describes the initial oil production usually occurs by expanding fluids that have been stuck under pressure in the rock. Expanding fluids can evolve from oil, a gas cap expansion, a bottom water drive, or a combination of these mechanisms. After the initial reservoir pressure drops to a low value, the oil no longer flows into the well hole, and pumps are installed to lift the crude oil to the surface. This mode of oil production refers to primary

recovery. Oil recovery associated with natural energy from the reservoir varies according to production mechanisms that are classified as a gas solution or depletion drive, gas cap drive, natural water drive, gravity drainage, and compaction drive. In some reservoirs, production can be attributed to one mechanism, in other cases, production can be the result of more than one mechanism.

According to Zoback (2007), depletion also has the potential to induce failure, both inside and outside the reservoirs in some geological environments. While these problems can be formidable in some reservoirs, depletion can also have a beneficial impact on reservoir performance. The reduction in the magnitude of the horizontal stress inside the reservoir, resulting from the decrease in the pore pressure associated with depletion, as shown in Figure 19, shows the changes in stress and strain that occur in the formations around a depleting reservoir, surface subsidence above compacted reservoirs is a well-known phenomenon.

Figure 19 – Reservoir changes during depletion.



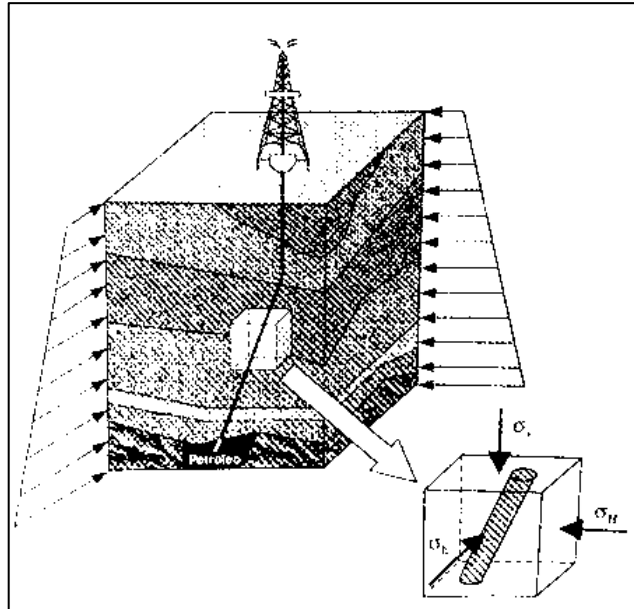
Source: Zoback, 2007.

Mohammadi *et al.* (2020), through the production life of a reservoir, recovery is summarized in three phases, primary, secondary, and tertiary. In primary recovery, the predominant mechanism is the natural energy driven from the reservoir. In this phase, no external fluid or heat is needed as energy, the main mechanism is the expansion of the rock and the fluid, gas solution, water inflow, gas cap, and gravitational drainage. Through secondary recovery, an external fluid such as water and/or gas is injected for pressure maintenance and volumetric scanning of the reservoir fluid. Tertiary recovery is described by the injection of special fluids such as chemicals, miscible gases, and thermal energy injection.

According to AadnØy (2014), the identification of the stress state is the first step in the process of conducting a stability analysis of the formation, as shown in Figure 20, which

displays a schematic diagram of the *in situ* stresses existing in the formation around an oil well hole.

Figure 20 - *In situ* stress around a well borehole.



Source: Aadnøy, 2014.

#### 2.14. Reservoir behavior

Zoback (2007) notes that reductions in reservoir pore pressure with production, depletion, can cause significant deformation in a reservoir, including loss of compaction and permeability, and occasionally induce failure in some reservoirs at normal failure regimes or around the region.

Applications in the petroleum industry require both an understanding of the porous flow of reservoir fluids and an understanding of reservoir stresses and displacements. Some processes, such as the high level of depletion in light rock or water injection in fractured reservoirs, involve stronger coupling between the porous flow and geomechanics (Dean *et al.* 2006).

Ahmed (2006) analyzes the material from which an oil reservoir rock can be composed, ranging from very loose and unconsolidated sand to very hard and dense sandstone, limestone, or dolomite. Knowledge of the physical properties of the rock and the interaction between the hydrocarbon system and formation is essential in understanding and assessing the performance of a given reservoir.

According to Rosa (2002), the knowledge of the average reservoir pressure is necessary to determine the PVT fluids and rock properties, while contact pressure is used in the calculation



resources to optimize fluid recovery by minimizing capital investments and operating expenses. Table 2 lists reasons for conducting a study with a flow model, as well as for reservoir flow modeling.

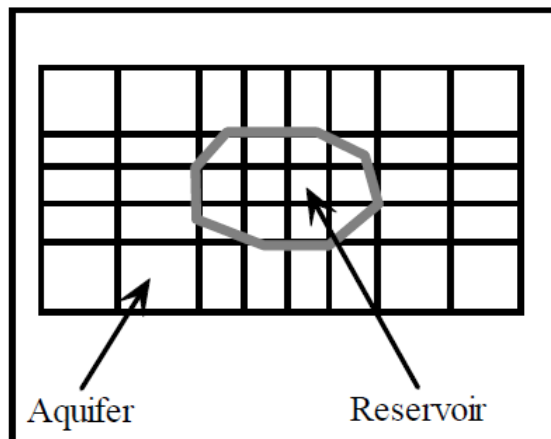
Table 2 – Reasons for simulation.

<p><b>Corporate Impact</b> Cash Flow Prediction Need Economic Forecast of Hydrocarbon • Price</p>
<p><b>Reservoir Management</b> Coordinate Reservoir Management Activities Evaluate Project Performance • Interpret/Understand Reservoir Behavior Model Sensitivity to Estimated Data Determine Need for Additional • Data Estimate Project Life Predict Recovery Versus Time Compare Different Recovery Processes Plan Development or Operational Changes Select and Optimize Project Design Maximize Economic Recovery</p>

Source: Fanchi, 2006 (Adapted).

A reservoir-aquifer system can be modeled using small mesh blocks to define the reservoir and increasingly larger mesh blocks to define the aquifer. This approach has the advantage of providing a numerically uniform analysis of the aquifer reservoir, and Figure 22 illustrates this block mesh design.

Figure 22 – Flow model mesh.



Source: Fanchi, 2006.

Ewing (1983) defines that the objective of reservoir simulation is to understand the chemical and physical complexity and fluid flow process that occurs in the oil reservoir. Enough to enable the optimization of hydrocarbon recovery. A numerical model is determined so that it has the necessary properties of precision and stability and which produces solutions representing the basic physical resources as best as possible, without introducing spurious phenomena associated with the specific numerical scheme.

Fluid movements in porous media are governed by the same fundamental laws that govern flow in conduits and rivers. These laws are based on the conservation of mass, momentum, and energy. Additional equations are usually Darcy's law and state equations.

Settari *et al.* (1999) describe the coupled modeling provide results that can be used to integral manage the reservoir, including reservoir engineering, drilling, and completions. the realism of reservoir modeling proposed by the coupled approach can lead to significant economic implications. This methodology can avoid equipment damage and oil spill due to pressure reservoir control.

The modeling geomechanical effects demand a rigorous integration of mechanical concepts in reservoir simulations, Longuemare *et al.* (2002). The partial coupling is named explicit when the methodology is only realized once for each time step and iterative if the methodology is repeated to the convergence of the stress and fluid flow unknowns.

Three coupling methods are presented by Dean et al. (2006) which are explicit coupling, which imposes timestep restrictions on runs because of concerns about stability and accuracy. The iterative coupling approach, multiphase porous flow and displacement are coupled through the nonlinear iterations for each timestep. During each iteration, a simulator performs computations sequentially for multiphase porous flow and for displacements. The final one is the fully coupled approach, porous-flow and displacement calculations are performed together, and the program's linear solver must handle both fluid-flow variables and displacement variables.

#### 2.16. New porosity and permeability calculation through iterative coupling

Connell (2009), developed a coupling study for coal joints under gas production, using the SIMED II and FLAC3D simulators, causing effects on permeability and porosity, due to changes in effective stress. Whereas Chalaturnyk (2010), proposed new porosity and

permeability models for reservoir coupling and geomechanics, discussing the relationship between permeability and pore pressure.

Tran *et al.* (2004), developed a new formula for porosity as a function of pressure, temperature, and mean total stress, which is used to improve the convergence speed of the iterative coupling used in CMG software. Only pore thermoelastic materials are considered in the study. Mikelic *et al.* (2014) discuss fixed stress iterative coupling for a compositional flow model and include the corresponding parallel computational result in the structured grid; The flow model used is the single-phase flow with finite element method.



### 3. METHODOLOGY

The methodology used in the numerical analysis for each case study is described, specifying the techniques used in each coupling and the approach used in the respective simulators.

#### 3.1. Problems description

The problems proposed in this paper refer to those described by Dean *et al.* (2006), four problems involving pore flow, geomechanical effects, and different boundary conditions. For all problems, the *Biot* parameter is equivalent to 1. All the described stresses are of compression and represent the total stress for the system. The constitutive model is elaborated on the elastic model.

These four problems were used in the development of the iterative coupling technique with the IMEX simulator (CMG 2019), with flow module and associated geomechanics. The explicit external iterative coupling technique is also developed for problem 1, with FLAC3D 6.0 (ITASACG) and IMEX (CMG 2019) simulators, with the support of FISH, PYTHON, and MATLAB programming languages.

##### 3.1.1. Problem 1

It is based on a single-phase reservoir, composed of water, which illustrates how depletion influences displacement behaviors and pore flow calculations. In this problem, displacement restriction conditions apply at the borders and the base of the reservoir, thus only allowing displacement along the top of the reservoir, characterizing a uniaxial deformation state.

The reservoir cells are distributed in 11 x 11 x 10 (x, y, z) with 200 ft (60.96 m) in the horizontal (x, y) and 20 ft (6.09 m) in the vertical z-direction, totaling 2,200 x 2,200 x 200 (ft), providing a bulk volume of  $9.68E^8$  ft<sup>3</sup>.

The top of the reservoir is at a depth of 6,000 ft (1828.8 m) and the porosity *in situ* is 20%. The permeability of the reservoir is 50 and 5 mD, in horizontal and vertical directions, respectively. The fluid that fills the reservoir is water, with a viscosity at 1 cP, volume formation factor of 1, fluid density of 62.4 lbm/ft<sup>3</sup>, and zero compressibility.

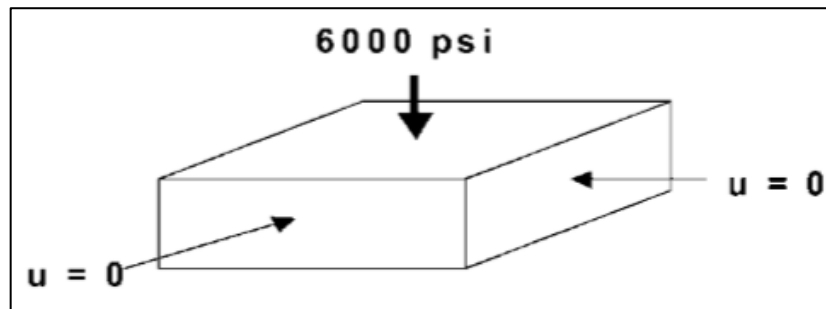
The reservoir *Young* modulus is  $10^4$  psi (68947.57 kPa) and the *Poisson* ratio is 0.3. Initial horizontal stress is 4,000 psi (27579.03 kPa), and vertical stress is 6,000 psi (41368.54

kPa), at a depth of 6,000 ft, with a vertical gradient of 1.0231 psi/ft along the reservoir, assuming uniaxial behavior and rock compressibility of  $3.74 \times 10^{-4} \text{ psi}^{-1}$ .

A vertical well with a radius of 0.25 ft (0.076 m) is completed in the center of the reservoir in all 10 layers, this well is a producer with a water rate of 15,000 b/d for 500 days, with time step simulation of 10 days.

No flow limit conditions are assumed for the fluid on all sides of the reservoir. Figure 23 shows the indication of displacement restriction on the sides of the reservoir.

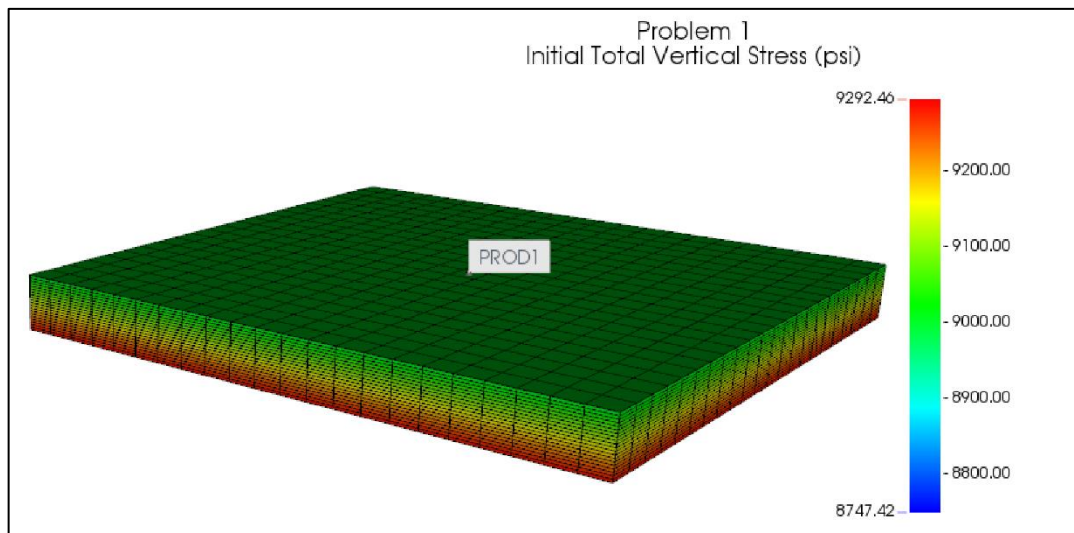
Figure 23 – Reservoir perspective of problem 1.



Source: Dean *et al.*, 2006.

The 3D representation generated in the IMEX 2019 simulator is shown in Figure 24, which also shows the variation of the initial vertical total stress along the reservoir and due to the vertical gradient applied.

Figure 24 – 3D display of problem 1 and initial vertical total stress.

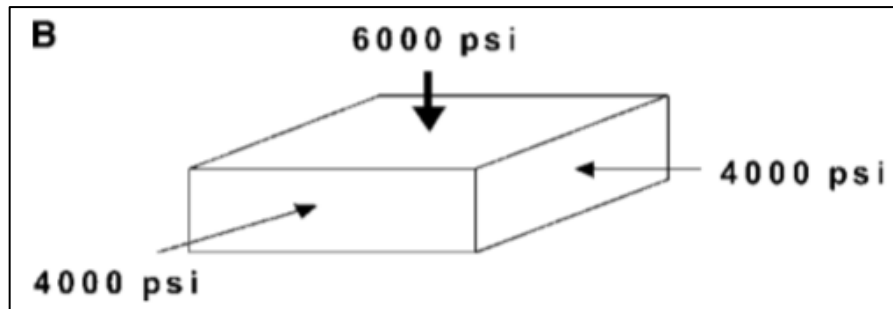


Source: Author, 2020.

### 3.1.2. Problem 2

Problem 2 has the same characteristics as problem 1, but with the difference of not restricting the displacement on the sides and there is the 4,000 psi application of horizontal stress on the reservoir sides. As well as the model compressibility presents the value of  $6.00 \times 10^{-4} \text{ psi}^{-1}$ . Figure 25 shows the application of horizontal stress on the sides of the reservoir.

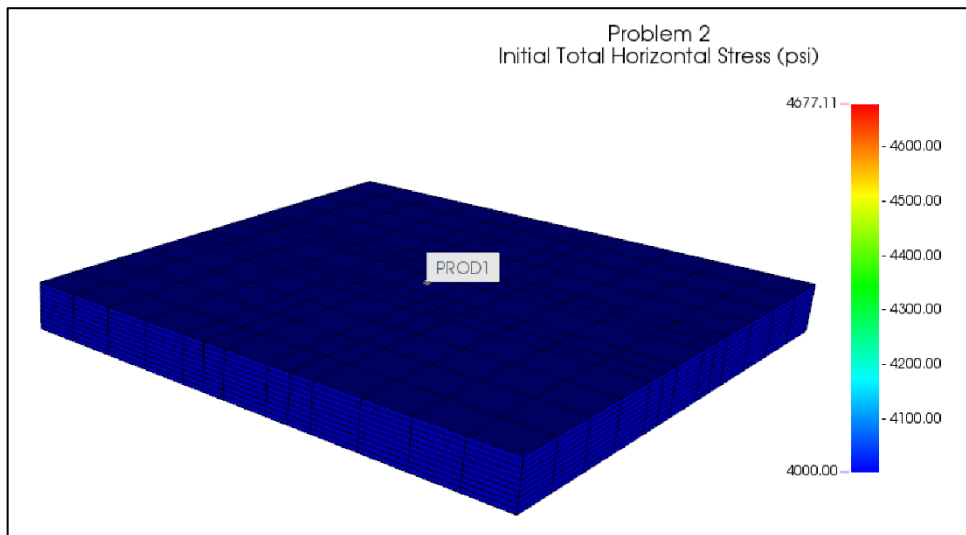
Figure 25 – Reservoir perspective of problem 2.



Source: Dean *et al.*, 2006.

The 3D representation generated in the IMEX 2019 simulator is shown in Figure 26, which also shows the initial horizontal total stresses applied to the reservoir.

Figure 26 - 3D display of problem 2 and initial horizontal total stress.



Source: Author, 2020.

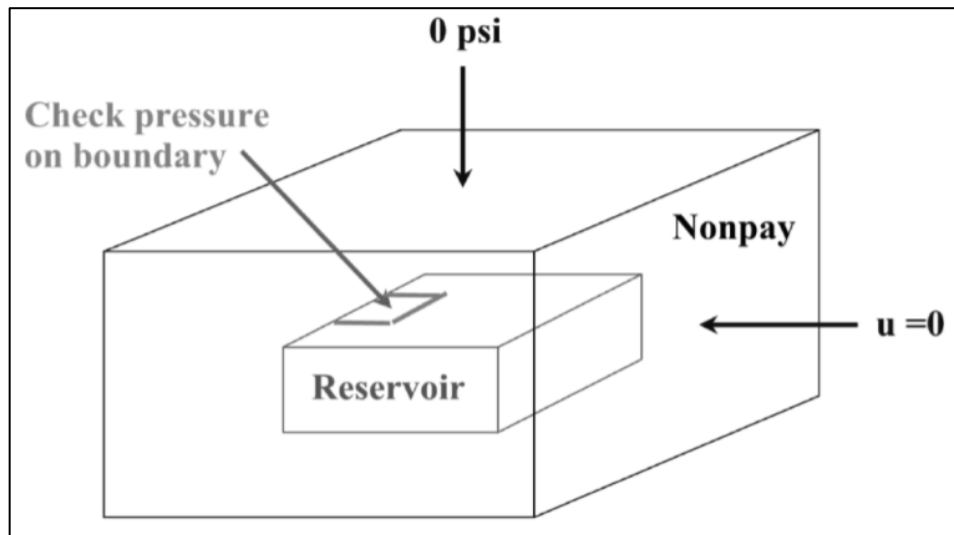
### 3.1.3. Problem 3

It consists of the depletion of a small single-phase reservoir contained in a rigid impermeable region. This problem presents geomechanical effects on the border of the reservoir, which cannot be observed in simulators that do not contain geomechanical calculations. For this problem, geomechanical effects cause an increase in fluid pressure in the early depletion stage.

The model cells are distributed in  $21 \times 21 \times 12$  (x,y,z) of which includes both the reservoir and the rigid region. The length in the X direction is distributed as follows, 4,000 ft (1219.2 m) for each of the first 5 cells, 2,000 ft (609.6 m) for each of the next 11 cells, and 4,000 ft for each of the last 5 cells. In the Y direction, the distribution follows the same orientation as the X direction, but with the value in the half for each cell.

The top of the model is at a depth of 0 ft, and the thickness of the vertical direction is distributed as follows, 4,000, 3,000, 2,000, 800, 200 (ft) for the first five cells, which represent the overload. The next five cells are 50 ft thick each and represent the reservoir. The last two cells are 100 ft thick each and represent the overload. Therefore, in Figure 27, it is shown the small reservoir contained in the rigid impermeable region.

Figure 27 – Reservoir perspective of problem 3.



Source: Dean *et al.*, 2006.

The horizontal and vertical permeabilities of the reservoir are 100 mD and 10 mD (MiliDarcy) respectively, while for the rigid region the permeability is zero and the porosity *in situ* is 25% for both the reservoir and the rigid region.

The reservoir is single-phase, consisting of water, with a volume formation factor of 1 at a pressure of 14.7 psi, viscosity of 1 cP, the fluid density of 62.4 lbm/ft<sup>3</sup> at 14.7 psi, and fluid

compressibility of  $3 \times 10^{-6} \text{ psi}^{-1}$ . Fluid compressibility other than zero is used in this problem because the effect of the zero value provides that the porous solid is incompressible in the rigid region.

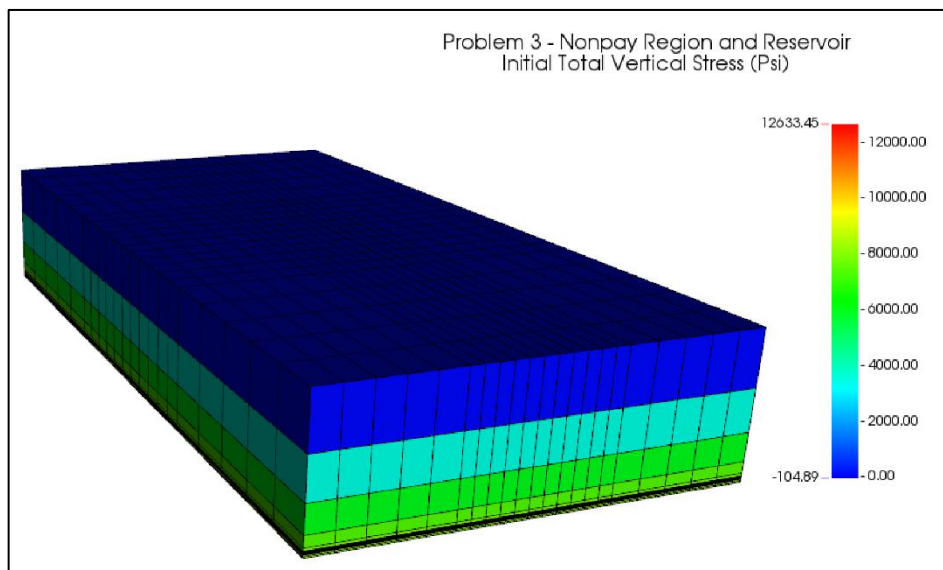
The initial fluid stress is 14.7 psi (101.35 kPa) on the surface with a hydrostatic gradient of 0.437 psi/ft. *Young's* module is  $1 \times 10^4$  psi for the reservoir and  $1 \times 10^6$  psi for the rigid region, and *Poisson's* ratio is 0.25 on the entire model. The initial solid density *in situ* (pore-free solid material) is  $2.7 \text{ g/cm}^3$ .

The initial vertical stress is 0 psi to the surface, with a gradient of 0.9869 psi/ft along with the mesh and the initial horizontal stress is equal to half the vertical stress. The base and sides of the mesh have zero normal displacement restriction and all mesh faces have zero tangential stress. Assuming uniaxial deformation behavior for this problem, the rock compressibility is  $3.33 \times 10^{-4} \text{ psi}^{-1}$  and  $3.33 \times 10^{-6} \text{ psi}^{-1}$  for the reservoir and rigid region, respectively.

A vertical well with a radius of 0.25 ft is completed in the center of the reservoir in all five layers. The well is producing, at a water rate of 50,000 stb/d to 4,000 days, with a time step of 20 days for the first 400 days, followed by a time step of 200 days, ending in 4,000 days. Small-time steps are applied at the beginning of the simulation to produce a precise solution for the pressure increase at the reservoir edge.

The 3D representation generated by the IMEX 2019 simulator is shown in Figure 28, which displays the variation of the initial vertical total stress along with the model due to the vertical gradient applied.

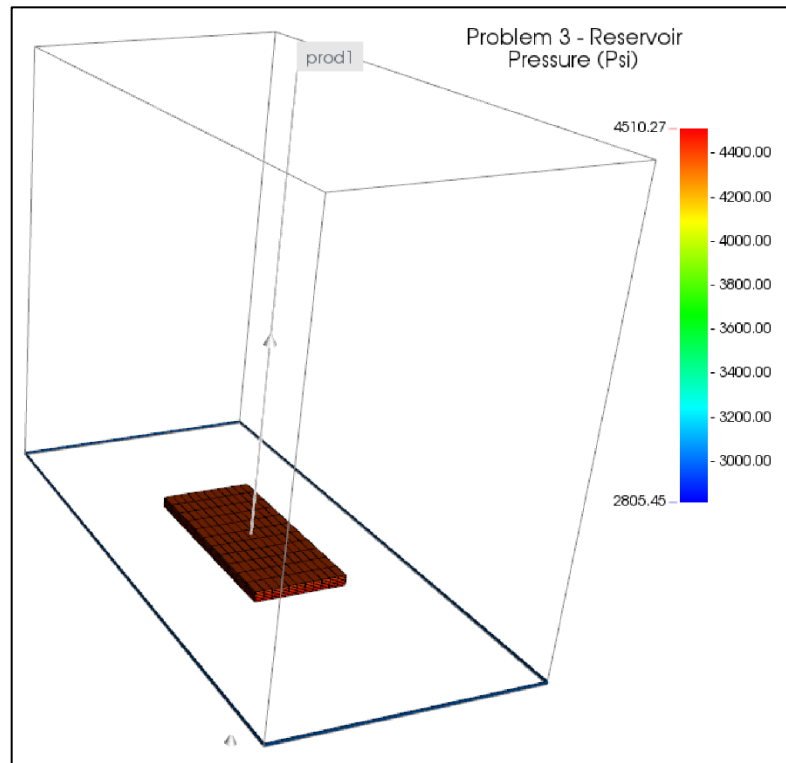
Figure 28 – 3D problem 3 display and vertical total stress.



Source: Author, 2020.

In Figure 29, the small reservoir contained in the rigid impermeable region, elaborated in the IMEX 2019 simulator, is shown, and the respective initial pressure value of the reservoir is displayed.

Figure 29 – Reservoir pressure.



Source: Author, 2020.

#### 3.1.4. Problem 4

This problem is developed for a three-phase, black oil type reservoir with a five-spot pattern, containing a producer well at one corner of the reservoir and an injection well opposed to the producer. The production ratio is higher than the injection ratio, so the reservoir pressure decreases during the simulation.

The model cells are made up of 21 x 21 x 11 (x, y, z), with a length in the horizontal direction of 60 ft (18.28 m) (x and y) and thickness of 20 ft in the vertical direction (z), totaling 1260 x 1260 x 220 (ft), providing a volume of 3.49E8 ft<sup>3</sup>. The top of the reservoir is at a depth of 4,000 ft and the initial in situ porosity is 30%.

The permeability of the reservoir varies along with the layers, with horizontal permeability starting from the first and along with the next layers with values equal to 5, 100, 20, 20, 100, 20, 100, 20, and 20 mD, respectively. The vertical permeability is equivalent to 0.01 times the horizontal permeability. The volume formation factor is equal to 1 at 14.7 psi

pressure, a viscosity of 1 cP, and a fluid density of 62.4 lbm/ft<sup>3</sup> at 14.7 psi pressure. Compressibilidade do fluid de  $3 \times 10^{-6}$  psi<sup>-1</sup>, as densities of oil and gas in the surface of 56,0 lbm/ft<sup>3</sup> and 57,0 lbm/Mcf, respectively.

The initial reservoir pressure is in hydrostatic equilibrium with fluid pressure from 3.010 psi to 4.010 ft, and initial fluid saturations are constant and have values equal to 20, 80, and 0% for water, oil, and gas, respectively. The oil is initially below saturation, with a bubble pressure of 3,000 psi and the compressibility of this oil is  $10^{-5}$  psi<sup>-1</sup> in all layers.

The *Young's* module is equal to  $5 \times 10^4$  psi, the *Poisson* ratio is 0.35 and the initial solid density *in situ* is 2.7 g/cm<sup>3</sup>. The initial vertical stress is 4,000 psi at the top of the reservoir, with a vertical stress gradient of 0.9256 psi/ft along the reservoir, and the initial horizontal stress is equal to half the vertical stress.

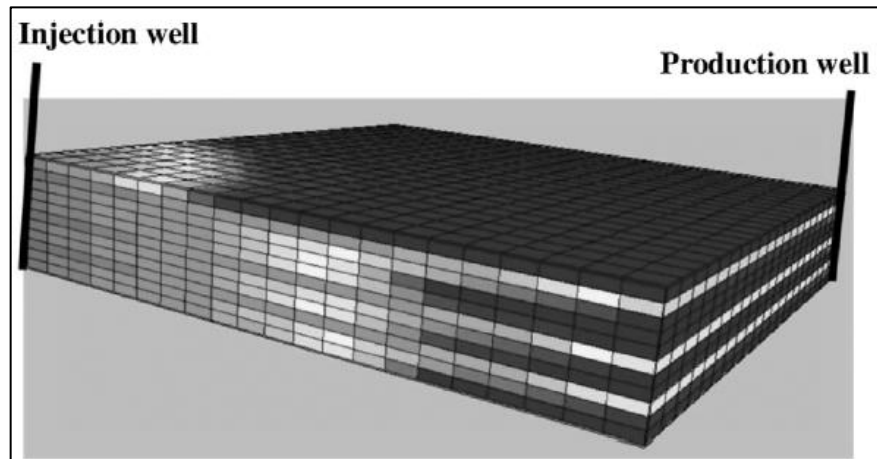
The base and mesh sides of the reservoir have normal displacement restriction equal to zero and all mesh faces have zero tangential stress, assuming uniaxial deformation behavior for this problem, the rock compressibility value is equal to  $4.15 \times 10^{-5}$  psi<sup>-1</sup>.

The vertical wells are completed and opposed to each other in all 11 layers. The water injection well is at a ratio of 500 stb/d (with 1/4 of the total well ratio), and the producing well is at a liquid ratio of 750 stb/d (with 1/4 of the total well ratio) with a bubble pressure limit at 500 psi.

The well radius is 0.069 ft instead of 0.25 ft so that it is possible to represent wells with a radius of 0.25 ft that are at the vertices of the mesh block. The multiplication factor of 0.25 is used for the well constant because only 1/4 of the well is being simulated.

The simulation is designed for 25 years, using time frames that are controlled by stability considerations. Figure 30 shows the 3D visualization of the reservoir, indicating the location of the producing well and the injection well, and shows the water saturation behavior at the end of the simulation.

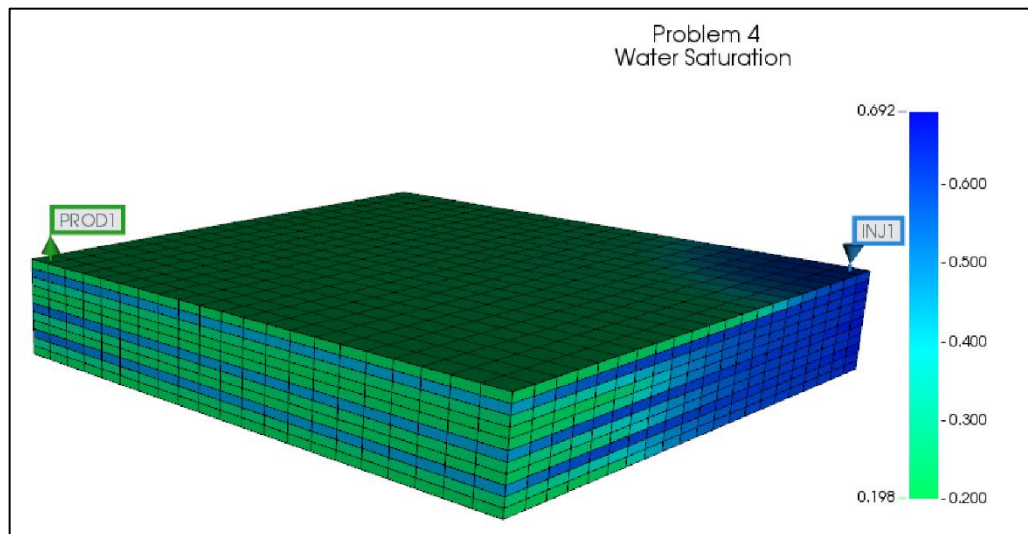
Figure 30 – 3D problem 4 representation and water saturation.



Source: Dean *et al.*, 2006.

Figure 31, shows the 3D display of the reservoir at the end of the simulation in the IMEX 2019 simulator, showing the same parameters and behaviors as the previous figure.

Figure 31 – Problem 4 3D view and water saturation.



Source: Author, 2020.

## 3.2. IMEX 2019 explicit iterative coupling

### 3.2.1. Problem 1

Initially, the model is assembled with input data and output data request in the results in the English unit system (Field), as well as the creation of a sector in the surface cell of the well for accurate visualization of specific parameters.

The model is created by defining the mesh, in the Cartesian model, the respective data is provided by Dean *et al.* (2006), with data on layer thickness and length, the number of



horizontal and vertical layers, top of the reservoir orientation, porosity value, permeability values, compressibility and reference pressure for the rock compressibility, as well as the creation of a sector for specific reservoir observation. The mesh developed for problem 1 is elaborated with 2 x 2 x 2 mesh refining to obtain accurate values.

Afterward, we have the definition of the fluid, with the respective PVT table provided by Dean *et al.* (2006) and adapted to the properties and units of the system used in the simulator, and inclusion of the fluid properties, such as density, compressibility, viscosity and formation volume factor, as the model of problem 1 is single-phase, complete with water, the gas-water fluid model is elaborated, but with the gas contact above the top of the reservoir, this way the reservoir region will present only the water fluid.

Next, the fluid-rock properties are included, with saturation parameters and relative water and gas permeabilities. 5,500 ft water/gas contact, so that the reservoir is complete with water, making it single phase. The numerical control applied to the simulation model is a maximum time step size of 10 days.

The initial depth and pressure reference conditions of 6,000 ft and 3,000 psi respectively apply.

Then the geomechanics module of the model is applied, with the respective data provided by Dean *et al.* (2006) and simulation and coupling parameters to the simulator.

As the *gcoupling* keyword of value 2, which the simulator will interpret the porosity of the fluid flow as a function of pressure, temperature, and mean total stress, defined according to the following equation 3.1, by Tran *et al.*:

$$\phi^{n+1} = \phi + (c_0 + c_2 a_1)(P - P^n) + (c_1 + c_2 a_2)(T - T^n) \quad (3.1)$$

$$c_0 = \frac{1}{V_b^0} \left( \frac{dV_p}{dP} + V_b \alpha c_b \frac{d\sigma_m}{dP} - V_p \beta \frac{dT}{d\rho} \right)$$

$$c_1 = \frac{V_p}{V_b^0} \beta$$

$$c_2 = -\frac{V_b}{V_b^0} \alpha c_b$$

$$a_1 = factor \left\{ \frac{2}{9} \frac{E}{(1-\nu)} \alpha c_b \right\}$$

$$a_2 = factor \left\{ \frac{2}{9} \frac{E}{(1-\nu)} \beta \right\}$$

Where:

$c_b$  – Porous rock compressibility;

$E$  – *Young* modulus;

$V_b$  – Bulk volume;

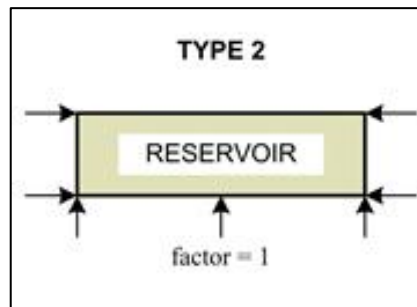
$\alpha$  – *Biot* coefficient;

$\nu$  – *Poisson* ratio;

$\sigma_m$  – Mean total stress.

The *gcfactor* function present value equal to 1 is used, which the simulator uses as a geomechanical coupling factor, providing the boundary condition with restricted behavior, as shown in Figure 32.

Figure 32 – Geomechanical coupling factor 1 and boundary conditions.



Source: CMG IMEX user's guide, 2020.

Among other parameters are included in the modeling, such as effective stress, rock properties, *Poisson* ratio, *Young* modulus, and rock cohesion.

As well as the *calib\_por* command, which calibrates the porosity, providing adjustment in the accuracy of the porosity coupling, and the *gptolmul* command, which adjusts the pressure tolerance to calculate the porosity formulas.

After completion of the geomechanics card, the well model is created at the end, consisting of a producing well located in the center of the reservoir and completed in all layers of the model, with respective dimensions and operation data provided by Dean *et al.* (2006), with total simulation for 500 days, performing specific time scheduling for better visualization of how the simulation and analysis of the model behavior occurs.

Therefore, all the formatting of problem 1, as well as the input cards, analysis, and the simulator keywords, can be found in Appendix A.

### 3.2.2. Problem 2

This problem is similar to problem 1, but with some changes, such as the behavior of the model outline conditions. Initially, the model is assembled with input data and output data request in the results, as well as the creation of a sector in the surface cell of the well for accurate visualization of specific parameters.

The model is created by defining the mesh, in the case of the Cartesian model, with the respective data provided by Dean *et al.* (2006), with data on layer thickness and length, the number of horizontal and vertical layers, top of the reservoir orientation, porosity value, permeability values, compressibility and reference pressure for the compressibility of the rock, as well as the creation of a sector for specific observation of the reservoir. In this model, manual refining is performed in the central cells of the reservoir to obtain accurate results from these zones.

One difference that can be noted at this stage is the compressibility value, since for problem 1 this value is  $3.71\text{E-}6 \text{ psi}^{-1}$ , and for problem 2 this value is  $6.0\text{E-}4 \text{ psi}^{-1}$ .

Afterward, we have the definition of the fluid, with the respective PVT table provided by Dean *et al.* (2006) and adapted to the respective properties and units of the system used in the simulator, and inclusion of the fluid properties, such as density, compressibility, viscosity and formation volume factor. The gas-water fluid model is prepared, but with the gas contact above the top of the reservoir, this way the reservoir region will have only the water fluid.

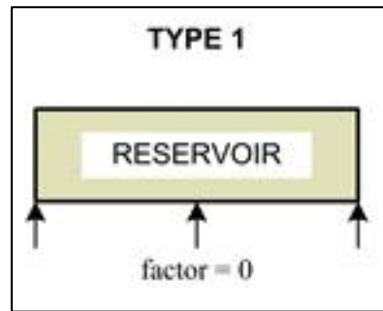
The properties of the fluid-rock zone, with saturation parameters, relative water, and gas permeabilities, are then included. The initial depth and pressure reference conditions of 6,000 ft and 3,000 psi respectively are then applied.

The gas/water contact at 5,500 ft, so that the reservoir is complete with water, making it a single-phase, as in problem 1. The numerical control applied to the simulation model is a maximum time step size of 10 days.

Then, the geomechanics module of the model is applied, with the respective data provided by Dean *et al.* (2006) and simulation and coupling parameters to the simulator, as *gcoupling* keyword, with a value equal to 2, as well as problem 1.

Application of the *gcfactor* keyword, presenting value equal to 0, which is used as a geomechanical coupling factor, providing behavior without displacement restriction, as shown in Figure 33.

Figure 33 - Geomechanical coupling factor 0 and boundary conditions.



Source: CMG IMEX user's guide, 2020.

Among other parameters are inserted into the model, such as effective model stress, rock properties, *Poisson* ratio, *Young* modulus, and rock cohesion. As well as the *calib\_por* command, which calibrates the porosity, providing adjustment in the accuracy of the porosity coupling and *gptolmul*, which adjusts the pressure tolerance to calculate the porosity formulas. The *presbc3d* control is used, which determines the contour conditions at the nodes of a 3D finite element, providing contour restriction only at the base of the reservoir.

After completion of the geomechanics card, the well model is created at the end, consisting of a producer well located in the center of the reservoir and completed in all reservoir layers, with respective dimensions and operation data provided by Dean *et al.* (2006), with total simulation for 500 days, but with specific time marking for better visualization of how the simulation and analysis of the model behavior occurs.

Therefore, all the formatting of problem 2, as well as the input cards, analysis, and the simulator keywords are in Appendix B.

### 3.2.3. Problem 3

Initially, the model is assembled with input data and output data request of the results, as well as the creation of a sector in the top cell of the reservoir, with the orientation to the well, in the surface cell of the model, oriented also in the region of the well and in the cell of the border of the model, located to the central region of the mesh for visualization of specific parameters in a refined way.

The model is created by defining the mesh, in the case of the Cartesian model, with the respective data provided by Dean *et al.* (2006), with data on layer thickness and length, the number of horizontal and vertical layers, the orientation of the top of the reservoir, porosity value, permeability values, compressibility, and reference pressure for rock compressibility.

Each parameter is determined specifically for the reservoir region and the waterproof rock region.

After that, the fluid is defined, with the respective PVT table adapted to the respective properties and units of the system used in the simulator, and the properties of the fluids, such as density, compressibility, viscosity, and formation volume factor are included.

Next, the properties of the fluid-rock zone are included, with saturation parameters and relative water and gas permeabilities. Initial conditions are bubble pressure of 3,000 psi, depth reference of 10,000 ft, and pressure reference of 4,370 psi for the reservoir. The water/gas contact of 0 ft respectively for the regions of the reservoir and waterproof rock, ensuring the condition of a single-phase reservoir.

The numerical control applied to the simulation model is set to a maximum time step size of 5 days, with normal pressure variation of 1,000 psi and maximum convergence in pressure tolerance of 0.0005. These are simulation parameters, of how the simulator should behave and perform the calculations.

Then, the geomechanics module of the model is applied, with the respective data and parameters of simulation and coupling to the simulator, as *gcoupling* keyword of value equal to 2, as in past problems. The *gcfactor* keyword with a value equal to 1 is also applied, as in problem 1. Among other parameters are inserted, such as effective model stress, rock properties, *Poisson* ratio, *Young* modulus, and rock cohesion for reservoir region and waterproof rock region.

As well as the *calib\_por*, which calibrates the porosity, providing adjustment in the accuracy of the porosity coupling, and the *gptolmul*, which adjusts the pressure tolerance to calculate the porosity formulas.

The well model is created at the end, consisting of a producing well located in the center of the reservoir and completed in all reservoir layers, with respective dimensions and operation data provided by Dean et. al. (2006), with total simulation for 4,000 days, but with specific time marking for better visualization of how the simulation occurs and model behavior.

Therefore, all the formatting of problem 3, as well as the input cards, analysis, and keywords of the simulator, can be found in Appendix C.

#### 3.2.4. Problem 4

Initially, the model is assembled with input data and output data request of the results, as well as the creation of a sector in the surface cell of the well for visualization of specific parameters in a refined manner.

The model is created by the definition of mesh, in the Cartesian model, with the respective data provided by Dean *et al.* (2006), with data on layer thickness and length, the number of horizontal and vertical layers, the orientation of the top of the reservoir, porosity value, permeability values, compressibility and reference pressure for the compressibility of the rock, as well as the creation of a sector for specific observation of the production well.

Afterward, it is defined the fluid properties, with the respective PVT table provided by Dean *et al.* (2006) and adapted to the respective properties and units of the system used in the simulator, and inclusion of the fluid properties, such as density, compressibility, viscosity and formation volume factor. Next, the properties of the fluid-rock zone are included, with parameters of saturation, capillary pressure, relative permeabilities of water, oil, and gas.

The initial conditions as well as the bubble pressure at 3,000 psi, depth reference, and pressure reference of 4,010 ft and 3,010 psi respectively apply. The water/oil and gas/oil contact at 4,310 ft and 3,900 ft respectively.

The numerical control applied to the simulation model is set to a maximum time step size of 365 days, with a normal pressure variation of 100 psi and maximum convergence in pressure tolerance of 2.0. These are simulation parameters, of how the simulator should behave and perform the calculations.

Then, the geomechanics module of the model is applied, with the respective simulation parameters and coupling to the simulator, as *gcoupling* keywords, with a value equal to 2, as in past problems, and *gcfactor* with a value equal to 1.

Among other parameters are inserted, such as effective model stress, rock properties, *Poisson* ratio, *Young* modulus, and rock cohesion, for reservoir region.

As well as the *calib\_por* command, which calibrates the porosity, providing adjustment in the accuracy of the porosity coupling and *gptolmul*, which adjusts the pressure tolerance to calculate the porosity formulas. Controls are also used to ensure the restriction of displacement in the contour of the reservoir, providing only the free top for movement.

The well model is created at the end, consisting of a producing well located at one vertex of the reservoir, cell 21, 21, 1 completed in all layers of the model, and another well, injector, located in the opposite region of the producer, in cell 1, 1, 1 completed in all layers of the model.

With simulation total time to 9,125 days, but with a specific time set for better visualization of how the simulation occurs and model behavior.

Therefore, all the formatting of problem 4, as well as the input cards, analysis, and keywords of the simulator, is in Appendix D.

### 3.3. External explicit iterative coupling with FLAC3D 6.0, IMEX e MATLAB

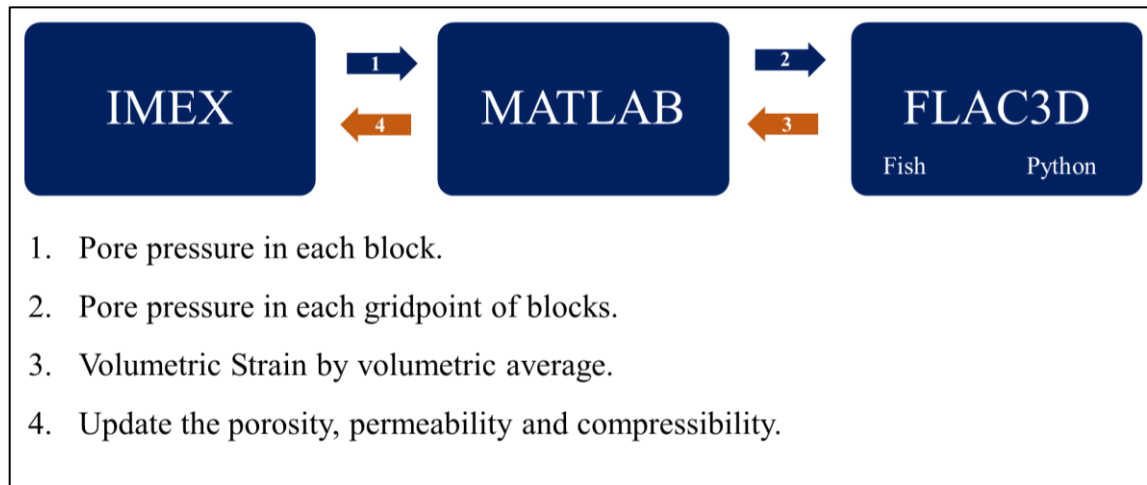
The external iterative coupling is performed to update the porosity, permeability, and compressibility of the reservoir throughout the simulation in 500 days for problem 1. In total, 10 couplings are elaborated with different development methodologies, the first one is used with the technique of performing all the simulation in the IMEX simulator and, later, performing the simulation in FLAC3D, therefore, a method not coupled, called one-way and that there is no updating of parameters such as porosity, permeability, and compressibility, only the activation of geomechanics in both models.

The next models are elaborated with the methodology called two-way, dynamic simulation in which the simulators interact with each new simulation cycle. Models with activation and without activation of geomechanics in the IMEX simulator are elaborated with different types of parameter updates, as well as with the use of different equations to calculate permeability.

Therefore, when simulating a time step in the IMEX simulator, a list of pore pressure per zone of the model is exported.

This list is adjusted through interpolation in the MATLAB software, providing another pore pressure list, but by gridpoint, ensuring that the FLAC3D software uses the pore pressure data by zone vertex. In this way, when simulating a step of time on the FLAC3D simulator, using the FISH language, a list of volumetric strain is exported. This list is used in MATLAB to calculate the new model porosity and compressibility. In Figure 34, a process flow with the activities between the simulation and programming software is presented.

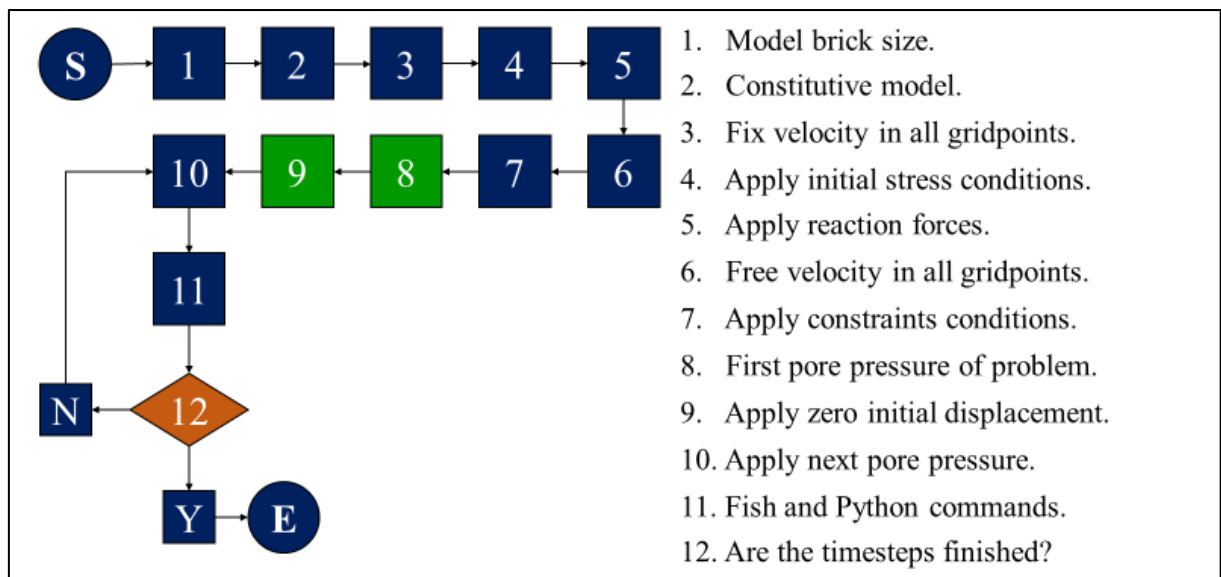
Figure 34 – Process flow between software.



Source: Author, 2020.

A flowchart is prepared for a detailed analysis of the steps that occur in the FLAC3D simulation, indicating the step-by-step and cycle of simulations that are carried out in this numerical analysis. Therefore, Figure 35 presents this flowchart of FLAC3D simulation steps.

Figure 35 - FLAC3D flow chart



Source: Author, 2020.

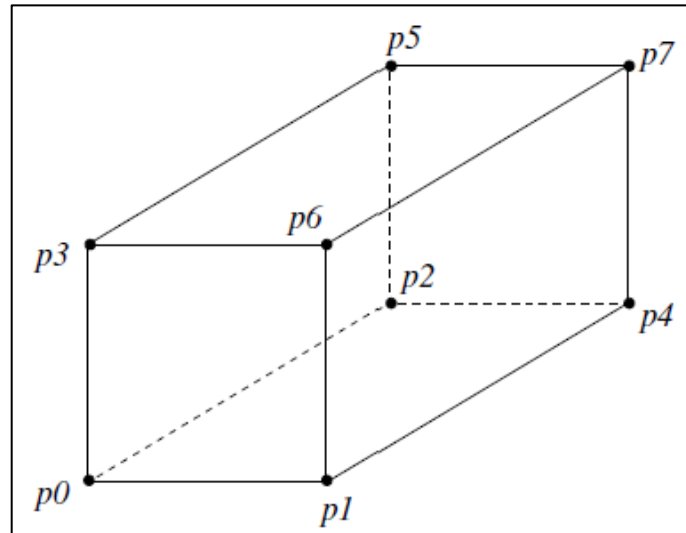
### 3.3.1. Mesh design

The simulation model mesh in FLAC3D was designed to follow the same orientation of the IMEX, therefore, the two simulators presenting the same orientation, there is no need for convergence for data transfer between the programs, this way facilitating the interpretation and use of data and results in each simulator.



The model design in the FLAC3D simulator was done through the block creation. Each block is generated through the vertex points, followed by an orientation with specific coordinates, as shown in figure 36.

Figure 36 – Zone block vertices configuration.



Source: FLAC3D 6.0 User guide, 2020.

The complete mesh of the model is made with the support of the MATLAB. Thus, the formatting of the grid of problem 1 is found in Appendix E.

### 3.3.2. Initial conditions

The following fluid configurations are applied for the reservoir model: activated *Biot* coefficient, Porosity equals to 0,2, and fluid anisotropy with horizontal permeability of 50 mD and vertical permeability of 5 mD. Then, the constitutive model, assigned for the elastic model, with the *Young* modulus of  $1 \times 10^4$  psi and *Poisson* ratio of 0.3.

The velocity is fixed in all directions of the model, and the reaction forces are then applied to the model. Afterward, the velocity is release, and then the specific problem restrictions are applied.

At the end of these steps, it is calculated numerically using the *Model solve* command, to ensure the state balance. In this way, the total stresses of the model are applied, through which the calculations and the strains are elaborated. For the model, a 1.0231 psi/ft gradient is presented for the vertical stress.

The model's initial conditions, as well as the formatting of these conditions with the respective keywords, are found in Appendix F.

### 3.3.3. Master file

It is created a master file of the programming to call the support files as Grid creation, constitutive properties, and constraints conditions, and then solve this step, it is elaborated to display a clean visualization of the programming steps. Which follows as such:

```

model new
call 'Grid'
call 'Gridinfo'
call 'Constitutive'
call 'Constraints'

model solve
; History graphs & list tables
model history mechanical ratio-average

model save 'Fundamental'

```

### 3.3.4. Initial pore pressure list

By exporting the list of Pore pressures per zone in the IMEX initial time, the MATLAB is used for interpolation of the values obtained for pore pressure values per vertex of each block. This gives the first pore list to insert in FLAC3D, however before inserting this list, the "*model solve*" command is used to balance the system.

The command used to insert each pore value into FLAC3D is the following:

```
"zone gridpoint fix pore-pressure <value>range id <area of the respective gridpoint block>".
```

There are other commands to insert the pore value, such as instead of using "*fix*" use "*initialize*", but when using this type of structure the values obtained in the results do not correspond to the behavior expected for the simulation.

In the user manual, the initialize command is: if the pore pressure is modified, it will not affect the total stress, but will change the effective stress. The setting of the fixed command is it will adjust the total stress, but it will keep the effective stress constant. However, it is obtained the converged behavior to the IMEX values with the command *fix*.

There is still another way to insert the pore pressure to the model, by inserting the pore pressure difference in each simulation time interval, using the "*add*" command after the pore pressure difference value. However, when using this method, the final value of each average pore pressure time step is extremely low. Therefore, there is a sudden drop in pore pressure, which is greater than the value of the pore pressure difference that occurs in the system.

Then, all displacements are pointed to zero to start counting the displacements and volumetric strains after the time zero.

Immediately after this, the "*model solve*" command is inserted again. For each iterative simulation process, the same procedure is followed minus the application of zeroing the displacements.

Therefore, the list of model's pore pressures, as well as the formatting with the respective keywords, are in Appendix G.

### 3.3.5. FISH programming

The next simulation step in FLAC3D is using the simulator's programming language, the FISH language. This language allows the user to interact and manipulate FLAC3D, defining new variables and functions if necessary.

In this way, FISH is used to provide the values of volumetric strain and average pore pressure per zone in each new time step, and the elaboration of the export file, with .dat extension, providing the results, as shown in table 3.

Table 3 – Exported file.

Volumetric Strain for time simulation 0 to 1 day.		
ID	Volumetric strain	Pore Pressure
1	3.32129e-05	3006.5
2	3.03777e-05	3006.5
3	2.922e-05	3006.5
4	3.27127e-05	3006.5
5	3.03459e-05	3006.5
6	2.43517e-05	3006.5
7	2.68276e-05	3006.5
8	2.63517e-05	3006.5
9	2.08579e-05	3006.5
10	1.98563e-05	3006.5

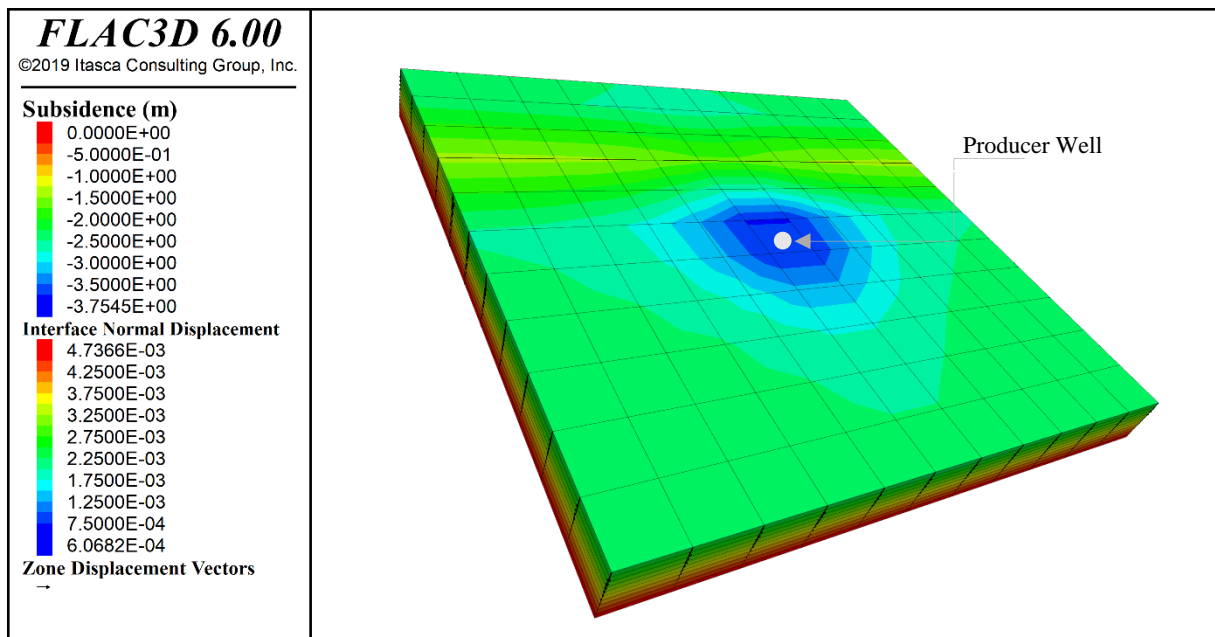
Source: Author, 2020.

Therefore, prepared for use in MATLAB, which will calculate through equation 2.1 the new porosity and compressibility values of the model. This creation of the programming, with FISH commands, is therefore presented in Appendix H.

### 3.4 Fractured model

The elaboration of a fractured model is made from the properties proposed in problem 1, but with the inclusion of a vertical fracture at a perpendicular distance of 152.40 m from the producing well, as shown in Figure 37. In this study, it was elaborated on the one-way method and on the two-way method with update only the porosity. Both cases with geomechanics activated. The fracture is inserted into FLAC3D with the interface attribute.

Figure 37 - Fractured reservoir



Source: Author, 2020.

This figure shows the final subsidence development of the one-way method. The fracture is distributed along with all the layers of the reservoir, thus along the entire vertical axis and with the following properties: cohesion 6.89E10 kPa, stiffness-shear 2.5E6 kPa, stiffness-normal 2.5E6 kPa, and friction angle 30°.

This way, the programming of the fracture in FLAC3D is performed as follows:

```
zone interface 'flt' create by-face separate range position-y 487 488
```

```
zone interface 'flt' node property cohesion 6.89E10 friction 30 stiffness-shear 2.5E6
stiffness-normal 2.5E6
```

```
zone interface 'flt' permeability on
```

```
zone interface 'flt' effective on
```

These commands are inserted in the constraints section.

## 4. RESULTS

Parameters that are influenced by the properties and behavior of the reservoir, as well as the boundary conditions of each scenario studied and the influence of rock geomechanics. Therefore, the results of mean reservoir pressure, subsidence along with the depletion, and properties of the fluid that constitutes the reservoir are presented.

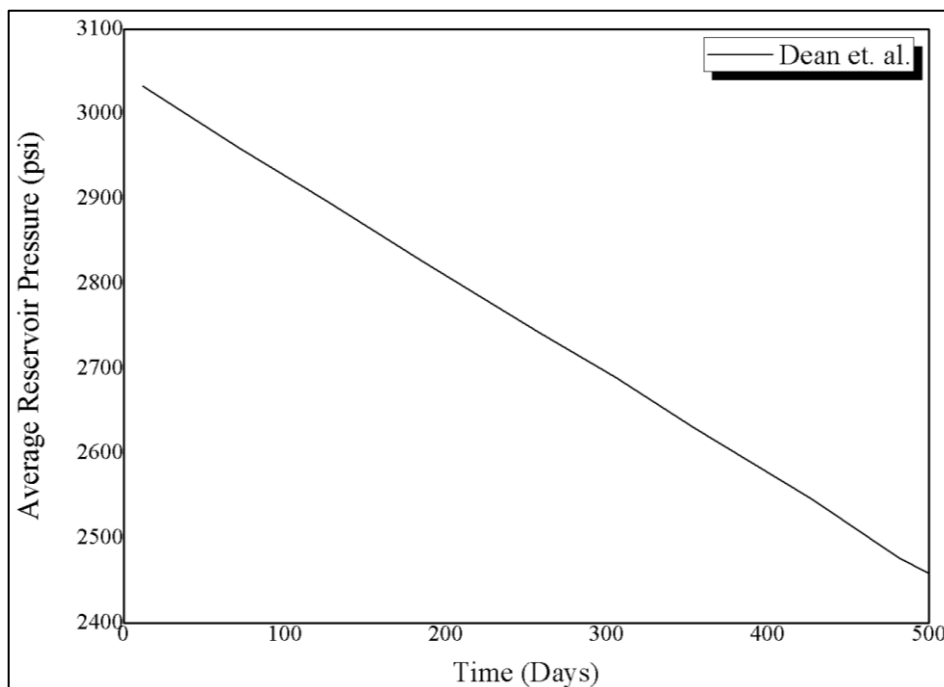
### 4.1. Description of results of Dean *et al.* (2006)

The results presented by Dean *et al.* (2006) are provided through graphs. Therefore, in this work, the graphs are reproduced in a way that allows the comparative analysis with the results obtained in the simulations.

#### 4.1.1. Problem 1

The average reservoir pressure results are observed in the central region where the producing well is located. Thus, Figure 38 shows the development of the average reservoir pressure, with the final value of 2.458,58 psi.

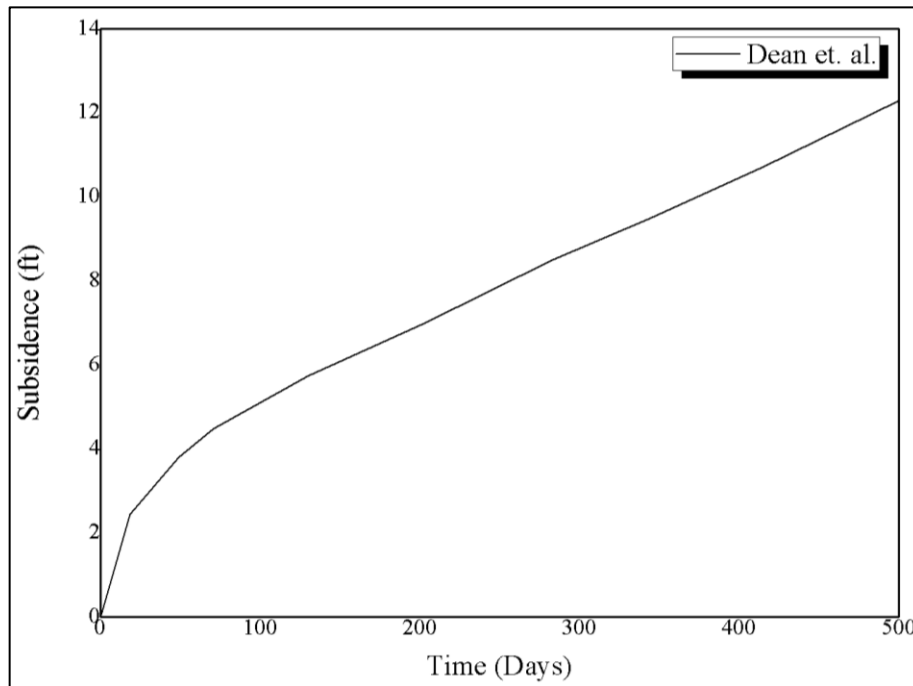
Figure 38 – Average reservoir pressure (problem 1).



Source: Author, 2020.

It is also observed for problem 1, the subsidence development at the reservoir top, in the central region, where the producing well is located. As shown in Figure 39, with a final value of 12.2 ft.

Figure 39 - Subsidence (problem 1).

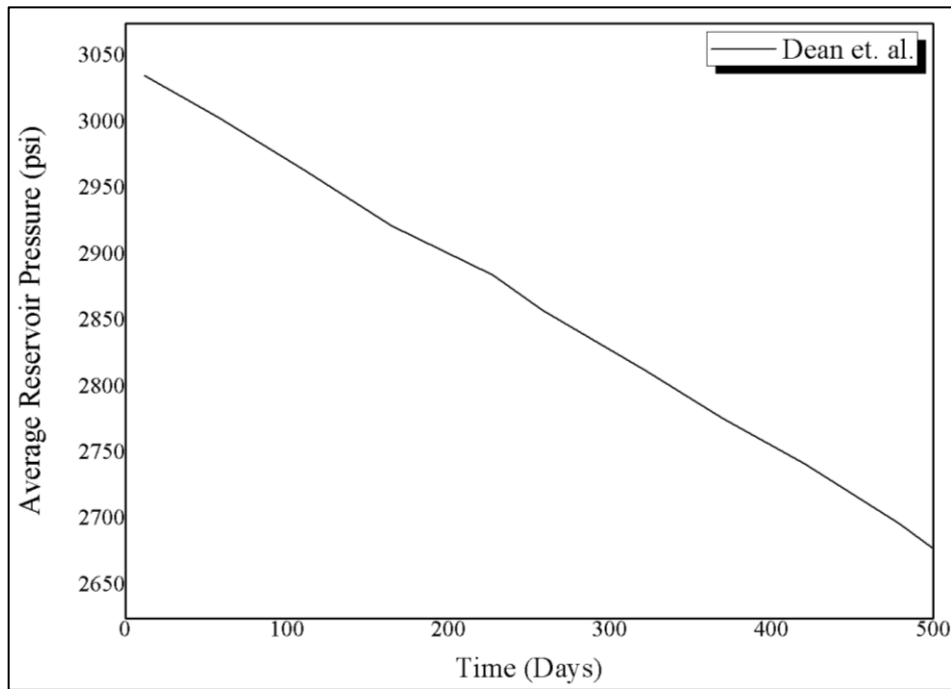


Source: Author, 2020.

#### 4.1.2. Problem 2

The results of the average reservoir pressure are observed in the central region where the producing well is located. Thus, Figure 40 shows the development of the average pressure, with the final value of 2,678.15 psi.

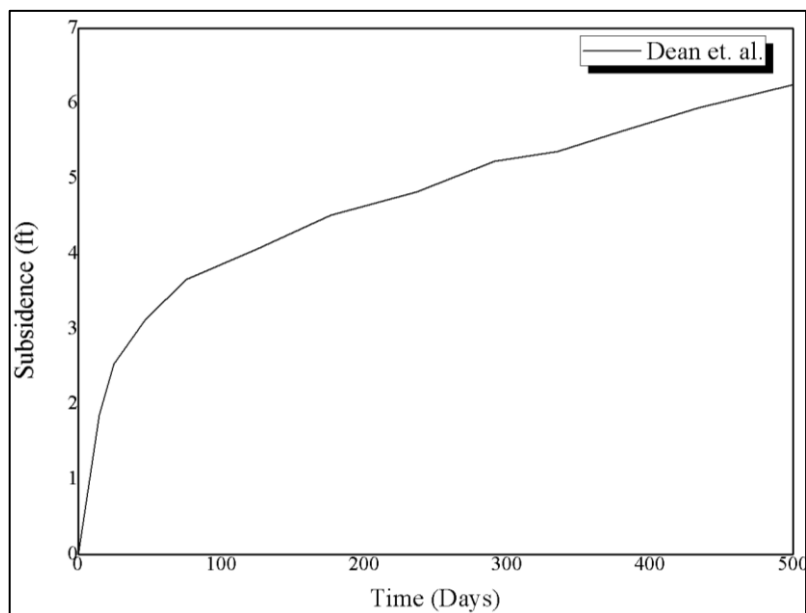
Figure 40 – Average reservoir pressure (problem 2).



Source: Author, 2020.

It is also observed for problem 2, the development of subsidence at the top of the reservoir, in the central region, where the producing well is located. As shown in Figure 41, with a final value of 6.30 ft.

Figure 41 - Subsidence (problem 2).

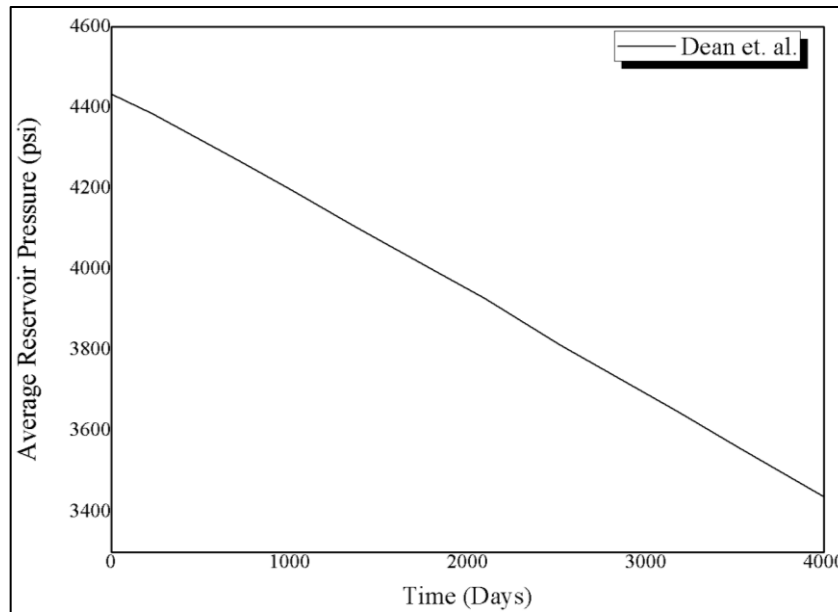


Source: Author, 2020.

#### 4.1.3. Problem 3

The results of the average reservoir pressure are observed in the central region where the producing well is located. Therefore, Figure 42 shows the development of the average pressure with the final value of 3,437.15 psi.

Figure 42 – Average reservoir pressure (problem 3).

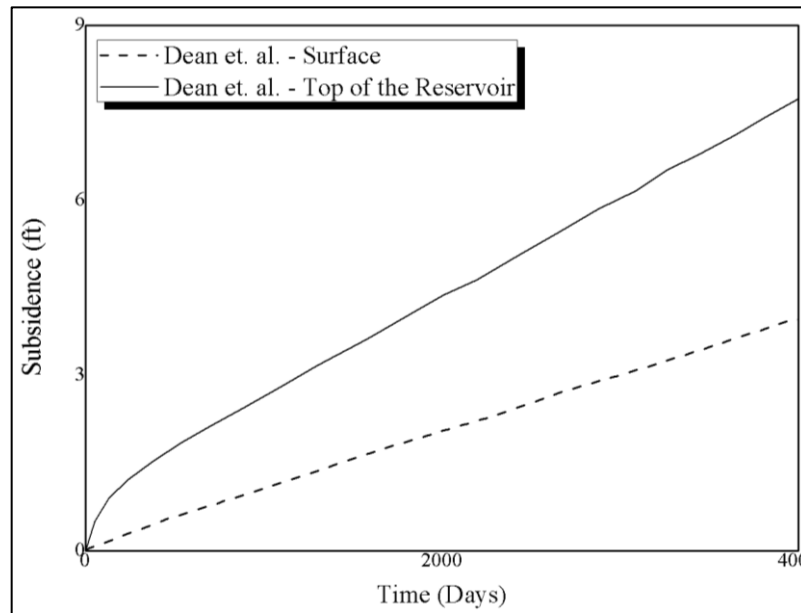


Source: Author, 2020.

It is also observed for problem 3, the development of subsidence at the surface and the top of the reservoir, both in the central region of the model, where the producing well at the top of the reservoir is located. As shown in Figure 43, with a final value of 3.96 ft at the surface and 7.74 ft at the top of the reservoir.



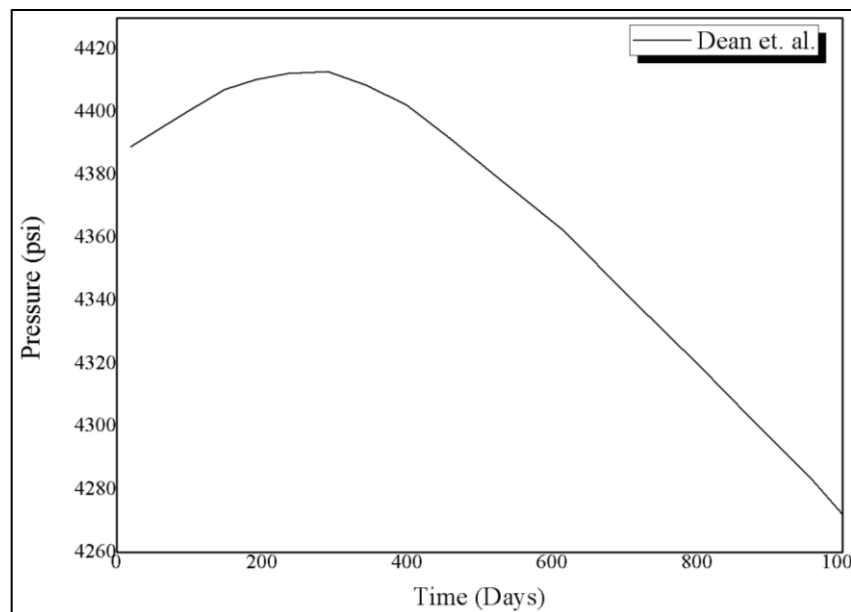
Figure 43 - Subsidence (problem 3).



Source: Author, 2020.

The pressure at the border of the model is also observed, in Figure 44, where there is an increase in pressure in the initial simulation periods, due to the geomechanical effects, with a subsequent decline in this pressure. This curve is analyzed up to 1,000 days to point out this behavior with an increase of pressure in the initial simulation period.

Figure 44 – Border pressure (problem 3).

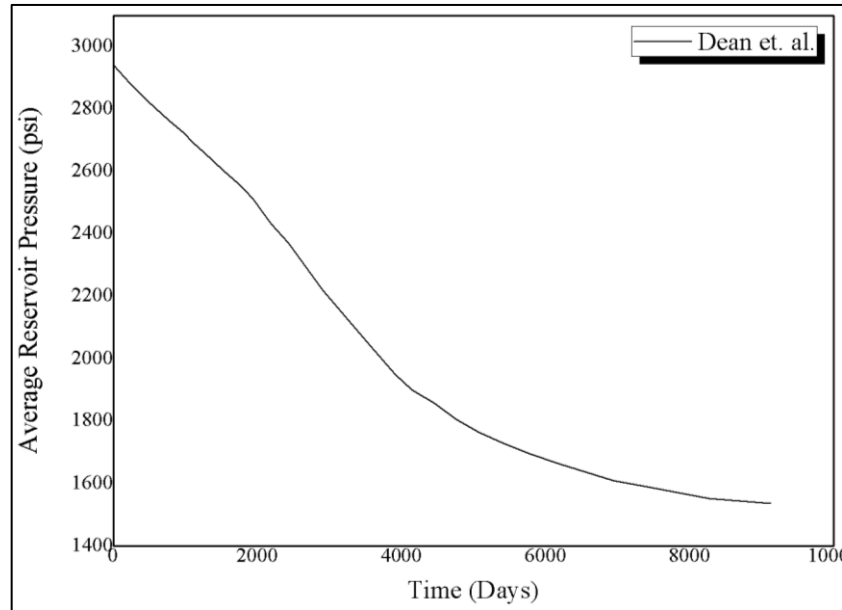


Source: Author, 2020.

#### 4.1.4. Problem 4

The results of the average reservoir pressure in the central region of the model are observed. Thus, Figure 45 shows the development of the average reservoir pressure with the final value of 1,535.79 psi.

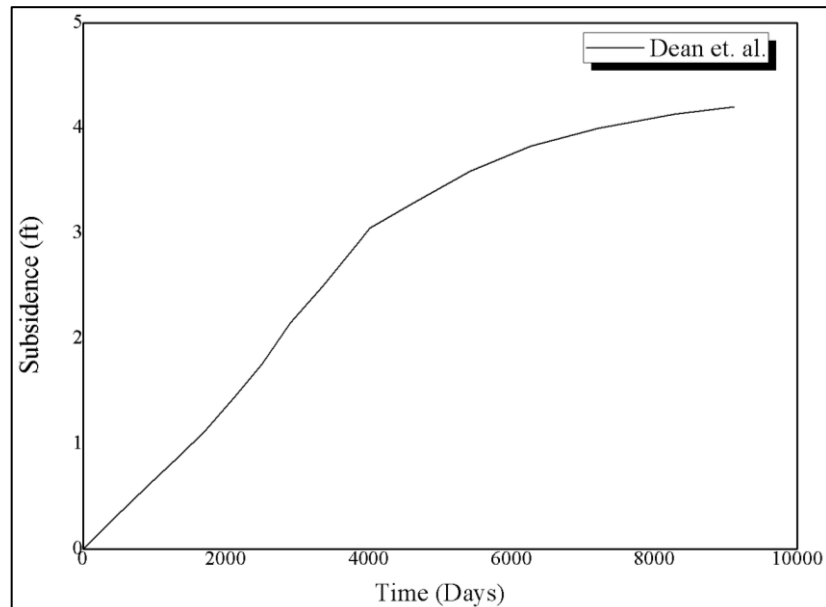
Figure 45 – Average reservoir pressure (problem 4).



Source: Author, 2020.

It is also observed for problem 4, the development of subsidence at the top of the reservoir. As shown in Figure 46, with a final value of 4.2 ft.

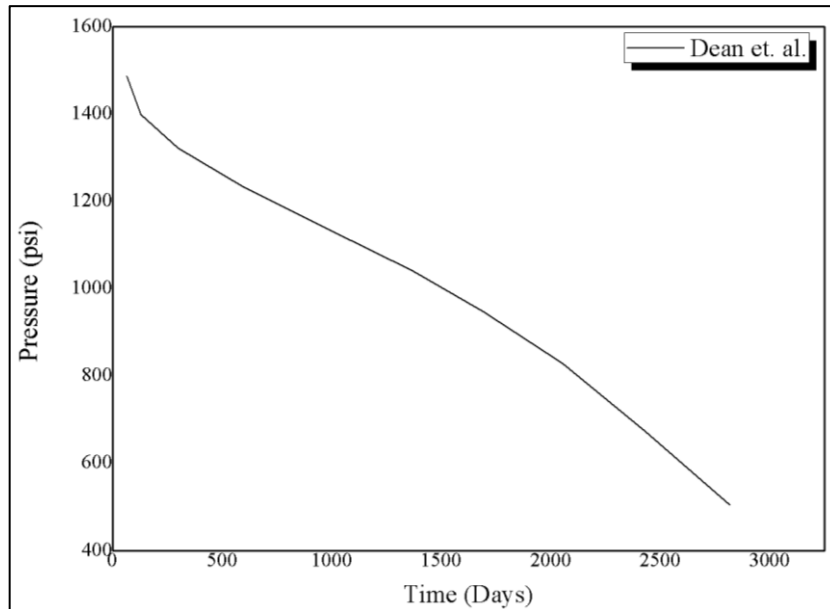
Figure 46 - Subsidence (problem 4).



Source: Author, 2020.

Still, on problem 4, the pressure parameter in the producing well is observed, which is obtained, at the end of the simulation, the value of 500 psi, as shown in Figure 47.

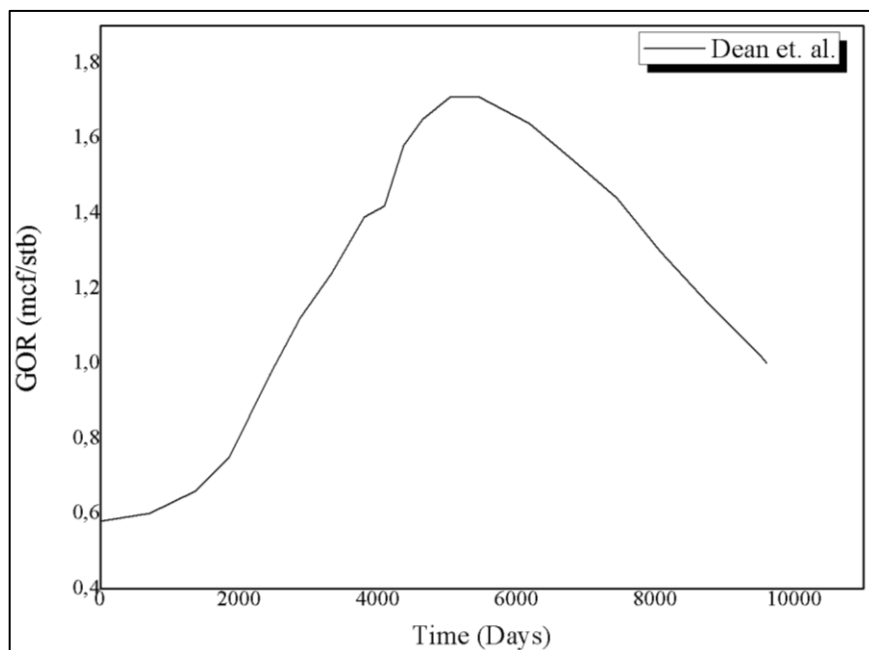
Figure 47 – Well's pressure (problem 4).



Source: Author, 2020.

The gas/oil ratio, observed in Figure 48, presents the development of this ratio along with the exploitation and injection, in which the value of 1.0 mcf/stb was obtained at the end of the simulation.

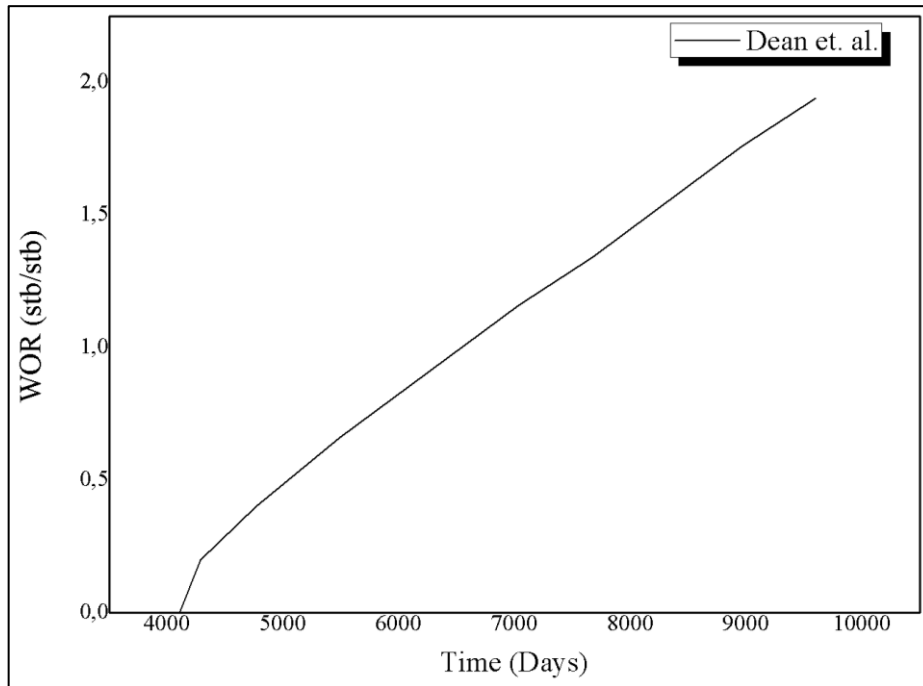
Figure 48 – Gas/Oil ratio (problem 4).



Source: Author, 2020.

And the water/oil ratio parameter, where 1.94 stb/stb was obtained at the end of the simulation, as shown in figure 49, recreated a graph from Dean.

Figure 49 – Water/Oil ratio (problem 4).



Source: Author, 2020.

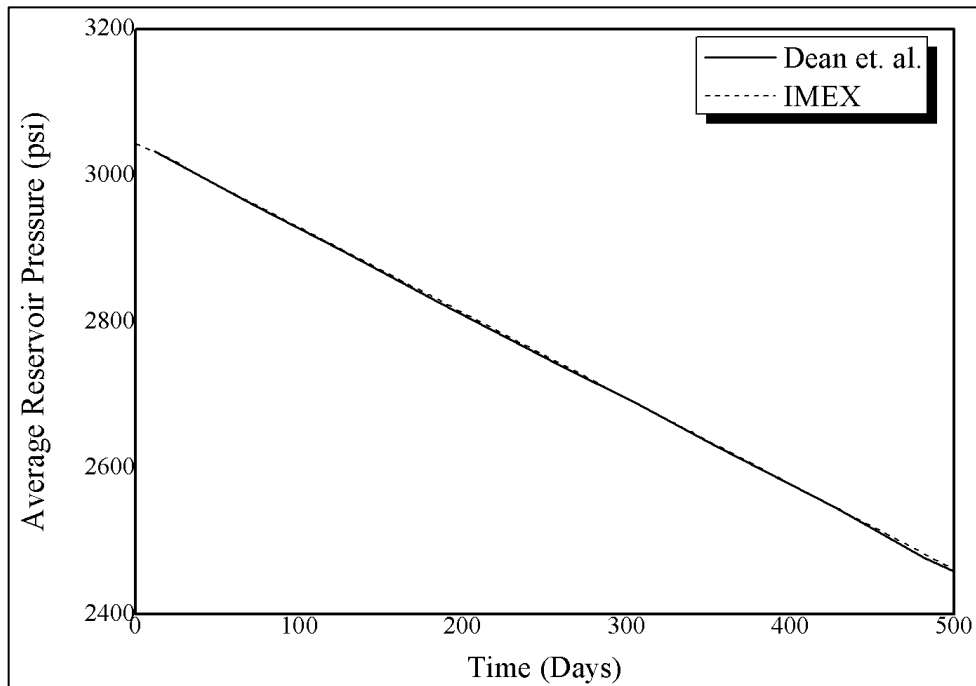
All graphs reported by Dean *et al.* (2006) and prepared by the author are in Appendix I.

## 4.2. IMEX 2019 results

### 4.2.1. Problem 1

The results observed for this problem are the developments in average reservoir pressure and subsidence. Therefore, the average reservoir pressure at the end of the simulation presented a value of 2.462,54 psi, as shown in Figure 50, the depletion behavior of an aquifer type reservoir.

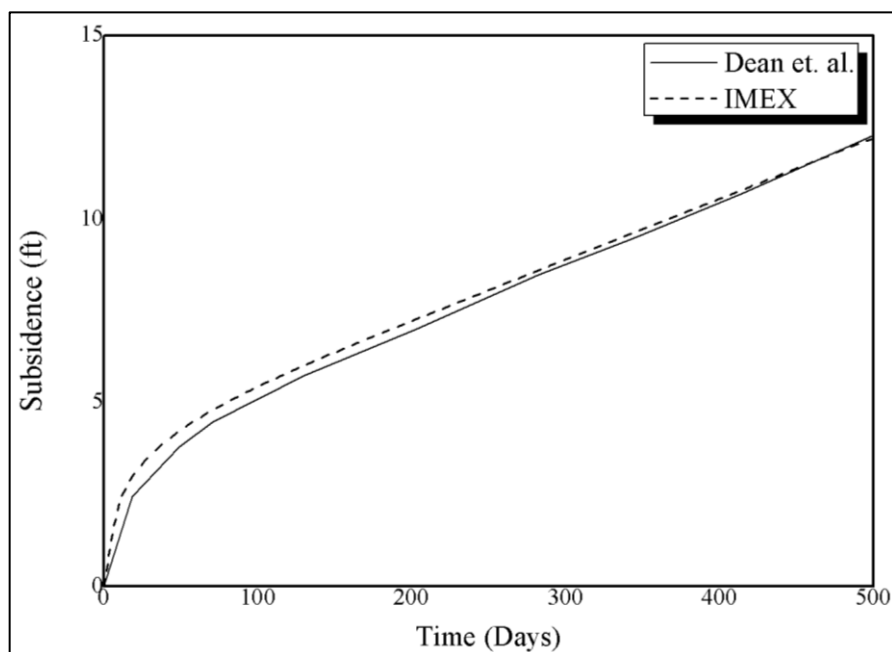
Figure 50 – Average reservoir pressure (problem 1, IMEX).



Source: Author, 2020.

Therefore, the average reservoir pressure maintained the behavior and result trend observed by Dean *et al.* (2006). The subsidence observed in the surface cell of the well is shown in Figure 51, in which the value of 12.20 ft is obtained at the end of the simulation. This way, the adjustment to problem 1 is in line with the results proposed by Dean *et al.* (2006).

Figure 51 – Subsidence (problem 1, IMEX).

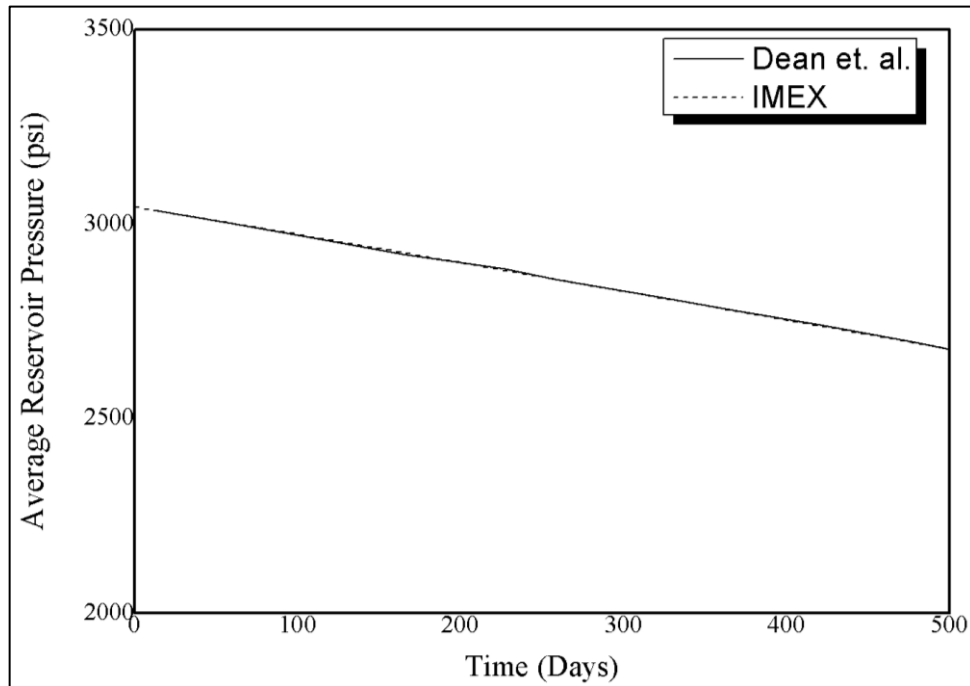


Source: Author, 2020.

#### 4.2.2. Problem 2

Os resultados observados para esse problema são os desenvolvimentos da pressão média do reservatório e da subsidência, assim como no problema 1. A pressão média do reservatório ao final da simulação apresentou valor de 2.679,27 psi, como mostra a Figura 52.

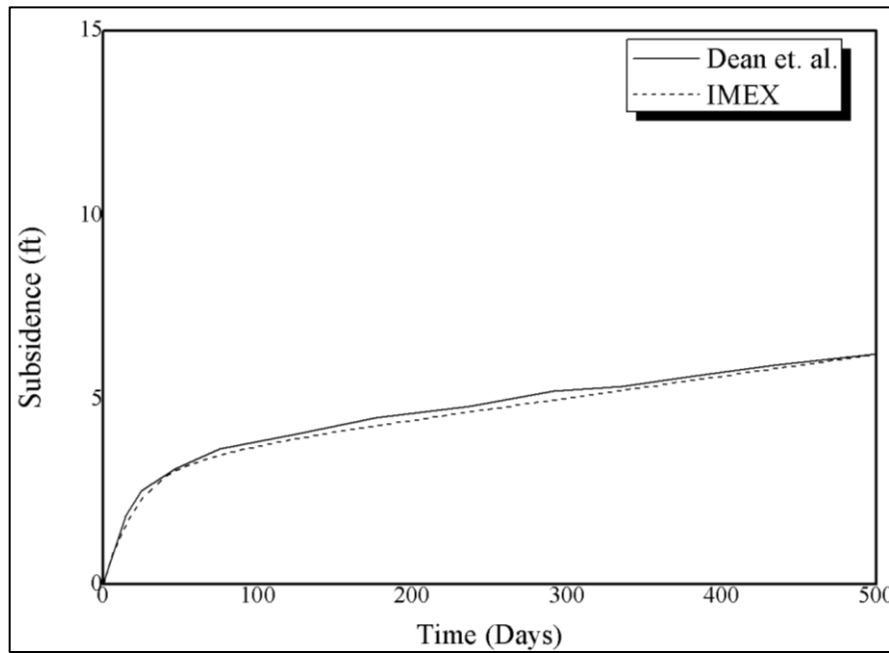
Figure 52 – Average reservoir pressure (problem 2, IMEX).



Source: Author, 2020.

The subsidence observed in the surface cell of the well is shown in Figure 53, in which the value of 6.23 ft is obtained at the end of the simulation.

Figure 53 - Subsidence (problem 2, IMEX).



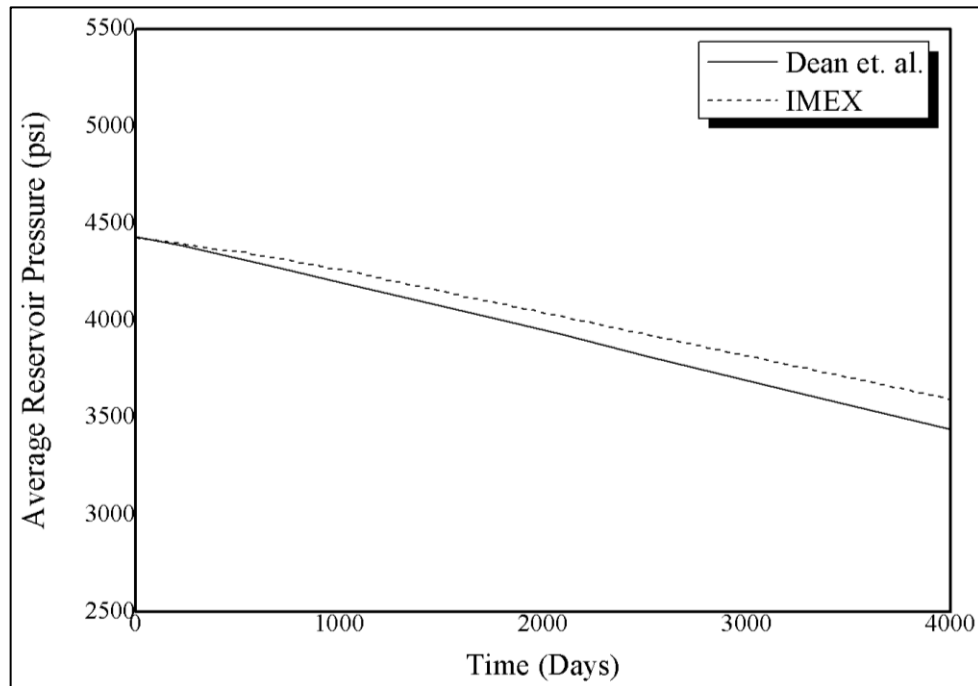
Source: Author, 2020.

The reservoir subsidence maintained the trend of behavior and result observed by Dean et. al. (2006). Therefore, the adjustment to problem 2 is in line with the results proposed by Dean et. al. (2006).

#### 4.2.3. Problem 3

The results observed for this problem are the developments of the average reservoir pressure, the subsidence on the surface of the model and the top of the reservoir, and the pressure at the border of the model. The average reservoir pressure at the end of the simulation had a value of 3,486.78 psi, as shown in Figure 54.

Figure 54 – Average reservoir pressure (problem 3, IMEX).

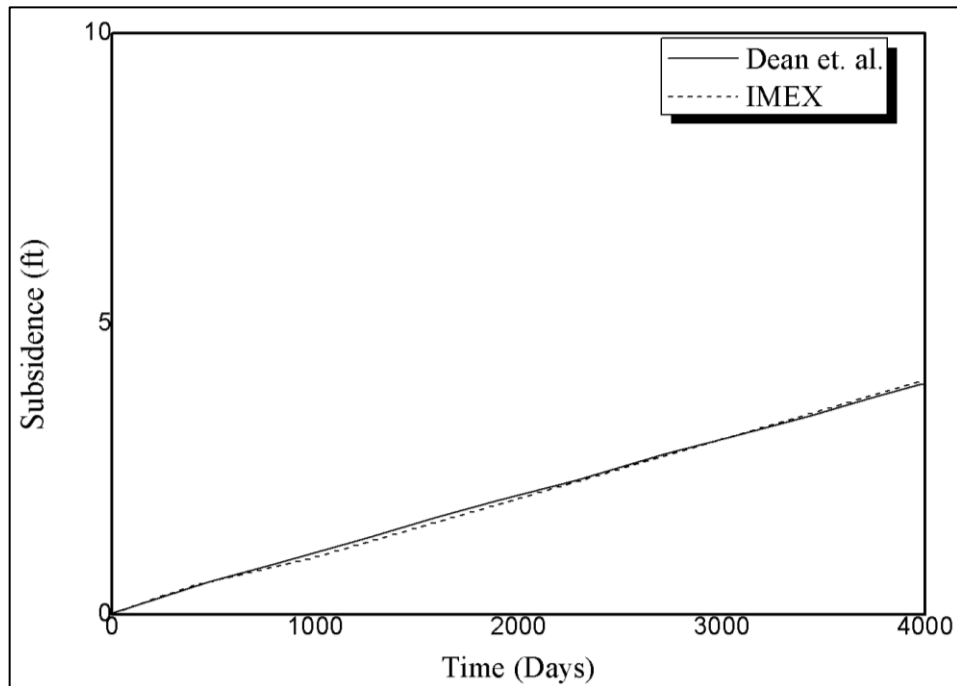


Source: Author, 2020.

Therefore, the average reservoir pressure maintained the behavior and result trend observed by Dean *et al.* (2006) but showing a difference of 155.96 psi at the end of the simulation. The subsidence observed in the superficial cell of the model, located in the central region of the model, is presented in Figure 55, in which the value of 4.43 ft is obtained at the end of the simulation.



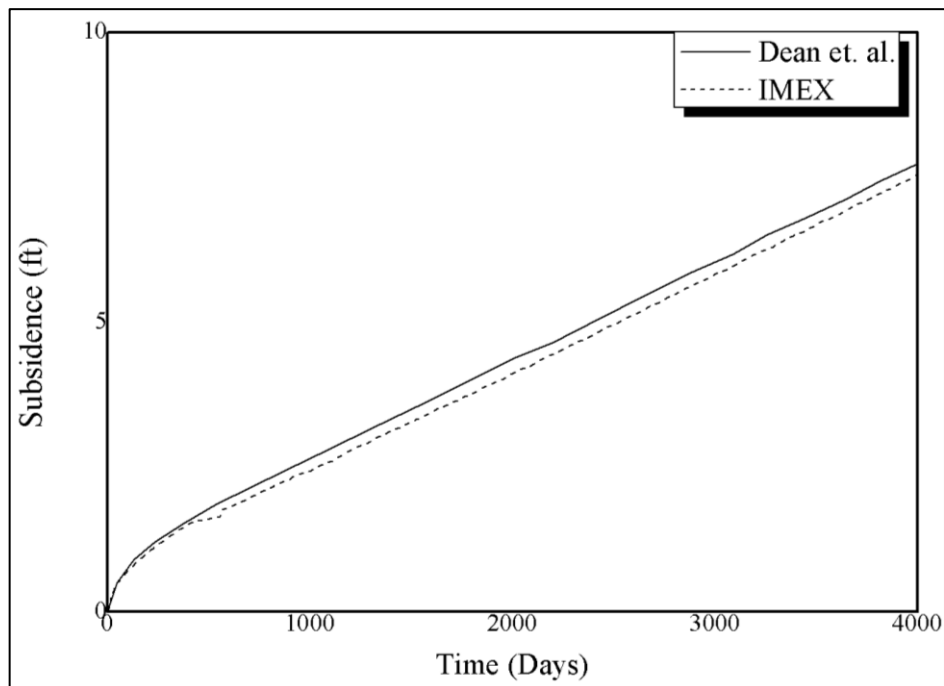
Figure 55 – Subsidence (problem 3, IMEX).



Source: Author, 2020.

The subsidence observed at the top of the reservoir, located in the central region of the model and where is located the producing well is presented in Figure 56, in which the value of 7.56 ft is obtained at the end of the simulation.

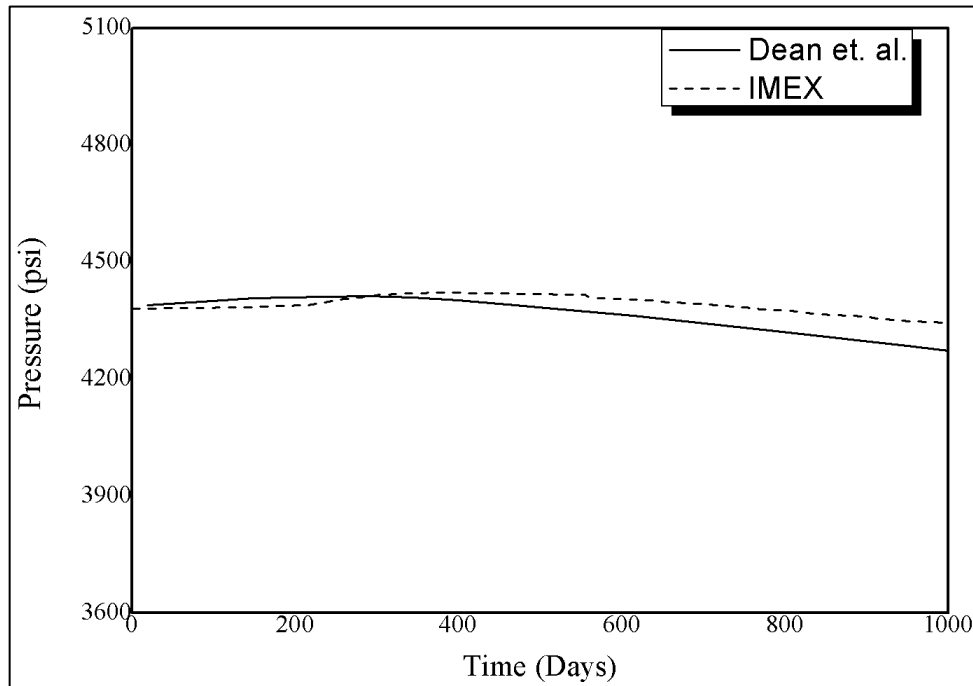
Figure 56 – Subsidence at the top of the reservoir (problem 3, IMEX).



Source: Author, 2020.

The model subsidence maintained the behavior and outcome trend observed by Dean *et al.* (2006). The pressure at the border of the model is analyzed up to 1,000 days of simulation, where an increase in pressure is observed due to the effects of geomechanics and the subsequent decline in that pressure, as shown in Figure 57. Ending at 4,344.04 psi.

Figure 57 – border pressure (problem 3, IMEX).



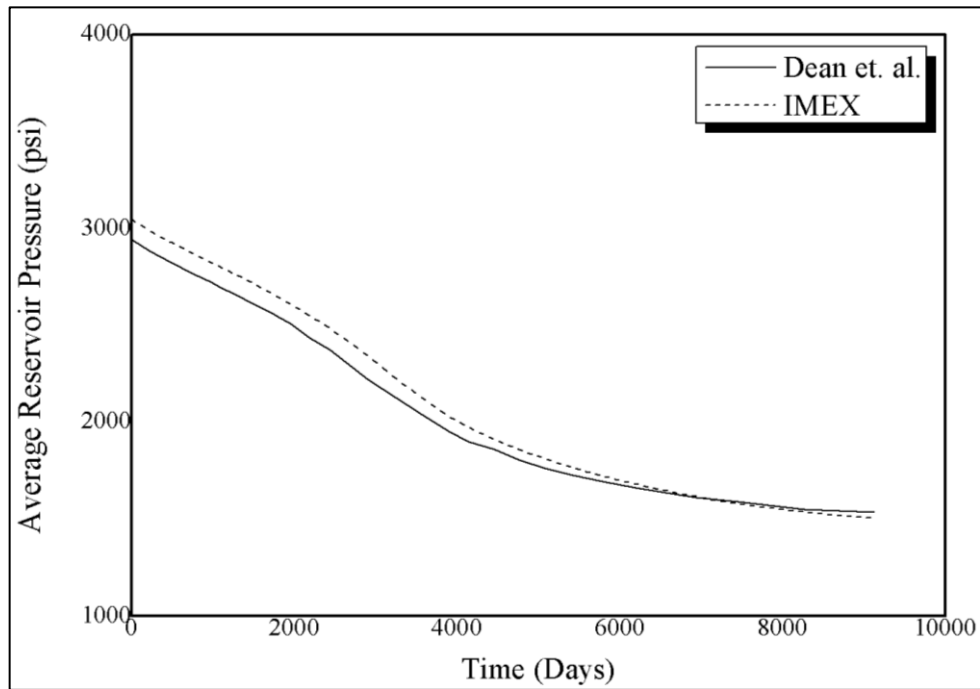
Source: Author, 2020.

The result at the end of the simulation was 72.03 psi different from the value observed by the compared literature. This way, the adjustment to problem 3 is considered as aligned with the results proposed by Dean *et al.* (2006).

#### 4.2.4. Problem 4

The results observed for this problem are the developments of the average reservoir pressure, the subsidence at the top of the reservoir, the pressure in the well, the gas/oil ratio, and the water/oil ratio. The average reservoir pressure obtained at the end of the simulation is 1,505.03 psi, as shown in Figure 58.

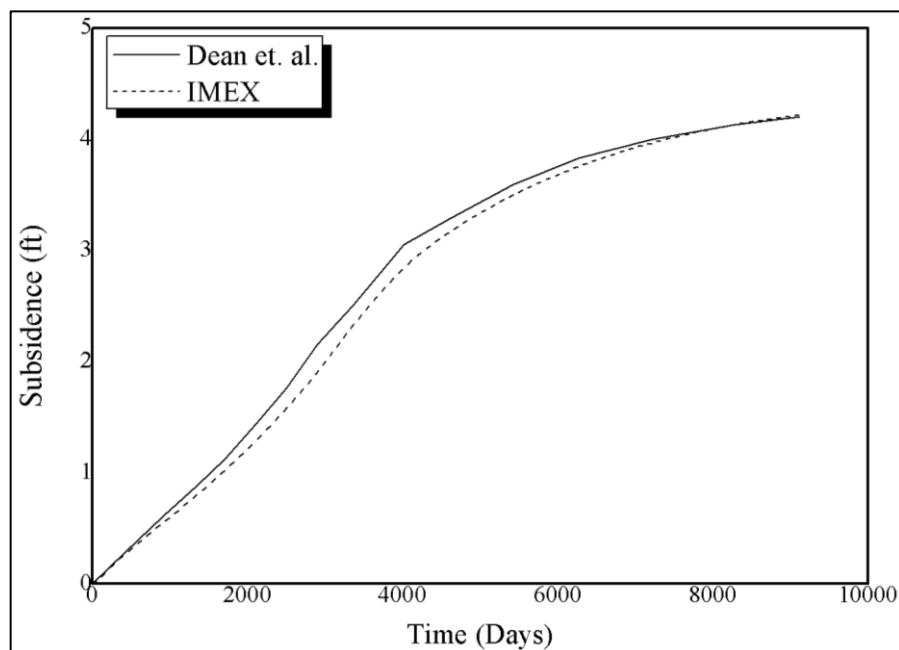
Figure 58 – Average reservoir pressure (problem 4, IMEX).



Source: Author, 2020.

As observed by the graph above, the average reservoir pressure values converged satisfactorily with the results presented by Dean *et al.* (2006). The development of subsidence at the top of the reservoir, in the central region of the model, is presented in Figure 59, with a final value of 4.22 ft.

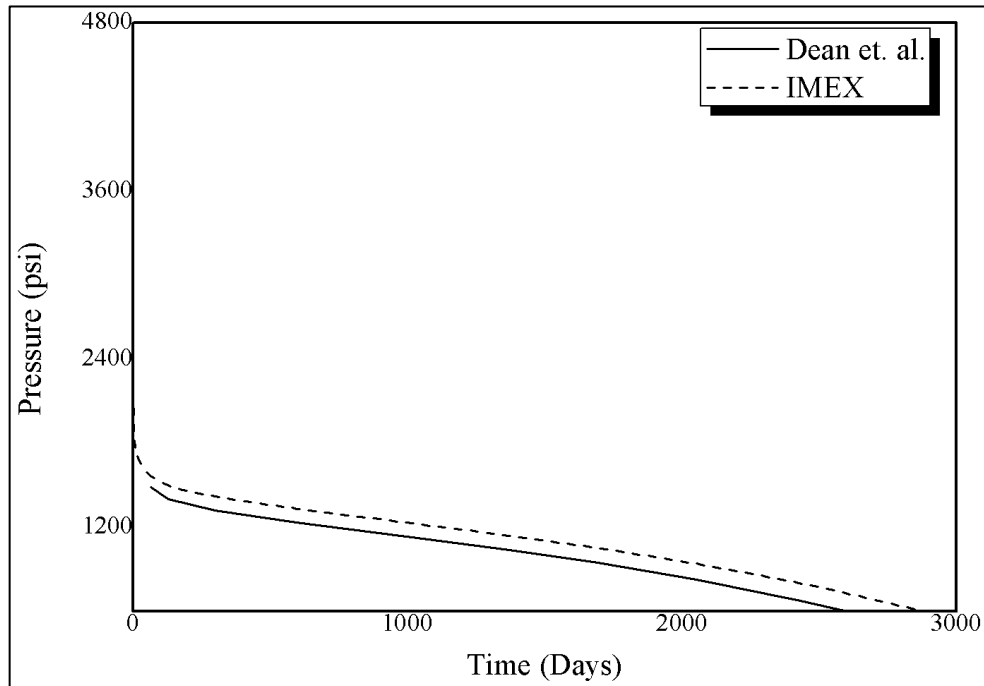
Figure 59 - Subsidence (problem 4, IMEX).



Source: Author, 2020.

As shown in the graph above, the reservoir subsidence values converged satisfactorily with the results presented by Dean *et al.* (2006). Still on problem 4, in the producing well, the pressure of 500 psi is obtained at the end of the simulation, as shown in Figure 60, with analysis up to 3,000 days of simulation, because after this analysis the pressure value in the well is constant.

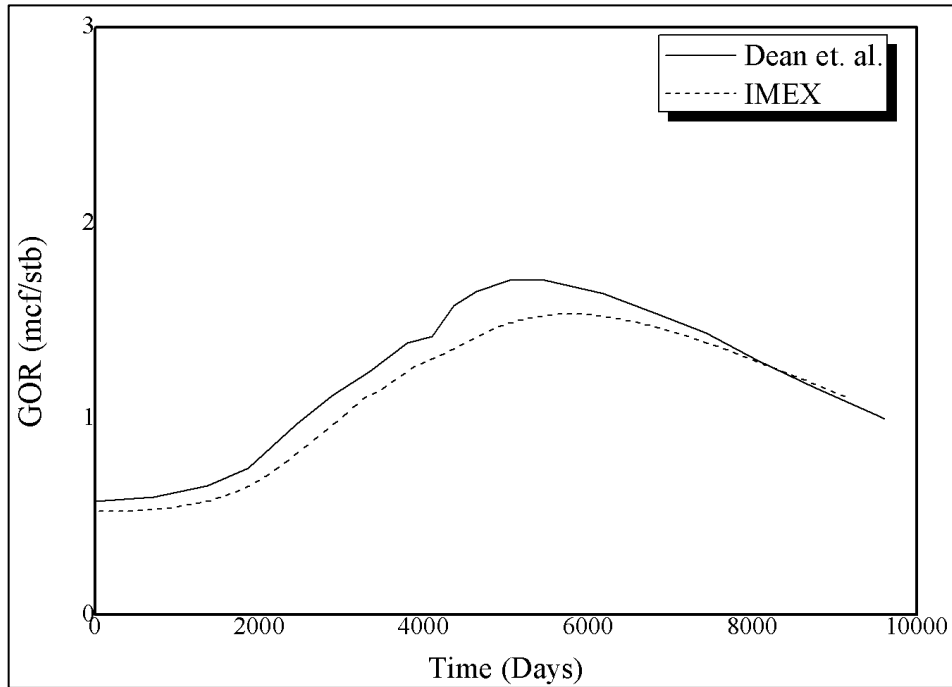
Figure 60 – Well's pressure (problem 4, IMEX).



Source: Author, 2020.

The result of pressure in the well at the end of the simulation shows a divergence of 4.71 psi. The gas/oil ratio is obtained at the end of the simulation at a value of 1.11 mcf/stb, as shown in Figure 61.

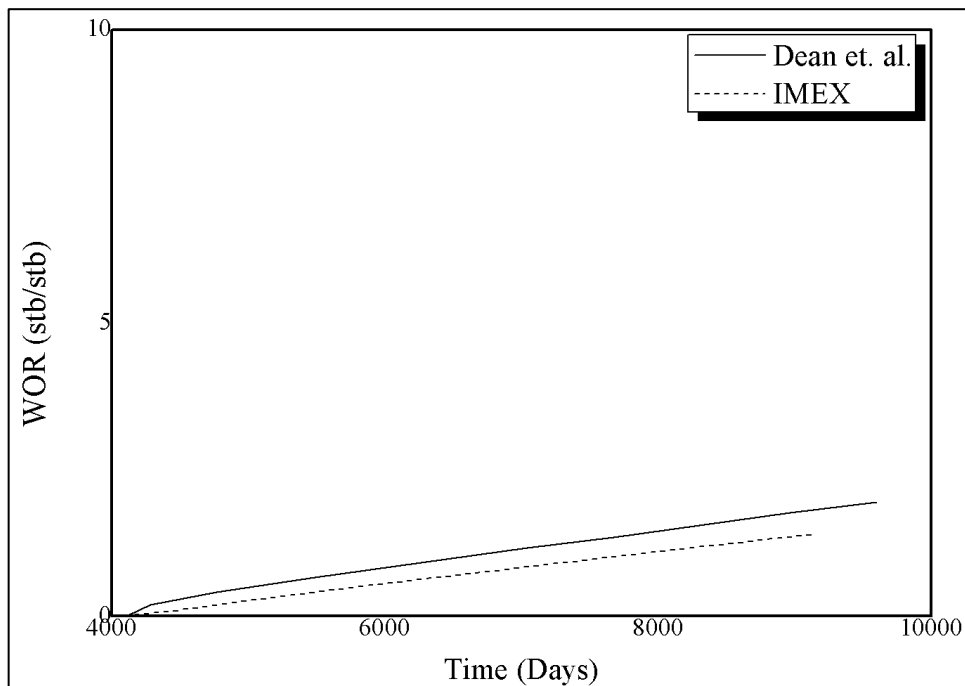
Figure 61 – Gas/Oil ratio (problem 4, IMEX).



Source: Author, 2020.

As seen in the graph above, the result obtained presents the same behavior trend as the one reported by Dean *et al.* (2006). As well as the water/oil ratio, at the end of the simulation, showing a value of 1.40 stb/stb, as shown in Figure 62.

Figure 62 – Water/Oil ratio (problem 4, IMEX).



Source: Author, 2020.

As observed in the graph above, the water/oil ratio behavior is of the same trend as presented by Dean *et al.* (2006), but with the divergence of 0.54 stb/stb. The graphs and plots prepared in the IMEX CMG 2019 simulator of all problems are presented in Appendix J.

#### 4.3. FLAC3D 6.0 results

It is possible to extract various results through FLAC3D, as well as using FISH language. The results that were analyzed through this language are the volumetric strain and the mean pore pressure of each zone, thus elaborating, with the support of the language, and output file with these respective data.

After this step, the list of volumetric strain per zone for the MATLAB to follow in the procedure of porosity and compressibility calculation is applied. Another result that is observed during the FLAC3D simulation is the vertical displacement, which is equivalent to the subsidence of the model, providing the interpretation of the geomechanical behavior of the reservoir. As well as the average mechanical rate, which indicates the steps in which the simulator elaborates the calculations until it is in an equilibrium state.

The first five models of the two-way method are elaborated with geomechanics deactivated in the IMEX simulator, distributed as follows: the first, the porosity, transmissibility factor, and pore compressibility are updated; the second, the porosity, permeability, and compressibility of the pore are updated; the third, the porosity and permeability are updated; the fourth, the porosity and compressibility of the pore are updated; and the fifth, the permeability and compressibility of the pore are updated. Four other models are elaborated with geomechanics activation in the IMEX simulator, distributed as follows: the sixth, only the porosity is updated; the seventh, the permeability is updated using equation 4.1:

$$\frac{k_n}{k_0} = \left(\frac{\phi_n}{\phi_0}\right)^3 \quad (4.1)$$

The eighth, pore porosity and compressibility are updated; and the ninth, permeability is updated using equation 4.2:

$$\frac{k_n}{k_0} = \left(\frac{1 - \phi_0}{1 - \phi_n}\right)^2 \left(\frac{\phi_n}{\phi_0}\right)^3 \quad (4.2)$$

Table 4 presents the subsidence results obtained with the above-mentioned models:

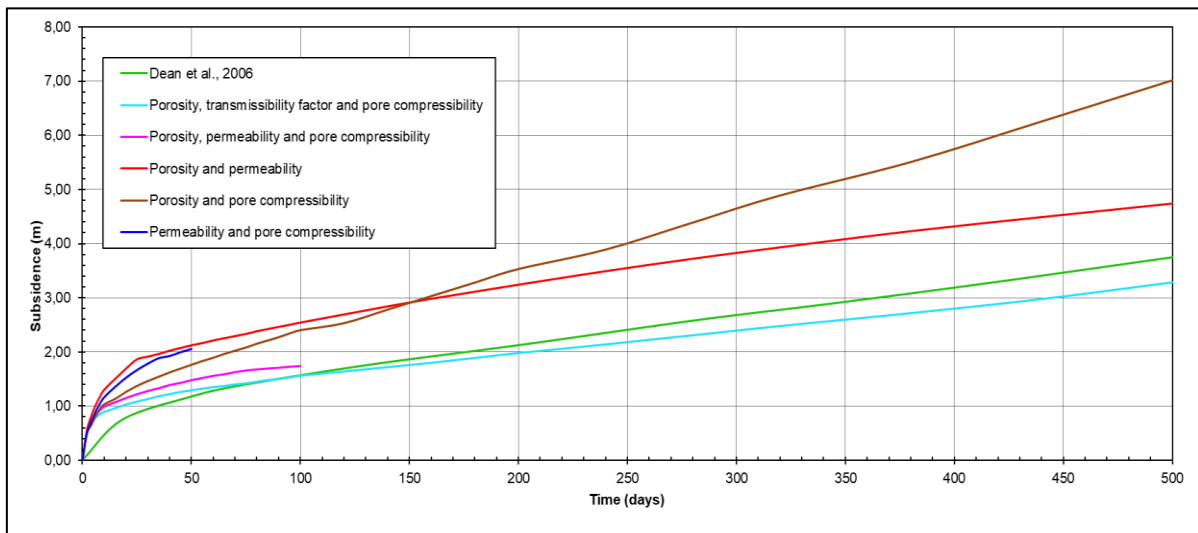
Table 4 - FLAC3D - IMEX models

Model	Type	Subsidence (m)
ONE WAY		
1	With geomechanics	3.81 (500 Days)
TWO WAY		
1	Without geomechanics; Porosity, transmissibility factor and pore compressibility	3.29 (500 Days)
2	Without geomechanics; Porosity, permeability and pore compressibility	1.74 (100 Days)
3	Without geomechanics; Porosity and permeability	4.74 (500 Days)
4	Without geomechanics; Porosity and pore compressibility	6.89 (500 Days)
5	Without geomechanics; Permeability and pore compressibility	2.15 (50 Days)
6	With geomechanics; Porosity	3.86 (500 Days)
7	With geomechanics; Permeability eq. 3.1	2.23 (140 Days)
8	With geomechanics; Porosity and pore compressibility	1.20 (100 Days)
9	With geomechanics; Permeability eq. 3.2	2.15 (140 Days)

Source: Author, 2020.

Figure 63, presents the results of subsidence of the models obtained without activated geomechanics in comparison with the results of Dean *et al.* (2006):

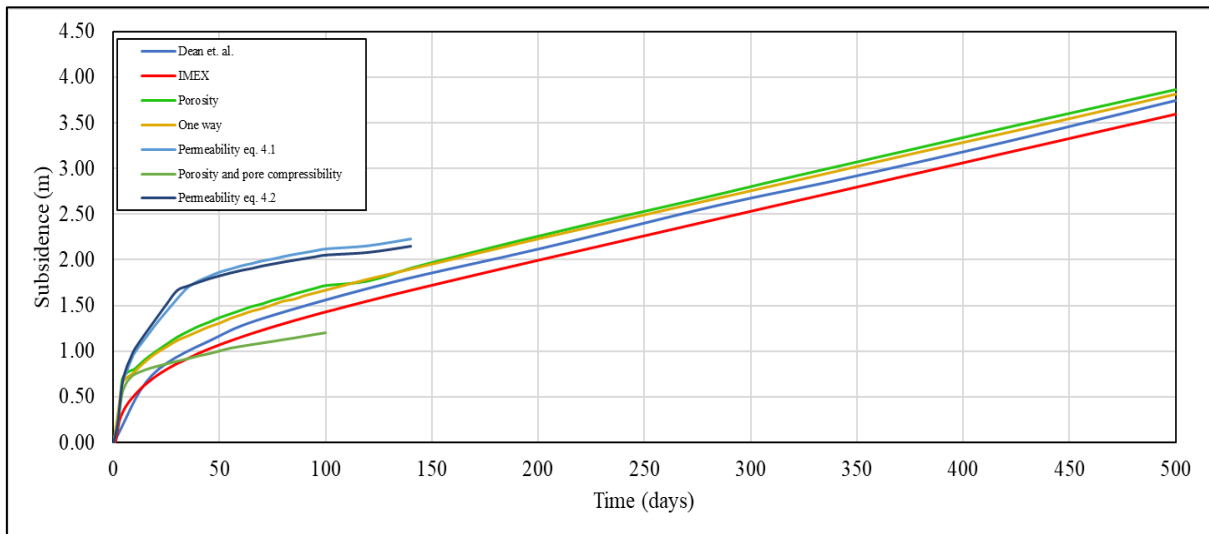
Figure 63 - Models without geomechanics



Source: Author, 2020.

The subsidence results of the models obtained with geomechanics activation, in comparison with the one-way model, with the result of the IMEX simulator model and with the result of Dean *et al.* (2006) are presented in the following figure 64:

Figura 64 - Models with geomechanics



Source: Author, 2020.

It is observed that of the models without geomechanics activation in the IMEX simulator, the representative result for the subsidence analysis is in the model with porosity update, transmissibility factor, and pore compressibility, although with final subsidence of 3.29 m. For the models with geomechanics activation in both simulators, the influence that permeability provides to the simulation model due to fluid-reservoir dynamics stands out, these models are not elaborated until the end of the simulation days, because there is a flow error in the reservoir. The one-way model is not representative, because it is not a coupled model between the simulators, this model is only used as an alignment checker between the simulators. Thus, the best model obtained is the one that updates only the porosity of the reservoir along the simulation timesteps, since the subsidy obtained is of the value of 3.86 m, which is close to the results of the simulation that uses only the IMEX, as well as with the one-way model and with the model of Dean *et al.* (2006).

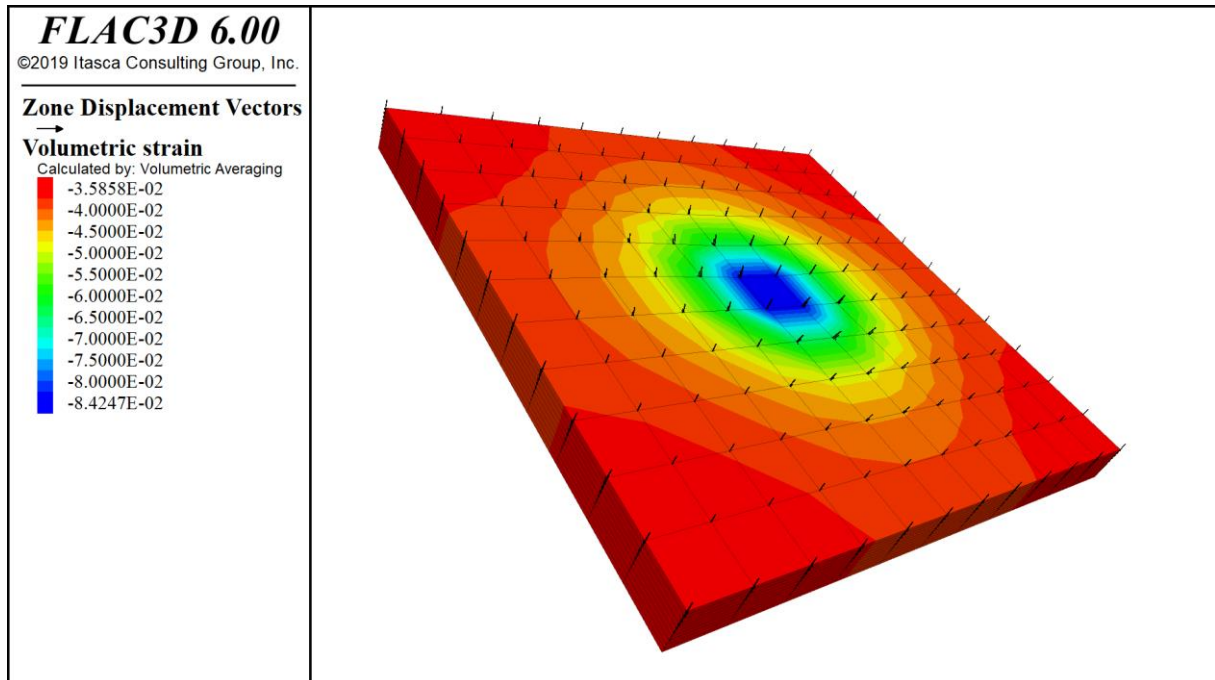
Therefore, the results of the coupled model are presented in greater detail with only the porosity parameter being updated throughout the simulation. Starting with the volumetric strain by the average volumetric, the subsidence, and the average mechanical ratio.

#### 4.3.1. Volumetric strain

At the end of the simulation, the volumetric strain along with the mesh of the reservoir obtained the value  $-8.42E-2$  as shown in Figure 65. It can be seen by the figure that greater deformations occur in the central region of the reservoir, in which the well is located and there is also a deformation gradient increasing along with the approach of this region, this is justified due to the deformation behavior of the reservoir.



Figure 65 – Volumetric strain.



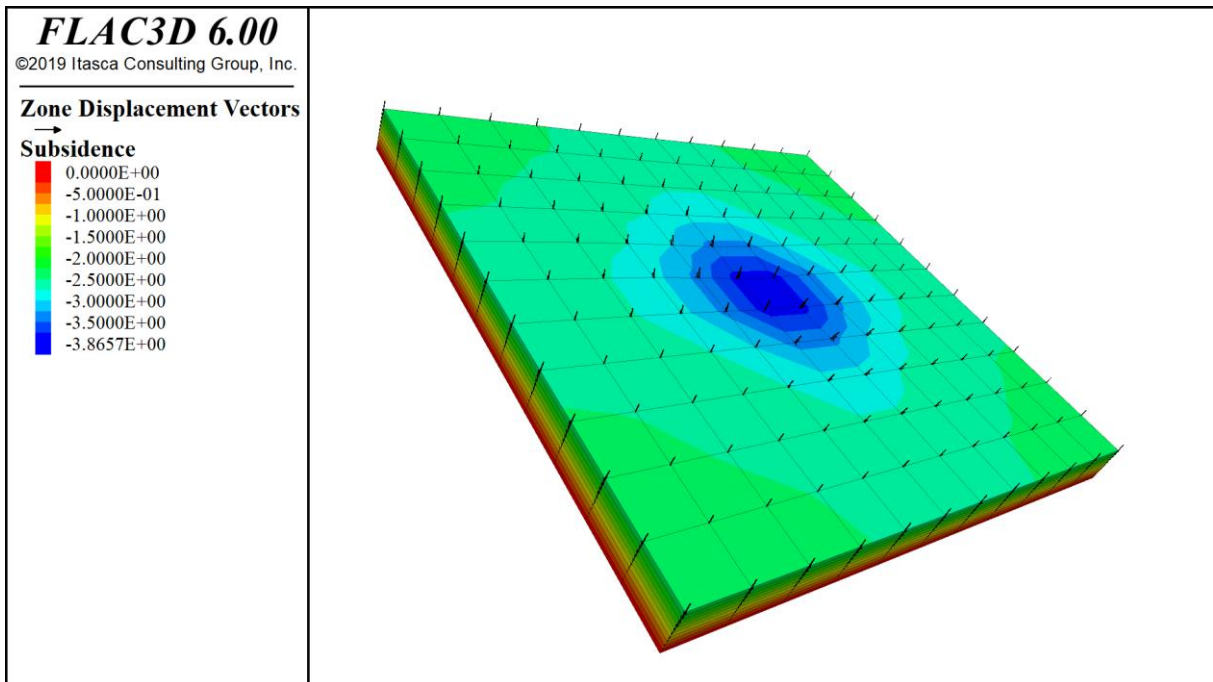
Source: Author, 2020.

#### 4.3.2. Subsidence

At the final of the simulation, the subsidence along the mesh of the reservoir model is presented as shown in Figure 66. Where there is also greater subsidence value in the center of the reservoir because it is the place of greatest deformation and where depletion occurs, naturally the greatest impacts of subsidence occur first in this region.

This behavior is justified by the uniaxial compression deformation to which the reservoir is subjected. In this way, an arc phenomenon occurs in unilateral compression. It is noted that there is an elevation gradient of subsidence between the zones approaching the reservoir well zone. Therefore, subsidence smoothing at the edges of the reservoir and a greater incidence in the center.

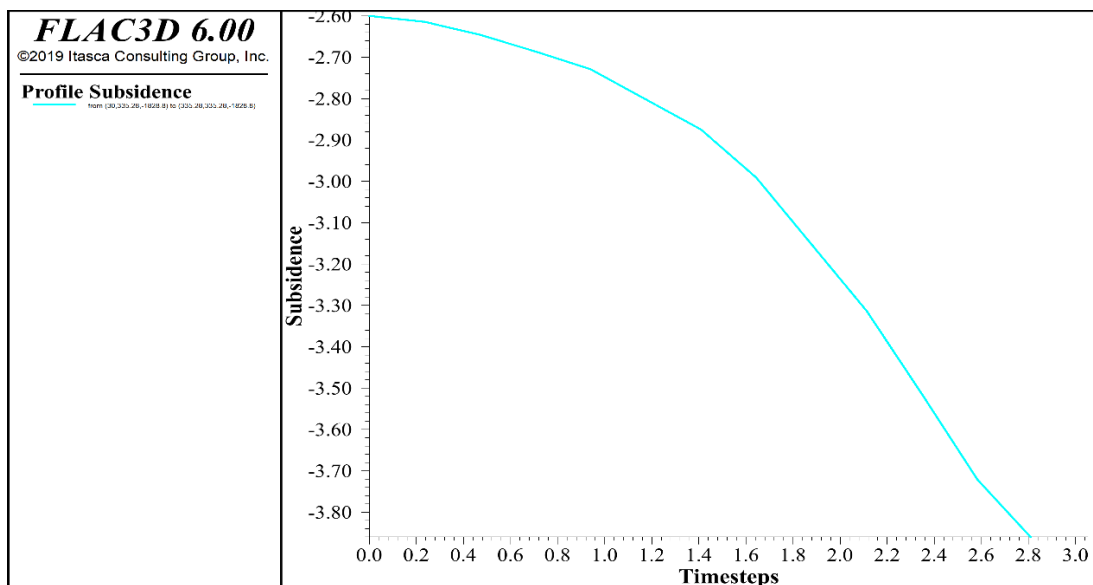
Figure 66 – Subsidence.



Source: Author, 2020.

The subsidence curve that develops on the reservoir surface is exported from FLAC3D, this way, the development of this curve is smoothed, since the development and storage of the subsidence values take place continuously and without losses, as seen in Figure 67.

Figure 67 – Subsidence profile in FLAC3D.

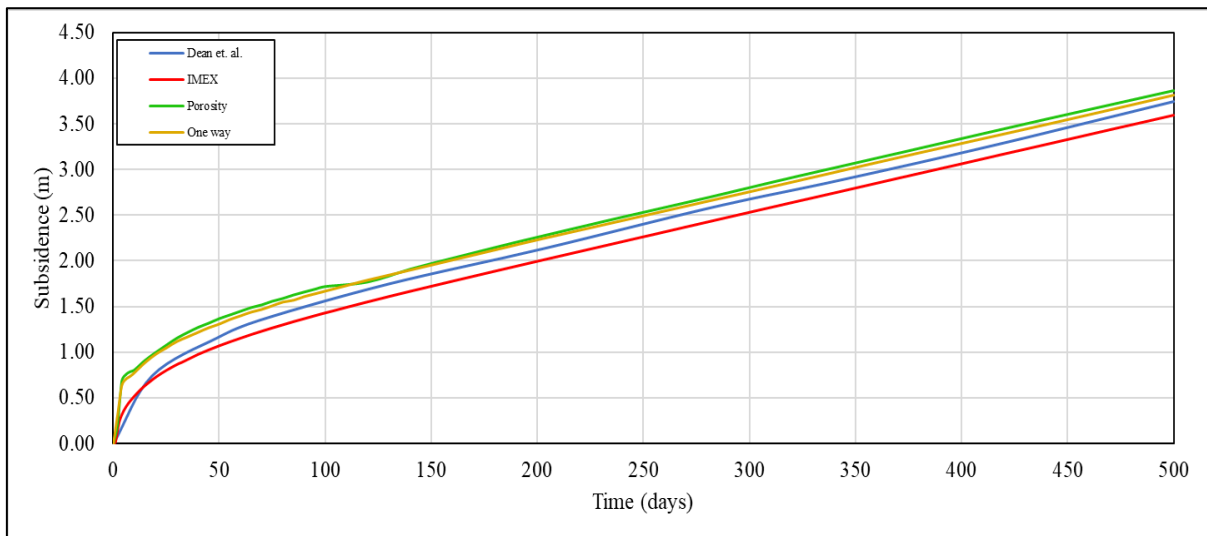


Source: Author, 2020.

It is observed that the curve is inverted in comparison with the other curves, this is since it is a compression, therefore the displacement is negative, importing the growth along the negative axis of the ordinates. FLAC3D informs the orientation graphically of the displacement in this way.

Therefore, the subsidence curve is applied in comparison to the three methods, by Dean *et al.* (2006), IMEX and one-way method, applied in positive values, to make a reliable comparison and using Excel for the graphic export. As shown in figure 68.

Figure 68 – Comparison of subsidence with the methodologies.



Source: Author, 2020.

A decline in a specific section of the FLAC3D method graph can be observed because the export occurs with the use of point values in each timestep of the result of each zone throughout the simulation. As in FLAC3D, the subsidence marking is dynamic throughout the simulation, the curve is obtained in a continuous way and without loss of information.

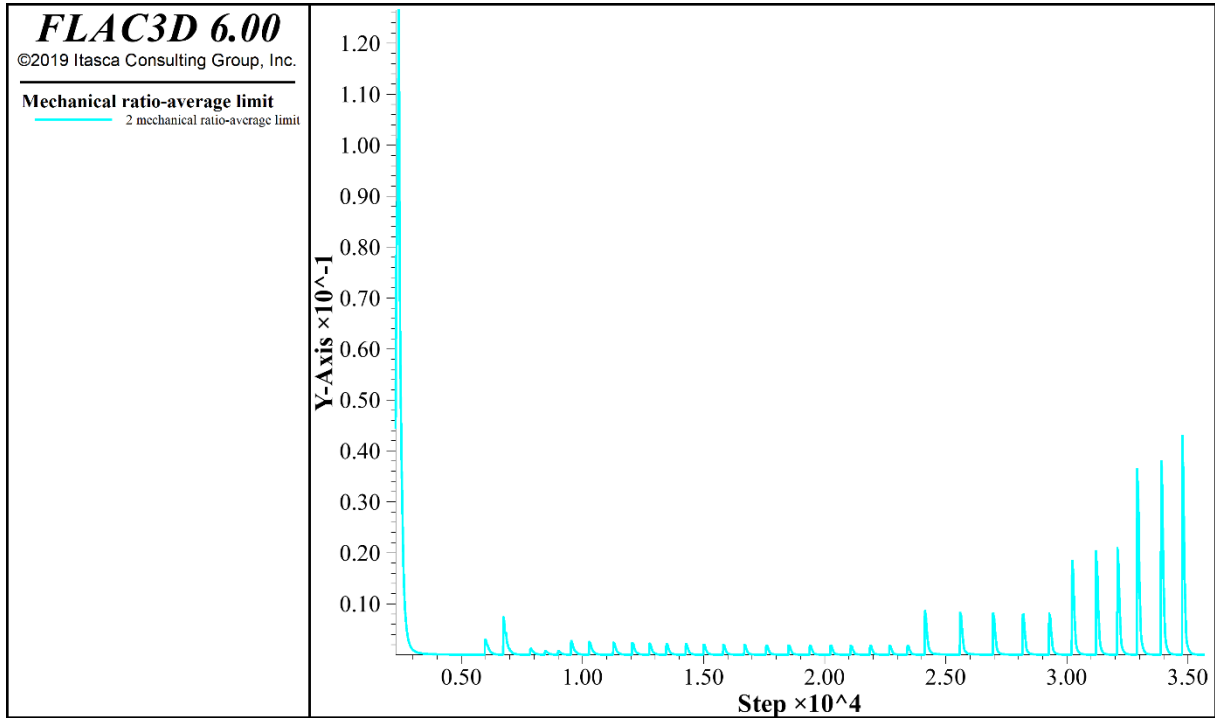
#### 4.3.3. Average mechanical ratio

It is also observed in the simulations with FLAC3D, the average mechanical ratio, which indicates the calculation rate that the simulator elaborates and the equilibrium trend that it reaches for the proposed model.

Figure 69 shows this average mechanical ratio, the first peak is about the initial calculations of the model, just after the model definitions and initial stresses, and it goes to a stable condition. The next peaks are of each timestep, it is noticed that there are different sizes

of peaks, it is because of the increase of the timesteps. This mechanical ratio-average limit shows the FLAC3D calculations and how it becomes in a stable condition.

Figure 69 – Mechanical ratio-average limit.

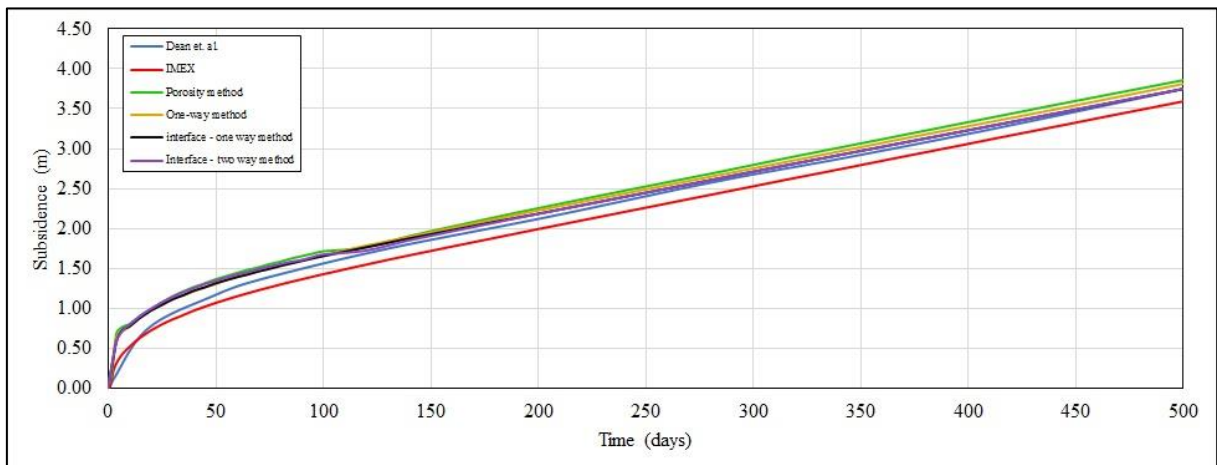


Source: Author, 2020.

#### 4.4. Fractured reservoir

Figure 70 presents the results of subsidence of the fracture of the two methods performed in FLAC3D, the one-way and the two-way methods. It is observed that the results converged to the same value, and when comparing with the result without fracture, the variation of values is subtle.

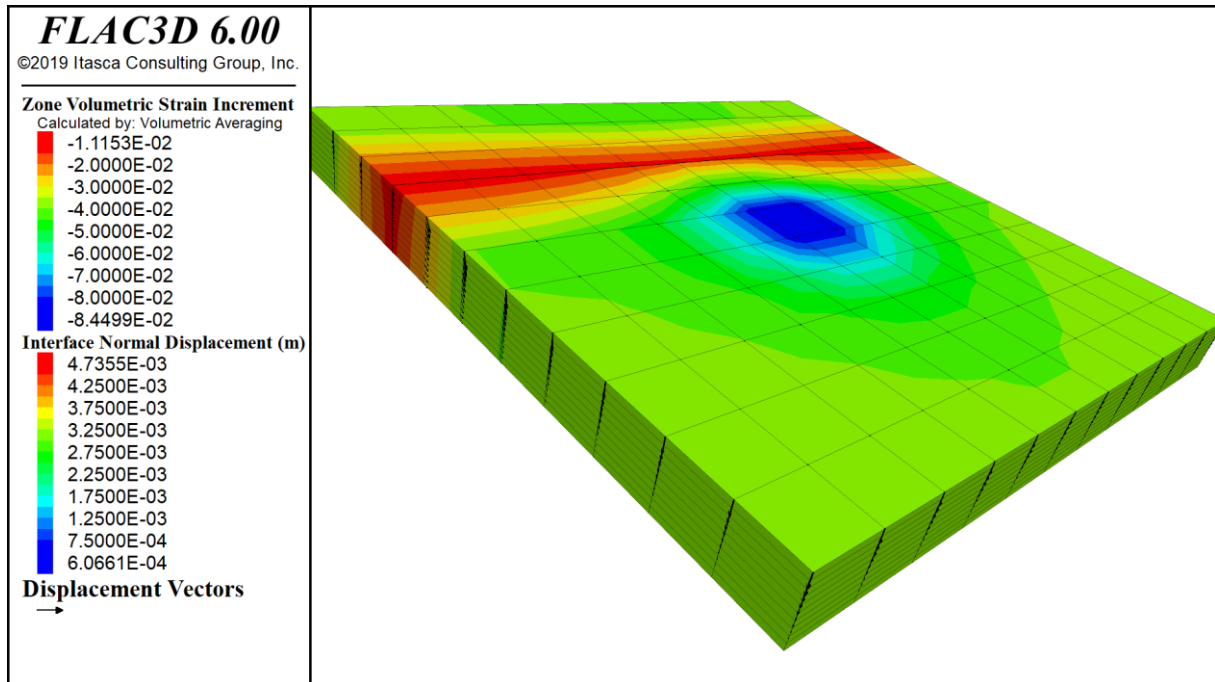
Figure 70 - Fractured reservoir subsidence



Source: Author, 2020.

The volumetric strain behavior along the reservoir shows how the fracture influences the reservoir in a general way, not in the production but in all the dynamics of the reservoir compression behavior. Therefore, Figure 71, 3D visualization of volumetric strain development by volumetric strain at the end of the 500 days simulation, is presented.

Figura 71 - Fractured reservoir volumetric strain 3D view



Source: Author, 2020.

In the interface region, a low volumetric strain is observed, which indicates that the interface has provided greater stiffness in this region, but low resistance behavior is generally expected in fractured regions, however, when fractures are in contact, the roughness and mechanical behavior can provide greater resistance to this region. Because of this, interface parameters are crucial to this determination.

## CONCLUSIONS AND RECOMMENDATIONS

The numerical analysis employed in oil reservoirs is important due to the variety of parameters and uncertainties associated with the reservoir system, given the geomechanical behavior associated with the performance during drilling, depletion, injection, and abandonment. All stages of these processes must be monitored to mitigate undesirable consequences and predict the actual behavior during operation.

It is observed that the simulations performed only with the software of CMG 2019, IMEX, guaranteed the satisfactory coupling in many aspects with the comparative paper in the study, but some parameters presented soft divergence, so it's propose as a future work the suggestion of analysis with the refining of the input data.

The iterative coupling between FLAC3D 6.0, MATLAB 2018, and CMG IMEX 2019 software presented a trend and satisfactory behavior to the problem of Dean *et al.* (2006), The model with updating methodology only in the porosity parameter of the reservoir through the variation of volumetric strain guaranteed the expected convergence of results, moreover, it is observed the influence that the variation of permeability causes to the reservoir system, providing scenarios with the inconsistency of behavior. It is also worth mentioning the model with the transmissibility factor, which presented satisfactory behavior when compared to the others.

The value of subsidence at the end of the model with fracture did not differ from the model without interface, but this is caused by the fact that the interface is far from the well and thus does not influence its behavior. However, the volumetric strain in the region of the fracture showed variation which indicates the influence that the fracture causes in the surroundings of this region.

Therefore, it is suggested as future works the approach in scenarios with the influence of the transmissibility factor and with the update of permeability, to obtain scenarios close to the reservoir dynamics found *in loco*, as well as the application of this type of numerical analysis in fractured environments and under the plastic deformation regime. In addition, it is suggested to validate this methodology with actual data from reservoirs and production wells.

Hence, it is observed that simulations elaborated with the iterative method, by association, provide results and simulation behaviors equivalent to the total coupling method, which is more complex, thus, with the iterative method of coupling, simplified methods are promoted allowing the elaboration of scenarios with greater complexity and less computational demand.

## 5. REFERENCES

- AADNØY, B.S; LOOYEH, R. **Mecânica das Rochas Aplicada: Perfuração e Projeto de Poços**. Elsevier. 1ª ed. Rio de Janeiro, BRA, 2014.
- AHMED, T. H. **Hydrocarbon Phase Behavior**. Gulf Publishing Company. Texas, USA, 1946.
- AHMED, T. H. **Reservoir Engineering Handbook**. Elsevier. 3ª ed. MA, USA, 2006.
- CHALATURNYK, R. **Permeability and Porosity Models Considering Anisotropy and Discontinuity of Coalbeds and Application in Coupled Simulation**. Elsevier Scientific Publishing Company, *Journal of Petroleum Science and Engineering* 74: 113-131. New York, USA, 2010.
- CHITSAZAN M; RAHMANI G; GHAFOURY H. **Investigation of Subsidence Phenomenon and Impact of Groundwater Level Drop on Alluvial Aquifer**, Case Study: Damaneh-Daran Plain in West of Isfahan Province, Iran. *Modeling Earth Systems and Environment*. 6: p. 1145-1161, 2020.
- CMG. **User's Guide IMEX**. Computer Modeling Group Ltd. Calgary, CAN, 2018.
- CONNELL, L. D. **Coupled flow and Geomechanical Processes During Gas Production from Coal Seams**. Elsevier Scientific Publishing Company, *International Journal of Coal Geology* 79: 18-28. New York, USA, 2009.
- CRAIG, F.F. Jr. **The Reservoir Engineering Aspect of Waterflooding, Monograph Series**. Society of Petroleum Engineers, SPE, Dallas, 134p, 1971.
- DEAN, R. H. et al. **A Comparison of Techniques for Coupling Porous Flow and Geomechanics**. Society of Petroleum Engineers, *SPE Journal* 79709: 132-140, 2006.
- DUSSEAULT, M. B. **Geomechanical challenges in petroleum reservoir exploitation**. *KSCE Journal of Civil Engineering*, 15(4):669-678. DOI: 10.1007/s12205-011-0007-5, 2011.
- EWING, R. E. **The Mathematics of Reservoir Simulation**. SIAM – Society for Industrial and Applied Mathematics. Philadelphia, USA, 1983.
- FANCHI, J. R. **Principles of Applied Reservoir Simulation**. Elsevier. 3 ed. Oxford, UK, 2006.
- GORAL, J. et al. **Confinement Effect on Porosity and Permeability of Shales**. Nature research. *Scientific Reports*. 10:49. <https://doi.org/10.1038/s41598-019-56885-y>, 11p, 2020.
- HOEK, E. **Strength of Jointed Masses**. Geotechnique. Vol. 33. No 3, p. 187-223, 1983.

- HOSSEINI, B. K; CHALATURNYK, R. **A Domain Splitting-Based Analytical Approach for Assessing Hydro-Thermo-Geomechanical Responses of Heavy-Oil Reservoirs**. Society of Petroleum Engineers, *SPE Journal* 170193: 300-315, 2017.
- HOWARD N. H. **Compressibility of Reservoir Rocks**. *Petroleum Transactions*, AIME. OKLA, USA, 1953.
- HUDSON, J.A; HARRISON J.P. **Engineering Rock Mechanics: An Introduction to the Principles**. Pergamon. 1<sup>a</sup> ed. London, UK, 1997.
- Itasca Consulting Group, Inc. **FLAC3D – Fast Lagrangian Analysis of Continua in 3 Dimensions**, Ver. 6.0 User's Manual. Itasca: Minneapolis, 2017.
- INOUE, N; FONTOURA, S. A. B. **Explicit Coupling Between Flow and Geomechanical Simulators**. International Conference on Computational Methods fo Coupled Problems in Science and Engineering, 2009.
- JAEGER, J.C; COOK, N.G.W. **Fundamentals of Rock Mechanics**. Chapman Hall, London, UK, 2007.
- JU, W. et al. **Stress Sensitivity in Naturally Fractured Reservoirs: A Case Study of the Lower Cretaceous Xiagou Formation, Qingxi Oilfield, Jiuxi Basin, Northwestern China**. *Geosciences Journal*. Vol 24, No. 3, p. 339-349. p ISSN 1226-4806 eISSN 1598-7477, 2020.
- LONGUEMARE, P. et al. **Geomechanics in Reservoir Simulation: Overview of Coupling Methods and Field Case Study**. *Oil & Gas Science and Technology – Rev. IFP*, Vol. 57. No. 5. p. 471-483, 2002.
- LYONS, W. **Working Guide to Reservoir Engineering**. Elsevier. 1<sup>a</sup> ed. MA, USA, 2010.
- MATLAB & Simulink for Building Simulation – State of the Art**, MathWorks, Inc. MA, USA, 2018.
- MCCAIN, W.D. Jr. **The Properties of Petroleum Fluids**. Peenwell. 2<sup>a</sup> ed. Oklahoma, USA, 1973.
- MIKELIC, A; WANG B; WHEELER M. F. **Numerical Convergence Study of Iterative Coupling for Coupled Flow and Geomechanics**. Springer Science + Business Media Dordrecht, *Comput Geosci* 18: 325-341 2014. Berlin, GER, 2014.
- MOHAMMADI, M. et al. **Experimental Study of the Relationship Between Porosity and Surface Area of Carbonate Reservoir Rocks**. *Journal of Petroleum Exploration and Production Technology*. 10: p. 1817-1834, 2020.
- PAN, F; SEPEHRNOORI K. **Development of a coupled geomechanics model for a parallel compositional reservoir simulator**. Society of Petroleum Engineers, *SPE Journal* 109867: 9p, 2007.



- PEREIRA, L.C; SÁNCHEZ M; GUIMARÃES L.J.N. **Uncertainty Quantification for Reservoir Geomechanics**. Geomechanics for Energy and the Environment. Vol. 8. p. 76-84, 2017.
- ROSA, A. J; CARVALHO R. S. **Previsão de Comportamento de Reservatórios de Petróleo: Métodos Analíticos**. Interciência. Rio de Janeiro, BRA, 2002.
- SEGURA, J.M et al. **Coupling a Fluid Flow Simulation With a Geomechanical Model of a Fractured Reservoir**. American Rock Mechanics Association – ARMA. 50th US Rock Mechanics / Geomechanics Symposium. Texas, USA, 2016.
- SETTARI, A; WATERS, D. A; BEHIE, G. A. **Reservoir Geomechanics: New Approach to Reservoir Engineering Analysis**. *Petroleum Society of CIM*. Paper NO. 99-116, 10p, 1999.
- STEVENSON, M; PINCZEWSKI, V. **SIMED II – Multi-Component Coalbed Gas Simulator**. User's Manual Version 1.21. Centre for Petroleum Engineering, University of New South Wales. Sydney, AUS, 1995.
- SUN, Z. et al. **Grain to Reservoir-Scale Modeling of Depletion-Induced Compaction and Implications on Production Rate**. Society of Petroleum Engineers, SPE Annual Technical Conference and Exhibition SPE 191390, 14p, 2020.
- TORTIKE, W. S; FAROUQ ALI, S. M. **Reservoir Simulation Integrated with Geomechanics**. The Journal of Canadian Petroleum Technology, 32, 5, 28-37, 1993.
- TRAN, D; SETTARI A; NGHIEM L. **New Iterative Coupling Between a Reservoir Simulator and a Geomechanics Module**. Society of Petroleum Engineers, *SPE Journal* 88989: 362-369, 2004.
- ZHAO, B. et al. **A Hybrid Approach for the Prediction of Relative Permeability Using Machine Learning of Experimental and Numerical Proxy SCAL Data**. Society of Petroleum Engineers, SPE Journal 196022: 16p, 2020.
- ZOBACK, M.D. **Reservoir Geomechanics**. Cambridge University Press. New York, USA, 2007.

## APPENDIX A –IMEX CMG 2019 Problem 1 programming.

## RESULTS SIMULATOR IMEX

```

** ===== INPUT/OUTPUT CONTROL =====
*TITLE1
'Dean Problem 1'
*TITLE2
'Dean Problem #1, Reservoir Embedded in Geomechanics Region'

*INUNIT *FIELD
*OUTUNIT *FIELD

*WPRN *GRID TIME
*OUTPRN *GRID *PRES

*WSRF WELL 1
*WSRF *GRIDDEFORM 2
*WSRF *GRID TIME
*WSRF SECTOR TIME
*OUTSRF *GRID *POROS *PRES *YOUNG *POISSON *VDISPL *STRESSH
*TSTRESI *TSTRESJ
*TSTRESK *STRAINVOL *YIELD *STRAINI *STRAINJ *STRAINK *STRESEFF
*STRESSM
*STRESI *STRESJ *STRESK *STRESEFF *VPOROSGEO *TSUBSIDGEO *SO *SG
*SW *REACFORCE

*OUTSRF *SPECIAL 6 6 1 / 2 2 2 *TSUBSIDGEO
*OUTSRF *SPECIAL 6 6 1 / 2 2 2 *PRES

*****
Definition of a fundamental cartesian grid
*****
GRID CART 11 11 10
KDIR DOWN

DI IVAR 11*200 DJ JVAR 11*200 DK ALL 1210*20

DTOP 121*6000

REFINE 1:11 1:11 1:10 INTO 2 2 2

NULL CON      1

PRPOR 3000
POR CON      0.2

```

CPOR 3.71E-4

PERMI CON 50

PERMJ CON 50

PERMK CON 5

PINCHOUTARRAY CON 1

\*\* ===== FLUID DEFINITIONS =====

**MODEL GASWATER**

PVTG EG 1

**	p	Eg	visg
14.696	4.80915	0.0125028	
213.716	71.4014	0.0126699	
412.737	140.731	0.0129125	
611.757	212.755	0.0132102	
810.777	287.342	0.0135585	
1009.8	364.241	0.0139562	
1208.82	443.071	0.0144024	
1407.84	523.314	0.0148959	
1606.86	604.33	0.0154345	
1805.88	685.393	0.0160148	
2004.9	765.753	0.016632	
2203.92	844.692	0.0172804	
2402.94	921.584	0.0179539	
2601.96	995.93	0.018646	
2800.98	1067.37	0.0193508	
3000	1135.67	0.0200628	

DENSITY GAS 0.0473

DENSITY WATER 62.4

REFPW 14.7

BWI 1.0

CW 0

VWI 1.0 CVW 0.0

\*\* ===== ROCK-FLUID PROPERTIES =====

**ROCKFLUID**

RPT 1

\*\* Sw krw krg

```

SWGT 0 0 1 0.0
0.1 0.1954 0.804562 0.0 0.2
0.3697 0.6303 0.0 0.3
0.5228 0.4772 0.0 0.4
0.6546 0.3454 0.0 0.5
0.7652 0.2348 0.0
0.6 0.8545 0.1455 0.0 0.7 0.9225 0.0775 0.0 0.8 0.9693 0.0307 0.0
0.9 0.9948 0.0052 0.0
1 1 0 0.0

```

\*\* ===== INTTAL CONDITIONS =====

### INITIAL

VERTICAL DEPTH\_AVE WATER\_GAS NOTRANZONE EQUIL

```

*REFDEPTH 6000
*REFPRES 3000
*DWGC 5500

```

\*\* ===== NUMERICAL CONTROL =====

### NUMERICAL

```

*DTMAX 10

```

\*\* ===== GEOMECHANIC MODEL =====

### GEOMECH

GEOM3D

```

GEOROCK 1
ELASTMOD 1e4
POISSRATIO 0.3
COHESION 1E10

```

```

GPTOLMUL 0.1

```

```

GEOGRID GCART 22 22 20
GDI GIVAR 22*100 GDJ GJVAR 22*100
GDK GKVAR 20*10

```

```

GEODEPTH *GTOP 1 1 1 6000.0

```

```

GCFACTOR 1

```

```

GCOUPLING 2
CALIB_POR
UTSTRESS

```

STRESS3D 0 0 6000.0 0.0 0.0 0.0 STRESSGRAD3D 0 0 -1.0231 0.0 0 0  
 YOUNGMAP CON 10E4 POISSONMAP CON 0.3 COHESIONMAP CON 1E10  
 \*GOUTSRF GGRID \*YOUNG \*POISSON \*VDISPL \*STRESI \*STRESJ \*STRESK  
 \*TSUBSIDGEO \*PRES \*STRAINK

**RUN**

\*\* =====RECURRENT DATA =====

DATE 2019 1 1 WELL 'PROD1'

PRODUCER 'PROD1'

OPERATE MIN BHP 100.0 CONT

OPERATE MAX STW 15000.0 CONT

\*\* rad geofac wfrac skin

GEOMETRY K 0.25 0.249 1.0 0.0 PERF GEO 'PROD1'

\*\* UBA ff Status Connection

6 6 1 / 2 2 1	1.0 OPEN FLOW-TO	'SURFACE'	REFLAYER	6 6 1 / 2 2 2
1.0 OPEN FLOW-TO	1 6 6 2 / 2 2 1	1.0 OPEN FLOW-TO	2 6 6 2 / 2 2 2	
1.0 OPEN FLOW-TO	3 6 6 3 / 2 2 1	1.0 OPEN FLOW-TO	4 6 6 3 / 2 2 2	
1.0 OPEN FLOW-TO	5 6 6 4 / 2 2 1	1.0 OPEN FLOW-TO	6 6 6 4 / 2 2 2	
1.0 OPEN FLOW-TO	7 6 6 5 / 2 2 1	1.0 OPEN FLOW-TO	8 6 6 5 / 2 2 2	
1.0 OPEN FLOW-TO	9 6 6 6 / 2 2 1	1.0 OPEN FLOW-TO	10 6 6 6 / 2 2 2	
1.0 OPEN FLOW-TO	11 6 6 7 / 2 2 1	1.0 OPEN FLOW-TO	12 6 6 7 / 2 2 2	
1.0 OPEN FLOW-TO	13 6 6 8 / 2 2 1	1.0 OPEN FLOW-TO	14 6 6 8 / 2 2 2	
1.0 OPEN FLOW-TO	15 6 6 9 / 2 2 1	1.0 OPEN FLOW-TO	16 6 6 9 / 2 2 2	
1.0 OPEN FLOW-TO	17 6 6 10 / 2 2 1	1.0 OPEN FLOW-TO	18 6 6 10 / 1 2	
2	1.0 OPEN FLOW-TO	19		

TIME 50

TIME 100

TIME 150

TIME 200

TIME 250

TIME 300

TIME 350

TIME 400

TIME 450

TIME 500

**\*STOP**

## APPENDIX B –IMEX CMG 2019 Problem 2 programming.

## RESULTS SIMULATOR IMEX

```

** ===== INPUT/OUTPUT CONTROL =====

*TITLE1
'Dean Problem 2'
*TITLE2
'Dean Problem #2, Reservoir Embedded in Geomechanics Region'

*INUNIT *FIELD
*OUTUNIT *FIELD

*WPRN *GRID 0
*OUTPRN *GRID *PRES

*WSRF *GRIDDEFORM 2
*WSRF *GRID 2
*WSRF WELL 1
WSRF GRID TIME
*OUTSRF *GRID *POROS *PRES *YOUNG *POISSON *VDISPL *STRESSH
*TSTRESI *TSTRESJ *TSTRESK *STRAINVOL *YIELD *STRAINI *STRAINJ
*STRAINK *STRESEFF *STRESSM
*STRESI *STRESJ *STRESK *STRESEFF *VPOROSGEO *TSUBSIDGEO *SO *SG
*SW *REACFORCE

OUTSRF SPECIAL 7 7 1 TSUBSIDGEO
OUTSRF SPECIAL 7 7 1 PRES
*****
Definition of a fundamental cartesian grid
*****
GRID VARI 13 13 10

DI IVAR 4*200 2*100 200 2*100 4*200 DJ JVAR 4*200 2*100 200 2*100 4*200
DK CON 20

KDIR DOWN

DTOP 169*6000

PERMI CON      50
PERMJ CON      50
PERMK CON      5

```

NULL CON 1

POR CON 0.2

PRPOR 3000

CPOR 6.0E-4

PINCHOUTARRAY CON 1

\*\* ===== FLUID DEFINITIONS =====

**MODEL GASWATER**

TRES 150

PVTG EG 1

**	p	Eg	visg
14.696	4.80915	0.0125028	
213.716	71.4014	0.0126699	
412.737	140.731	0.0129125	
611.757	212.755	0.0132102	
810.777	287.342	0.0135585	
1009.8	364.241	0.0139562	
1208.82	443.071	0.0144024	
1407.84	523.314	0.0148959	
1606.86	604.33	0.0154345	
1805.88	685.393	0.0160148	
2004.9	765.753	0.016632	
2203.92	844.692	0.0172804	
2402.94	921.584	0.0179539	
2601.96	995.93	0.018646	
2800.98	1067.37	0.0193508	
3000	1135.67	0.0200628	

DENSITY GAS 0.0473

DENSITY WATER 62.4

REFPW 14.7

BWI 1.0

CW 0

VWI 1.0 CVW 0.0

\*\* ===== ROCK-FLUID PROPERTIES =====

**ROCKFLUID**

RPT 1

\*SWT

```
**   SW   KRW   KRO
0           0 1           1
```

```
*SLT
```

```
**SL   KRG   KROG
0       1
1       0
```

```
** ===== INTTTAL CONDITIONS =====
```

### INITIAL

```
VERTICAL DEPTH_AVE WATER_GAS NOTRANZONE EQUIL
```

```
*REFDEPTH 6000
*REFPRES 3000
*DWGC 5500
```

```
** ===== NUMERICAL CONTROL =====
```

### NUMERICAL

```
*DTMAX 10
```

```
** ===== GEOMECHANIC MODEL =====
```

### GEOMECH

```
GEOM3D
GEOROCK 1
ELASTMOD 1e4
POISSRATIO 0.3
COHESION 1E10
```

```
GPTOLMUL 0.01
```

```
GCFACTOR 0
```

```
GCOUPLING 2
```

```
CALIB_POR
```

```
YOUNGMAP CON 10E4 POISSONMAP CON 0.3 COHESIONMAP CON 1E10
```

### UTSTRESS

```
STRESS3D 4000 4000 6000 0 0 0 STRESSGRAD3D 0 0 -1.0231 0 0 0
```

```
PRESCBC3D
```

```
IJK 1:13 1:13 10 5:8 03 0.0
```

```
GEOGRID GCART 13 13 10
```



GDI GIVAR 4\*200 2\*100 200 2\*100 4\*200 GDJ GJVAR 4\*200 2\*100 200 2\*100  
 4\*200  
 GDK GKVAR 10\*20

GEODEPTH \*GTOP 1 1 1 6000.00

\*GOUTSRF GGRID \*YOUNG \*POISSON \*VDISPL \*STRESI \*STRESJ \*STRESK  
 \*TSUBSIDGEO \*PRES \*STRAINK

**RUN**

\*\* =====RECURRENT DATA =====

DATE 2019 1 1 WELL 'PROD1'

PRODUCER 'PROD1'

OPERATE MIN BHP 100.0 CONT

OPERATE MAX STW 15000.0 CONT

\*\* rad geofac wfrac skin

GEOMETRY K 0.25 0.249 1.0 0.0 PERF GEO 'PROD1'

\*\* UBA ff Status Connection

7 7 1 1.0 OPEN FLOW-TO 'SURFACE' REFLAYER 7 7 2 1.0 OPEN  
 FLOW-TO 1 7 7 3 1.0 OPEN FLOW-TO 2 7 7 4 1.0 OPEN FLOW-TO  
 3 7 7 5 1.0 OPEN FLOW-TO 4 7 7 6 1.0 OPEN FLOW-TO 5 7 7 7  
 1.0 OPEN FLOW-TO 6 7 7 8 1.0 OPEN FLOW-TO 7 7 7 9 1.0 OPEN  
 FLOW-TO 8 7 7 10 1.0 OPEN FLOW-TO 9

TIME 50

TIME 100

TIME 150

TIME 200

TIME 250

TIME 300

TIME 350

TIME 400

TIME 450

TIME 500 **\*STOP**

## APPENDIX C –IMEX CMG 2019 Problem 3 programming.

## RESULTS SIMULATOR IMEX

\*\* ===== INPUT/OUTPUT CONTROL =====

\*TITLE1

'Dean Problem 3'

\*TITLE2

'Dean Problem #3, Reservoir Embedded in Geomechanics Region'

\*INUNIT \*FIELD

\*OUTUNIT \*FIELD

\*WPRN \*GRID TIME

\*OUTPRN \*GRID \*ALL

\*OUTPRN \*GRID \*PRES

\*OUTPRN \*WELL \*ALL

\*OUTSRF \*WELL \*LAYER \*ALL

\*OUTSRF \*FLUX-SECTOR \*ALL

\*WSRF \*SECTOR \*TIME

\*WSRF \*GRIDDEFORM \*TIME

\*WSRF \*GRID \*TIME

\*OUTSRF \*GRID \*POROS \*PRES \*YOUNG \*POISSON \*VDISPL \*STRESSH

\*TSTRESI \*TSTRESJ \*TSTRESK \*STRAINVOL \*YIELD \*STRAINI \*STRAINJ

\*STRAINK \*STRESEFF \*STRESSM

\*STRESI \*STRESJ \*STRESK \*STRESEFF \*VPOROSGEO \*TSUBSIDGEO \*SW

\*GEORTYPE \*SBDZ

\*OUTSRF \*SPECIAL 1 6 1 \*PRES

\*OUTSRF \*SPECIAL 1 6 1 \*POROS

\*OUTSRF \*SPECIAL 1 6 1 \*VPOROSGEO

\*OUTSRF \*SPECIAL 1 6 1 \*STRESMNP

\*OUTSRF \*SPECIAL 1 6 1 \*STRESMXP

\*OUTSRF \*SPECIAL 1 6 1 \*TSUBSIDGEO

\*OUTSRF \*SPECIAL 6 6 1 \*PRES

\*OUTSRF \*SPECIAL 6 6 1 \*POROS

\*OUTSRF \*SPECIAL 6 6 1 \*VPOROSGEO

\*OUTSRF \*SPECIAL 6 6 1 \*STRESMNP

\*OUTSRF \*SPECIAL 6 6 1 \*STRESMXP

\*OUTSRF \*SPECIAL 6 6 1 \*TSUBSIDGEO

\*OUTSRF \*SPECIAL 11 11 1 \*PRES

\*OUTSRF \*SPECIAL 11 11 1 \*POROS

\*OUTSRF \*SPECIAL 11 11 1 \*VPOROSGEO  
 \*OUTSRF \*SPECIAL 11 11 1 \*STRESMNP  
 \*OUTSRF \*SPECIAL 11 11 1 \*STRESMP  
 \*OUTSRF \*SPECIAL 11 11 1 \*TSUBSIDGEO  
 \*OUTSRF \*SPECIAL 11 11 6 \*PRES  
 \*OUTSRF \*SPECIAL 11 11 6 \*POROS  
 \*OUTSRF \*SPECIAL 11 11 6 \*VPOROSGEO  
 \*OUTSRF \*SPECIAL 11 11 6 \*STRESMNP  
 \*OUTSRF \*SPECIAL 11 11 6 \*STRESMP  
 \*OUTSRF \*SPECIAL 11 11 6 \*TSUBSIDGEO

\*OUTSRF \*SPECIAL 6 11 6 \*PRES  
 \*OUTSRF \*SPECIAL 6 11 6 \*POROS  
 \*OUTSRF \*SPECIAL 6 11 6 \*VPOROSGEO  
 \*OUTSRF \*SPECIAL 6 11 6 \*STRESMNP  
 \*OUTSRF \*SPECIAL 6 11 6 \*STRESMP

\*\* ===== DEFINITION OF FUNDAMENTAL CARTESIAN GRID =====

### **GRID VARI 21 21 12**

DI IVAR 5\*4000 11\*2000 5\*4000  
 DJ JVAR 5\*2000 11\*1000 5\*2000  
 DK KVAR 4000 3000 2000 800 200 5\*50 2\*100

### **KDIR DOWN**

\*DTOP 441\*0

\*POR \*CON 0

\*Mod 6:16 6:16 6:10 = 0.25

\*PERMI \*CON 0

\*Mod 6:16 6:16 6:10 = 100

\*PERMJ \*CON 0

\*Mod 6:16 6:16 6:10 = 100

\*PERMK \*CON 0

\*Mod 6:16 6:16 6:10 = 10

\*PRPOR 14.7

\*CPOR 3.33E-4

\*CCPOR \*MATRIX 3.33E-4

```

*CPRPOR *MATRIX 14.7
*CROCKTYPE 2
*CCPOR *MATRIX 3.33E-6
*CPRPOR *MATRIX 14.7

*CTYPE *MATRIX *IJK 1:21 1:21 1:12 2
*CTYPE *MATRIX *IJK 6:16 6:16 6:10 1

*SECTOR 'RESERVOIR' 6:16 6:16 6:10

```

```
** ===== FLUID DEFINITIONS =====
```

```
*MODEL *GASWATER
```

```
*PVTG EG 1
```

```

1000. 5.000 0.010
1500. 300.000 0.015
2000. 600.000 0.019
2500. 800.000 0.021
3000. 1000.000 0.023
5000. 2000.000 0.030

```

```

*DENSITY *GAS 0.7575
*DENSITY *WATER 62.4
*BWI 1
*CW 3E-6
*REFPW 14.7
*VWI 1
*CVW 0.0

```

```
** ===== ROCK-FLUID PROPERTIES =====
```

```
*ROCKFLUID
```

```
*RPT 1
```

```
*SWT
```

```

** SW KRW
0 0 1
1

```

```
*SLT
```

```
**SL KRG
```

```
0 1
```

1 0

\*\* ===== INTTAL CONDITIONS =====

**\*INITIAL**

\*VERTICAL\_DEPTH\_AVE \*WATER\_GAS

\*NREGIONS 2

\*ITYPE \*IJK

1:21 1:21 1:12 1

6:16 6:16 6:10 2

PB \*CON 0

PB \*CON 3000

REFDEPTH 0

\*REFDEPTH 10000

\*REFPRES 0

\*REFPRES 4370

\*DWGC 0

\*DWGC 0

\*\* ===== NUMERICAL CONTROL =====

**\*NUMERICAL**

\*DTMAX 5.0

\*NORM \*PRESS 1000

\*CONVERGE \*PRESS 0.0005

\*NCUTS 10

\*\* ===== GEOMECHANIC MODEL =====

**\*GEOMECH** \*\* geomechanics main keyword

\*GEOM3D

\*GCOUPLING 2

\*CALIB\_POR

\*GCFACOR 1

\*GPTOLMUL 0.5

```

GEOGRID GCART 21 21 12
GDI *GIVAR 5*4000 11*2000 5*4000

GDJ *GJVAR 5*2000 11*1000 5*2000

GDK *GKVAR 4000 3000 2000 800 200 5*50 2*100

*GEODEPTH *GTOP 1 1 1 0

*GEOROCK 1
*ELASTMOD 1E6
*POISSRATIO .25
*COHESION 1.0E10
**
*GEOROCK 2
*ELASTMOD 1E4
*POISSRATIO .25
*COHESION 1.0E10

*GEOTYPE ijk
**      i      j      k      rocktype
1:21   1:21   1:12           1
6:16   6:16   6:10           2

*UTSTRESS
*STRESS3D 0.0 0.0 0.0 0.0 0.0 0.0
*STRESSGRAD3D 0.0 0.0 -0.9869 0.0 0.0 0.0
*GOUTSRF GGRID *YOUNG *POISSON *VDISPL *STRESI *STRESJ *STRESK
*TSUBSIDGEO *GEORTYPE *STRESSM PRES *TSTRESI *TSTRESJ *TSTRESK
*GEODOMAIN ALL

*RUN

** =====RECURRENT DATA =====

*DATE 2018 12 31
*DTWELL 1.0

*WELL 1 'prod1'
*PRODUCER 'prod1'
*OPERATE *MAX *STW 50000
*GEOMETRY *K 0.25 0.41 1.0 0.0
*PERF *GEO 'prod1'

```

11 11 6 1.0 flow-to 'SURFACE' reflater  
11 11 7 1.0 flow-to 1  
11 11 8 1.0 flow-to 2  
11 11 9 1.0 flow-to 3  
11 11 10 1.0 flow-to 4

\*TIME 1

\*TIME 3

\*TIME 30

\*TIME 100

\*TIME 250

\*TIME 400

\*DTMAX 200

\*TIME 1000

TIME 2000

TIME 3000

TIME 4000

\*STOP

## APPENDIX D –IMEX CMG 2019 Problem 4 programming.

## RESULTS SIMULATOR IMEX 201710

\*\* ===== INPUT/OUTPUT CONTROL =====

\*TITLE1

'Dean Problem 4'

\*TITLE2

'Dean Problem #4, Water Flood - Single \*CART Grid'

\*INUNIT \*FIELD

\*OUTUNIT \*FIELD

\*WPRN \*GRID 10

\*OUTPRN \*GRID \*PRES

OUTSRF GRID VISO

OUTSRF GRID VISG

OUTSRF GRID STRMLN VELOCRC

OUTSRF FLUX\_SECTOR ALL SC

OUTPRN FLUX\_SECTOR ALL

\*WSRF \*GRIDDEFORM 1

\*WSRF \*GRID 1

\*OUTSRF \*GRID \*POROS \*PRES \*YOUNG \*POISSON \*VDISPL \*STRESSH

\*TSTRESI \*TSTRESJ \*TSTRESK \*STRAINVOL \*YIELD \*STRAINI \*STRAINJ

\*STRAINK \*STRESEFF \*STRESSM

\*STRESI \*STRESJ \*STRESK \*STRESEFF \*VPOROSGEO \*TSUBSIDGEO \*SO \*SG

\*SW \*REACFORCE BULKVOL SBDZ

\*OUTSRF \*SPECIAL 11,11,1 \*PRES

\*OUTSRF \*SPECIAL 11,11,1 \*POROS

\*OUTSRF \*SPECIAL 11,11,1 \*VPOROSGEO

\*OUTSRF \*SPECIAL 11,11,1 \*TSUBSIDGEO

\*\* ===== DEFINITION OF FUNDAMENTAL CARTESIAN GRID =====

**GRID CART 21 21 11**

DI CON 60

DJ CON 60

DK CON 20

KDIR DOWN



\*DTOP 441\*4000

NULL CON 1

\*POR \*CON 0.30

\*PERMI \*KVAR

5.0 100.0 20.0 20.0 20.0 100.0 20.0 20.0 100.0 20.0 20.0

\*PERMJ \*KVAR

5.0 100.0 20.0 20.0 20.0 100.0 20.0 20.0 100.0 20.0 20.0

\*PERMK \*KVAR

0.05 1.0 0.2 0.2 0.2 1.0 0.2 0.2 1.0 0.2 0.2

PINCHOUTARRAY CON 1

\*PRPOR 14.7

\*CPOR 4.15E-5

SECTOR 'PROD1' 21:21 21:21 1:11

\*\* ===== FLUID DEFINITIONS =====

**\*MODEL \*BLACKOIL**

\*PVT

** p	rs	bo	eg	viso	visg
300.00	61.00	1.0663	97.48299	1.50	0.02
600.00	116.10	1.0931	200.48919	1.50	0.02
900.00	168.10	1.1173	308.06198	1.50	0.02
1200.00	219.70	1.1408	419.19933	1.50	0.02
1600.00	289.40	1.1718	570.71111	1.50	0.02
2000.00	360.80	1.2030	722.64778	1.50	0.02
2400.00	434.20	1.2346	871.15602	1.50	0.02
2800.00	510.20	1.2667	1012.55569	1.50	0.02
3000.00	552.10	1.2843	1084.48108	1.50	0.02
3200.00	588.90	1.2996	1143.77216	1.50	0.02
3600.00	670.80	1.3334	1262.46686	1.50	0.02
4000.00	756.10	1.3683	1367.61488	1.50	0.02
4500.00	868.50	1.4137	1478.63374	1.50	0.02

\*DENSITY \*GAS 0.057

\*DENSITY \*WATER 62.4

\*DENSITY \*OIL 56.0

\*CO 1E-5

\*CVO 0.0

\*BWI 1.0

\*CW 3.0E-6

\*REFPW 14.7  
 \*VWI 1.0  
 \*CVW 0.0

\*\* ===== ROCK-FLUID PROPERTIES =====

**\*ROCKFLUID**

\*RPT 1

\*SWT       \*\*Water-oil relative permeabilities

** Sw	Krw	Krow	Pwc
** ----	-----	-----	-----
0.2	0.0	0.5102	6.4
0.25	0.0039	0.4133	5.6
0.3	0.0156	0.3266	4.9
0.35	0.0352	0.2500	4.2
0.4	0.0625	0.1837	3.6
0.45	0.0977	0.1276	3.0
0.50	0.1406	0.0816	2.5
0.55	0.1914	0.0459	2.0
0.60	0.2500	0.0204	1.6
0.65	0.3164	0.0051	1.2
0.70	0.3906	0.0	0.9
0.80	0.5625	0.0	0.4
0.90	0.7656	0.0	0.1
1.00	1.0	0.0	0.0

\*SLT       \*\*Liquid-gas relative permeabilities

** Sl	Krg	Krog	Pgc
** ----	-----	-----	-----
0.2	0.6303	0.0	3.2
0.25	0.5511	0.0 2.8 0.3	0.4772 0.0 2.5
0.35	0.4086	0.0026 2.1 0.4	0.3454 0.0104
1.8			
0.45	0.2874	0.0234	1.5
0.5	0.2348	0.0416	1.3
0.55	0.1875	0.0651	1.0
0.6	0.1455	0.0937	0.8
0.65	0.1089	0.1275	0.6
0.7	0.0775	0.1666 0.5 0.75	0.0514 0.2108
0.3 0.8	0.0307	0.2709 0.2	

0.85		0.0153	0.3149		0.1
0.9		0.0052	0.3748		0.0
0.95		0.0004	0.4398		0.0 0.97
	0.0		0.4673	0.0	
1.0		0.0	0.5102		0.0

\*\* ===== INTTAL CONDITIONS =====

**\*INITIAL**

\*VERTICAL \*BLOCK\_CENTER \*WATER\_OIL\_GAS

\*PB \*CON 3000

\*REFDEPTH 4010.

\*REFPRES 3010.

\*DWOC 4310.

\*DGOC 3900.

\*\* ===== NUMERICAL CONTROL =====

**\*NUMERICAL**

\*DTMAX 365

\*NORM \*PRESS 100

\*CONVERGE \*PRESS 2.0

\*\* ===== GEOMECHANIC MODEL =====

**\*GEOMECH**      **\*\* geomechanics main keyword**

\*GEOM3D

\*GCOUPLING 2

\*CALIB\_POR

\*GCFACTOR 1.0

\*GPTOLMUL 0.1

GEOGRID GCART 21 21 11

GDI \*GCON 60

GDJ \*GCON 60

GDK \*GCON 20

\*INTPOWER 5

\*RCONBT \*ALL

\*\* CONSTRAINT ON THE BOTTOM OF RESERVOIR

```

*RCONLF *ALL          ** CONSTRAINT ON THE LEFT OF RESERVOIR
*RCONRT *ALL          ** CONSTRAINT ON THE RIGHT OF RESERVOIR
*RCONBK *ALL          ** CONSTRAINT ON THE BACK OF RESERVOIR
*RCONF T *ALL         ** CONSTRAINT ON THE FRONT OF RESERVOIR

```

```
*GEODEPTH *GTOP 1 1 1 4000
```

```

*GEOROCK 1
*ELASTMOD 5.0e4
*POISSRATIO .35
*COHESION 1E10
*GEOTYPE ijk
**   i   j   k  rocktype
1:21  1:21  1:11  1

```

```
*UTSTRESS
```

```
*STRESS3D 2000 2000 4000 0.0 0.0 0.0
```

```
*STRESSGRAD3D -0.4628 -0.4628 -0.9256 0.0 0.0 0.0
```

```
*RUN
```

```
** =====RECURRENT DATA =====
```

```
*DATE 2019 01 29
```

```
*DTWELL 1.0
```

```
WELL 'INJ1'
```

```
INJECTOR MOBWEIGHT 'INJ1'
```

```
*INCOMP WATER
```

```
OPERATE MAX BHP 4000.0
```

```
OPERATE MAX STW 500.0
```

```
**   rad geofac wfrac skin
```

```
GEOMETRY          K 0.25 0.3 1.0 0.0
```

```
PERF   GEO 'INJ1'
```

```
** UBA          ff      Status Connection
```

```

1 1 1      0.2 OPEN  FLOW-FROM 'SURFACE' REFLAYER
1 1 2      0.2 OPEN  FLOW-FROM 1
1 1 3      0.2 OPEN  FLOW-FROM 2
1 1 4      0.2 OPEN  FLOW-FROM 3
1 1 5      0.2 OPEN  FLOW-FROM 4
1 1 6      0.2 OPEN  FLOW-FROM 5
1 1 7      0.2 OPEN  FLOW-FROM 6
1 1 8      0.2 OPEN  FLOW-FROM 7
1 1 9      0.2 OPEN  FLOW-FROM 8

```

1 1 10 0.2 OPEN FLOW-FROM 9  
 1 1 11 0.2 OPEN FLOW-FROM 10

WELL 'PROD1'

PRODUCER 'PROD1'

OPERATE MIN BHP 500.0

OPERATE MAX STO 750.0

\*\* rad geofac wfrac skin

GEOMETRY K 0.25 0.3 1.0 0.0

PERF GEO 'PROD1'

** UBA	ff	Status	Connection
21 21 1	0.2	OPEN	FLOW-TO 'SURFACE' REFLAYER
21 21 2	0.2	OPEN	FLOW-TO 1
21 21 3	0.2	OPEN	FLOW-TO 2
21 21 4	0.2	OPEN	FLOW-TO 3
21 21 5	0.2	OPEN	FLOW-TO 4
21 21 6	0.2	OPEN	FLOW-TO 5
21 21 7	0.2	OPEN	FLOW-TO 6
21 21 8	0.2	OPEN	FLOW-TO 7
21 21 9	0.2	OPEN	FLOW-TO 8
21 21 10	0.2	OPEN	FLOW-TO 9
21 21 11	0.2	OPEN	FLOW-TO 10

\*TIME 3650

\*TIME 9125

**STOP**

## APPENDIX E – Grid block creation in FLAC3D.

**zone** create brick size 1 1 1 ...

point 0 (0.00,609.60,-1834.90) point 1 (60.96,609.60,-1834.90) point 2  
(0.00,670.56,1834.90) point 3 (0.00,609.60,-1828.80) ...

point 4 (60.96,670.56,-1834.90) point 5 (0.00,670.56,-1828.80) point 6 (60.96,609.60,-  
1828.80) point 7 (60.96,670.56,-1828.80)

**zone** create brick size 1 1 1 ...

point 0 (60.96,609.60,-1834.90) point 1 (121.92,609.60,-1834.90) point 2  
(60.96,670.56,1834.90) point 3 (60.96,609.60,-1828.80) ...

point 4 (121.92,670.56,-1834.90) point 5 (60.96,670.56,-1828.80) point 6  
(121.92,609.60,-1828.80) point 7 (121.92,670.56,-1828.80)

**zone** create brick size 1 1 1 ...

point 0 (121.92,609.60,-1834.90) point 1 (182.88,609.60,-1834.90) point 2  
(121.92,670.56,-1834.90) point 3 (121.92,609.60,-1828.80) ...

point 4 (182.88,670.56,-1834.90) point 5 (121.92,670.56,-1828.80) point 6  
(182.88,609.60,-1828.80) point 7 (182.88,670.56,-1828.80)

**zone** create brick size 1 1 1 ...

point 0 (182.88,609.60,-1834.90) point 1 (243.84,609.60,-1834.90) point 2  
(182.88,670.56,-1834.90) point 3 (182.88,609.60,-1828.80) ...

point 4 (243.84,670.56,-1834.90) point 5 (182.88,670.56,-1828.80) point 6  
(243.84,609.60,-1828.80) point 7 (243.84,670.56,-1828.80)

**zone** create brick size 1 1 1 ...

point 0 (243.84,609.60,-1834.90) point 1 (304.80,609.60,-1834.90) point 2  
(243.84,670.56,-1834.90) point 3 (243.84,609.60,-1828.80) ...

point 4 (304.80,670.56,-1834.90) point 5 (243.84,670.56,-1828.80) point 6  
(304.80,609.60,-1828.80) point 7 (304.80,670.56,-1828.80)

**zone** create brick size 1 1 1 ...

point 0 (304.80,609.60,-1834.90) point 1 (365.76,609.60,-1834.90) point 2  
(304.80,670.56,-1834.90) point 3 (304.80,609.60,-1828.80) ...

point 4 (365.76,670.56,-1834.90) point 5 (304.80,670.56,-1828.80) point 6  
(365.76,609.60,-1828.80) point 7 (365.76,670.56,-1828.80)

...

## APPENDIX F – Initial conditions

; Fluid model

**model configure** fluid  
**zone** fluid active on  
**zone** fluid cmodel assign anisotropic **zone**  
 fluid biot on

; Constitutive model

**model gravity** 9.81 **zone**  
 cmodel assign elastic  
**zone** property young 68947 poisson 3e-1 density 2.7

**zone** face skin

; Constraint conditions **zone**

gridpoint fix velocity-x 0 **zone**  
 gridpoint fix velocity-y 0  
**zone** gridpoint fix velocity-z 0

; INITIAL CONDITIONS (TOTAL STRESSES OF PROBLEM 1) ;  
 AT PLANE XX:

**zone** initialize stress-xx -27578.8

;AT PLANE YY:

**zone** initialize stress-yy -27578.8

;AT PLANE ZZ:

**zone** initialize stress-zz -41368.2 gradient (0,0,23.1431)

; Reaction forces **zone**

gridpoint force-reaction-x **zone**  
 gridpoint force-reaction-y  
**zone** gridpoint force-reaction-z

; Free velocity

**zone** gridpoint free velocity-x **zone**  
 gridpoint free velocity-y  
**zone** gridpoint free velocity-z

; APPLY PROBLEMS CONSTRAINTS

**zone** gridpoint fix velocity-x 0 range group 'East' or 'West' **zone**  
 gridpoint fix velocity-y 0 range group 'North' or 'South' **zone**  
 gridpoint fix velocity-z 0 range group 'Bottom'

## APPENDIX G – Pore pressure list

;Pressure its ids and IDs ;Block ID 1

**zone** gridpoint fix pore-pressure 20744.03 range id 1 1  
**zone** gridpoint fix pore-pressure 20744.02 range id 2 2 **zone**  
 gridpoint fix pore-pressure 20744.03 range id 3 3 **zone**  
 gridpoint fix pore-pressure 20714.15 range id 4 4 **zone**  
 gridpoint fix pore-pressure 20744.03 range id 5 5 **zone**  
 gridpoint fix pore-pressure 20714.15 range id 6 6 **zone**  
 gridpoint fix pore-pressure 20714.15 range id 7 7 **zone**  
 gridpoint fix pore-pressure 20714.15 range id 8 8

;Block ID 2

**zone** gridpoint fix pore-pressure 20744.02 range id 2 2 **zone**  
 gridpoint fix pore-pressure 20744.02 range id 9 9 **zone**  
 gridpoint fix pore-pressure 20744.03 range id 5 5 **zone**  
 gridpoint fix pore-pressure 20714.15 range id 7 7 **zone**  
 gridpoint fix pore-pressure 20744.03 range id 10 10 **zone**  
 gridpoint fix pore-pressure 20714.15 range id 8 8 **zone**  
 gridpoint fix pore-pressure 20714.15 range id 11 11 **zone**  
 gridpoint fix pore-pressure 20714.15 range id 12 12

;Block ID 3

**zone** gridpoint fix pore-pressure 20744.02 range id 9 9 **zone**  
 gridpoint fix pore-pressure 20744.02 range id 13 13 **zone**  
 gridpoint fix pore-pressure 20744.03 range id 10 10 **zone**  
 gridpoint fix pore-pressure 20714.15 range id 11 11 **zone**  
 gridpoint fix pore-pressure 20744.03 range id 14 14 **zone**  
 gridpoint fix pore-pressure 20714.15 range id 12 12 **zone**  
 gridpoint fix pore-pressure 20714.15 range id 15 15 **zone**  
 gridpoint fix pore-pressure 20714.15 range id 16 16



## APPENDIX H – FISH programming

; Fish command to export volumetric strain and pore pressure results in a output file

```
fish define setup  
global a_size = 20  
global IO_READ = 0  
global IO_WRITE = 1  
global IO_FISH = 0  
global IO_ASCII = 1  
    global filename = 'vs.txt'  
end @setup
```

```
fish define io  
array b(a_size)
```

```
local status = file.open(filename, IO_WRITE, IO_ASCII)  
    loop foreach local zone zone.list  
id = zone.id(zone)  
    vsa = zone.strain.vol.inc (zone)  
pp = zone.pp(zone)
```

```
    b(1) = string(id) + ' ' + string(vsa) + ' ' + string(pp)  
status = file.write(b,1)
```

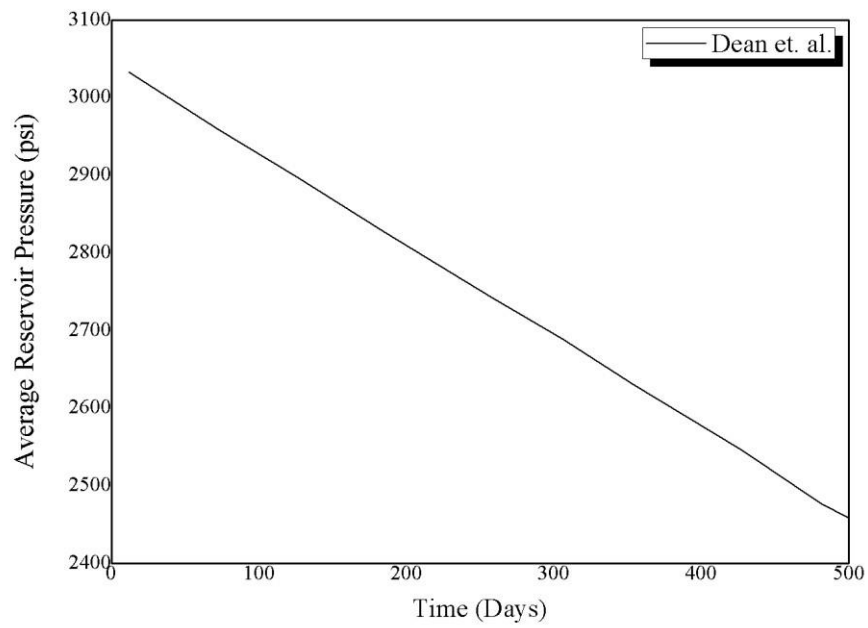
```
endloop
```

```
status = file.close  
end @io
```

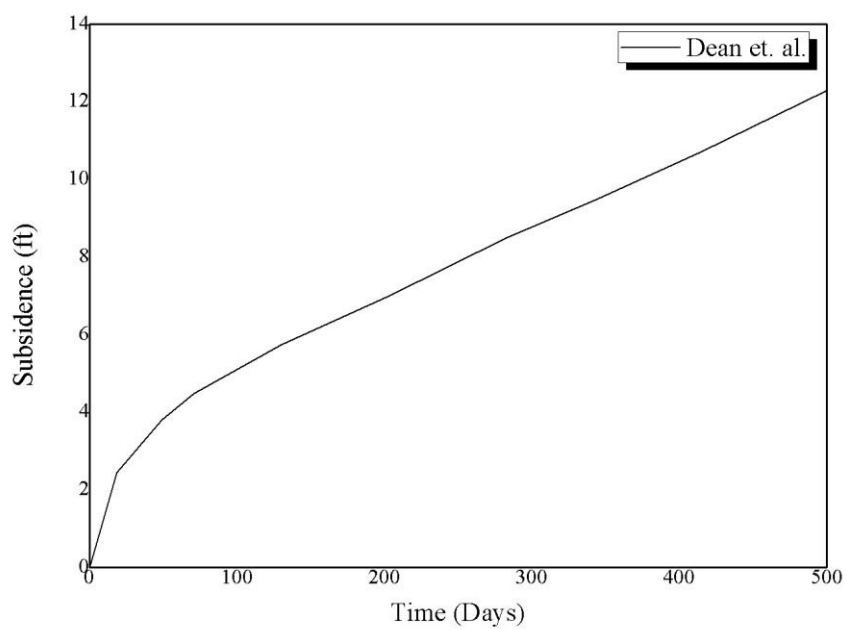
APPENDIX I – DEAN *et al.* RESULTS (2006)

## PROBLEM 1

Average reservoir pressure.

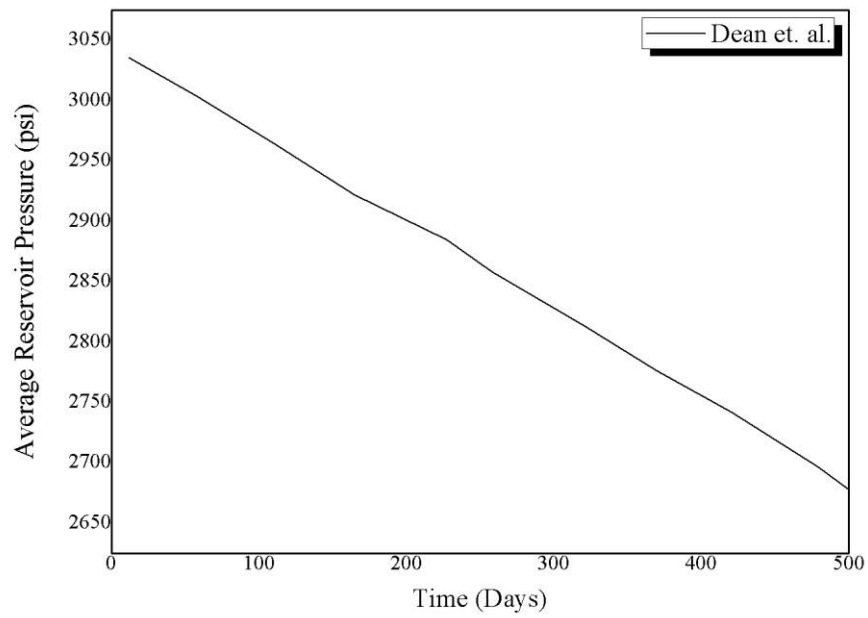


Subsidence.

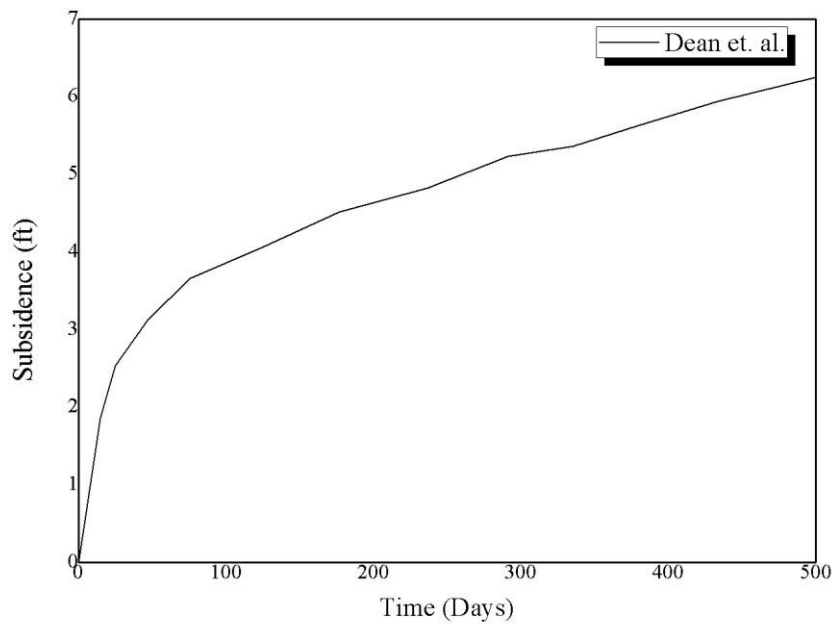


## PROBLEM 2

Average reservoir pressure.

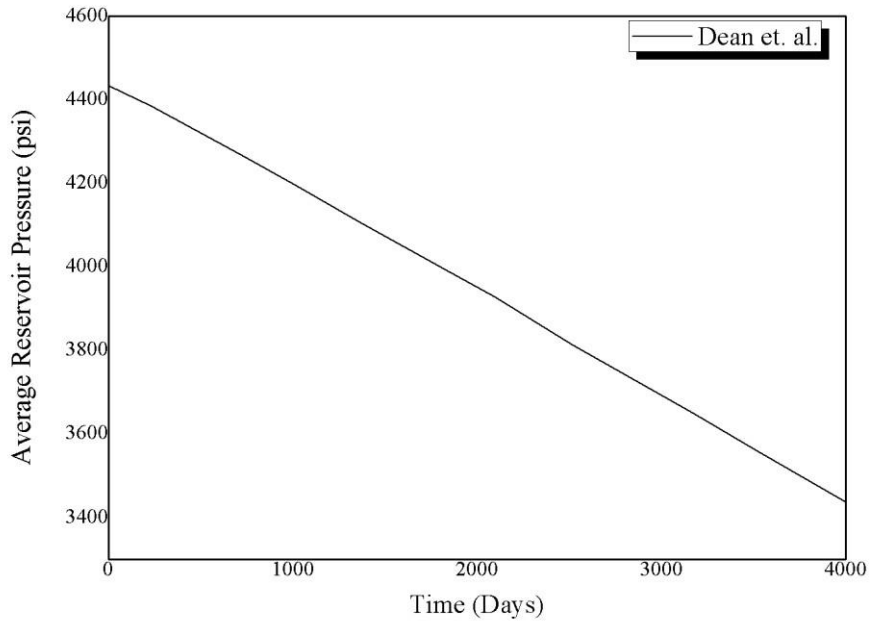


Subsidence.

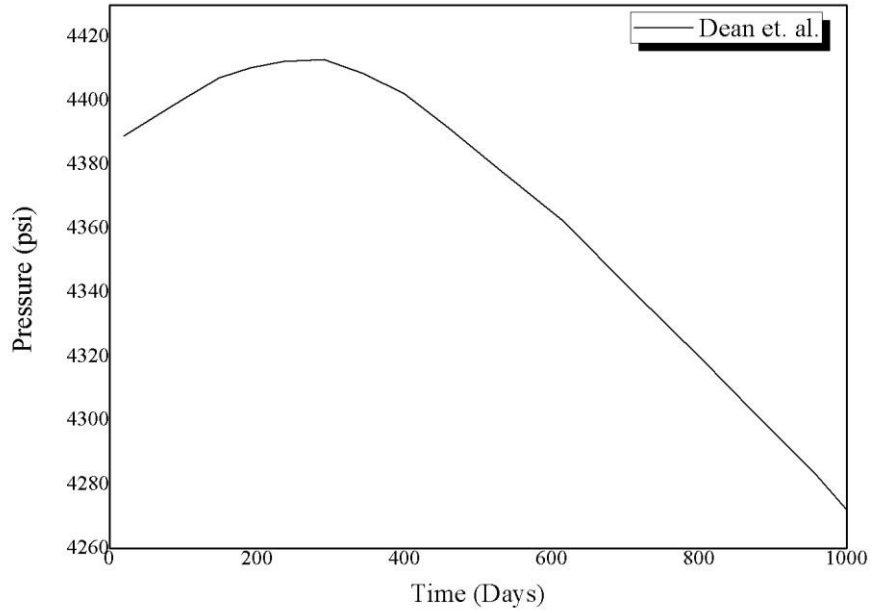


## PROBLEM 3

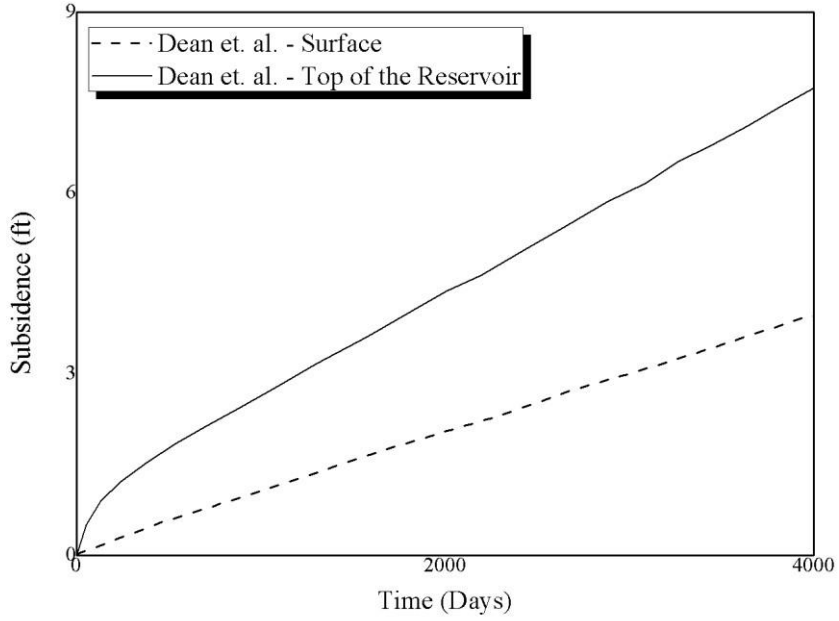
Average reservoir pressure.



Reservoir border pressure until 1000 days.

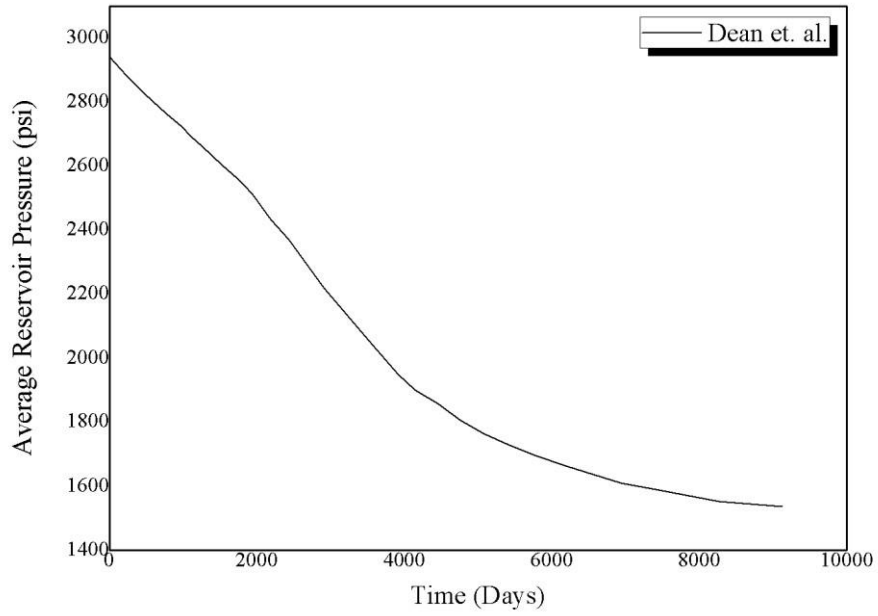


Subsidence.

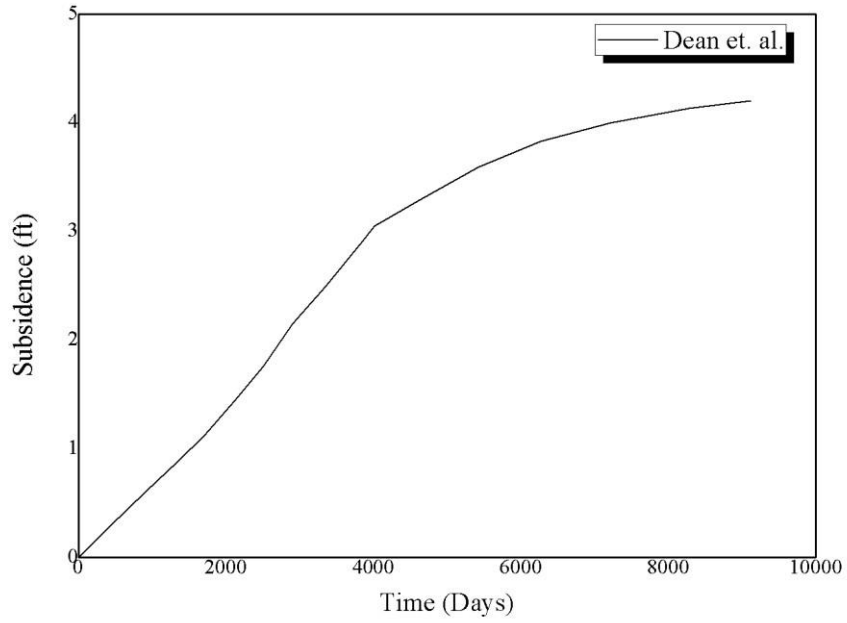


PROBLEM 4

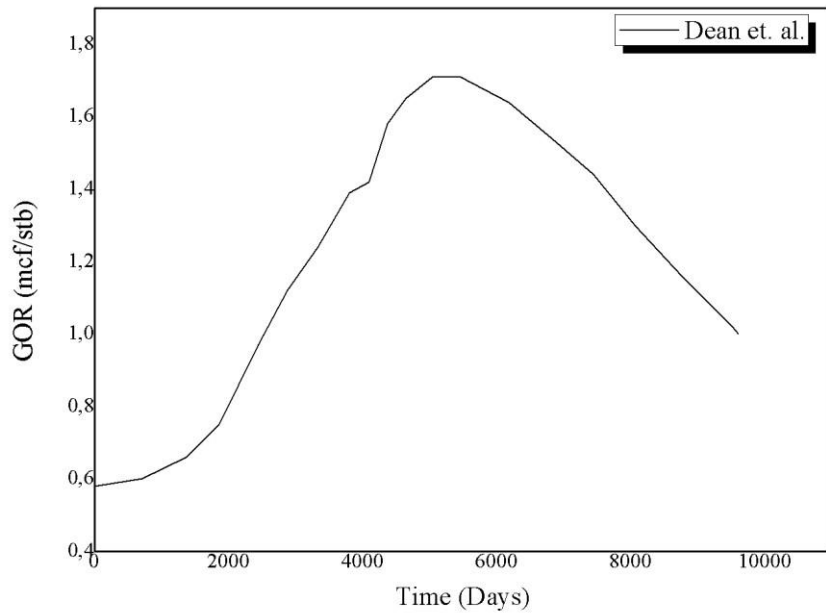
Average reservoir pressure.



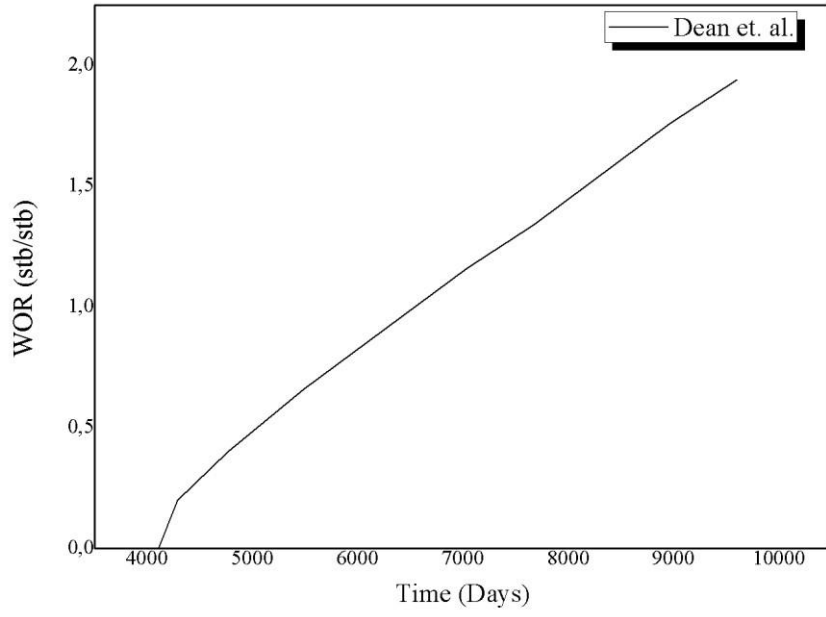
Subsidence



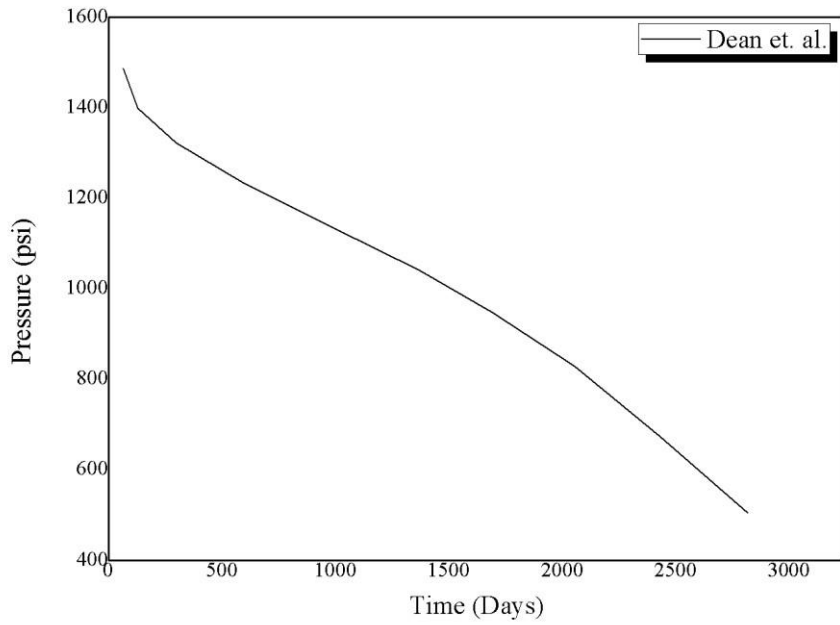
Producer well gas-oil ratio.



Producer well water-oil ratio.

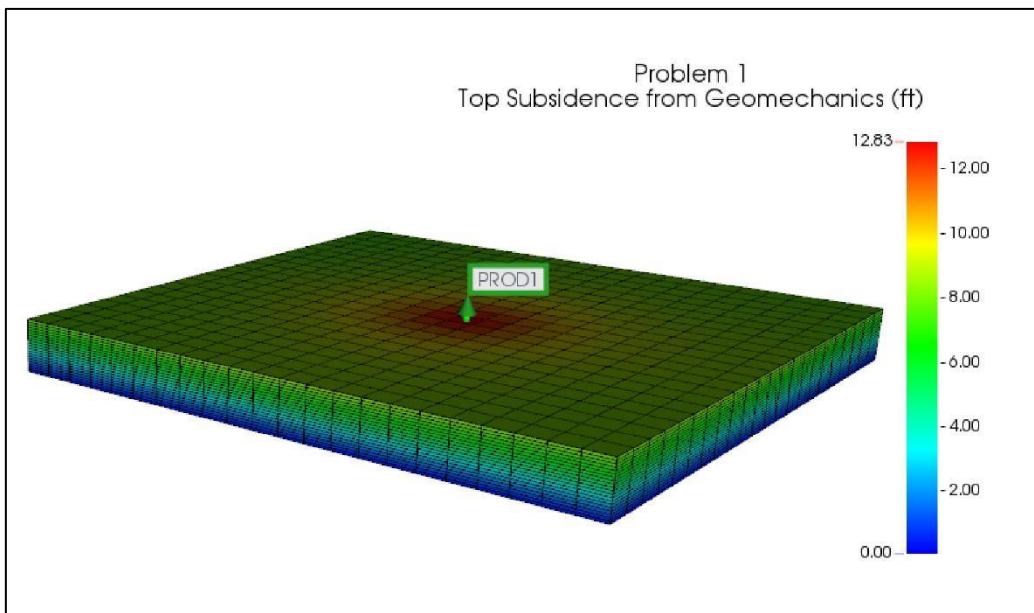
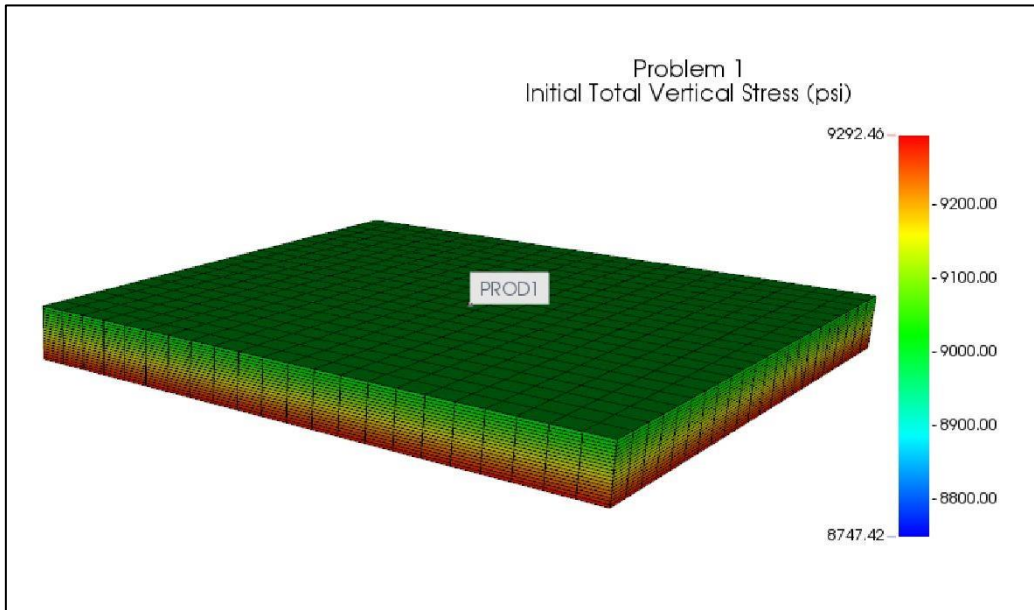


Producer well pressure.



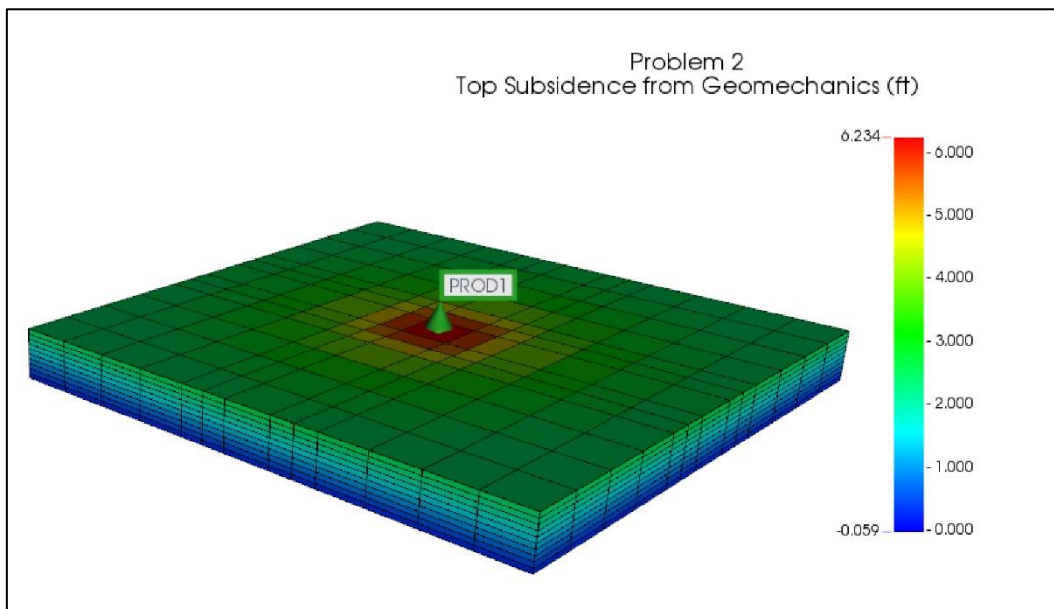
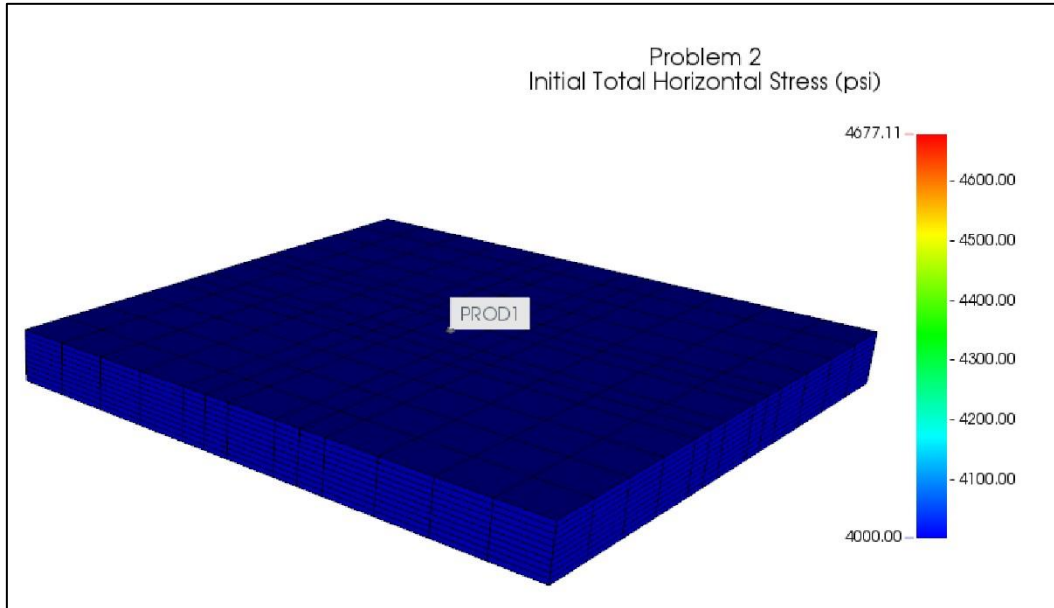
APPENDIX J – IMEX CMG 2019 EXPLICIT ITERATIVE COUPLING.

PROBLEM 1

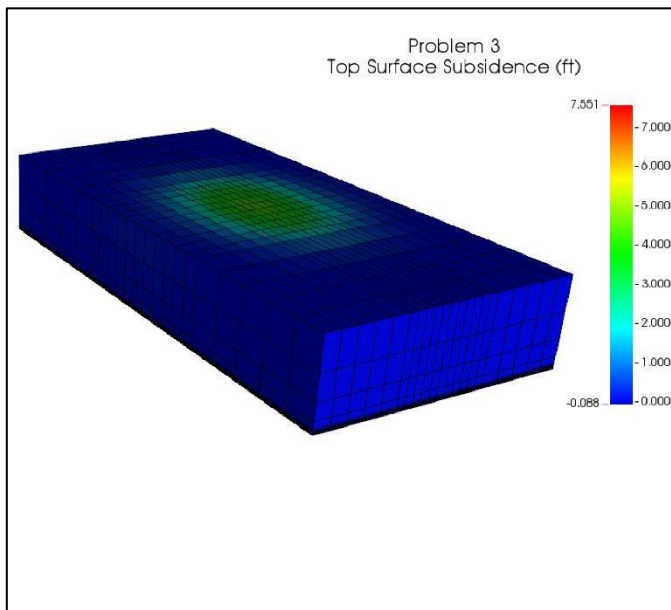
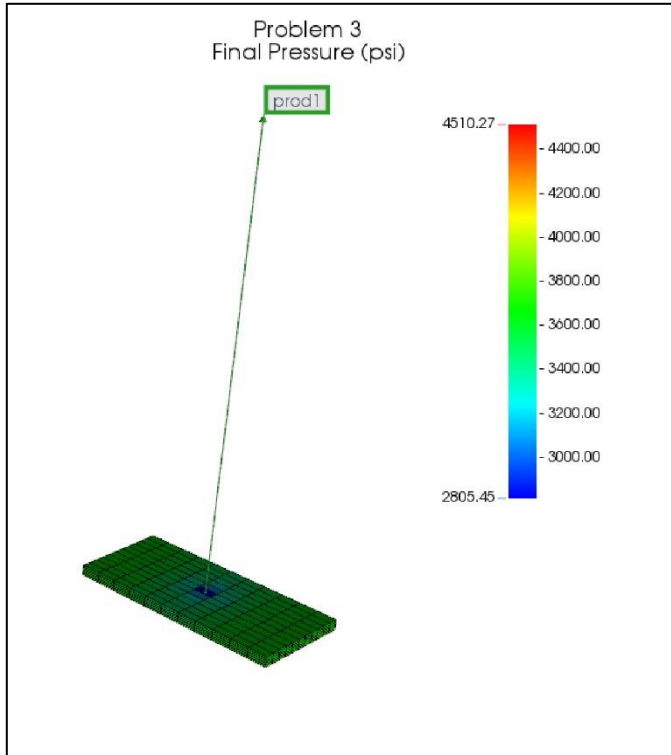


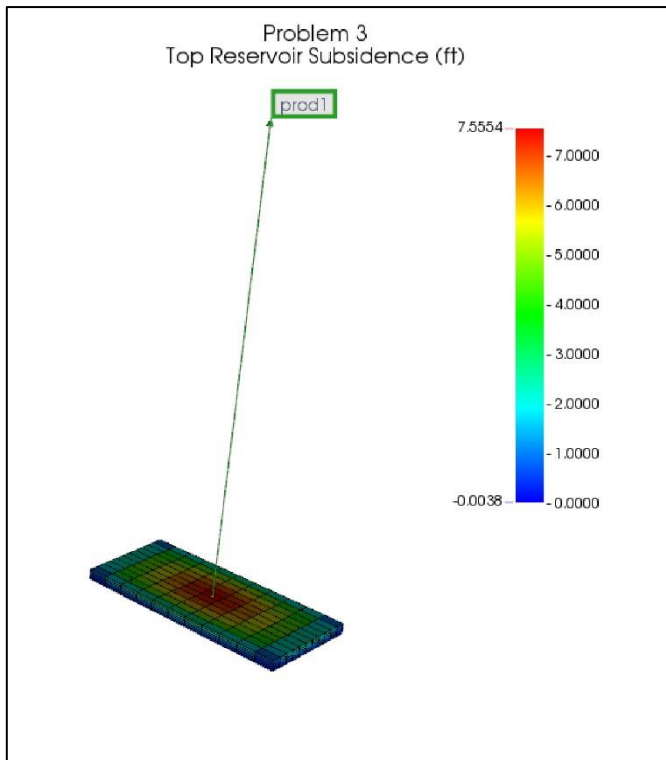


## PROBLEM 2



## PROBLEM 3





PROBLEM 4

